I. QUANTITATIVE STUDIES OF THE NO_2-N_2O_4
SYSTEM IN THE INFRARED

II. EMISSION OF DIFFUSE BANDS OF SODIUM
BEHIND SHOCK FRONTS

Thesis by

Andrew Guttman

In Partial Fulfillment of the Requirements
For the Degree of
Doctor of Philosophy

California Institute of Technology
Pasadena, California
1962

ACKNOWLEDGEMENTS

ABSTRACT

The integrated intensities as a function of temperature have been measured for one NO_2 and for four N_2O_4 combination bands in the spectral region from one to five microns. The temperature was varied from 50 to $100^{\circ}C$ for the gas-phase studies and from 25 to $100^{\circ}C$ for the liquid-phase experiments. In the spectral region from 5 to 15 microns, integrated intensities at $25^{\circ}C$ were measured for one NO_2 and for three N_2O_4 fundamental bands. Results from a series of absorption spectra were interpreted in accordance with the Wilson-Wells-Penner-Weber method. Saturated vapors were used in all experiments; the optical depth was varied by using a series of spacers in a specially designed infrared absorption cell capable of handling both liquid and gas. Measured intensities for N_2O_4 combination bands in the liquid and gas phases were compared and found to differ by less than 16% for three out of four combination bands studied; for the fourth band, the observed difference was about 50%. Results for all of the combination bands investigated indicate that the integrated intensities vary approximately as $1/T$ in the temperature range under consideration.

Absolute intensity data may be used for a spectroscopic determination of the heat of dissociation for gases in chemical equilibrium. For the reaction $N_2O_4 \rightleftharpoons 2NO_2$, we have found the value of ΔH°, using the temperature dependence of the absorption bands, to be 13.1 Kcal/(mole N_2O_4); this value is in fair agreement with the value of 13.7 Kcal/(mole N_2O_4) obtained by techniques utilizing density measurements.

In Chapter II, shock tube studies are described of a diffuse emission band, centered near the resonance lines of sodium and attributed to van der Waals molecules Na_2. A small quantity of finely ground sodium salt (e.g., NaCl, NaBr, or Na_2CO_3) was placed at the end of the low-pressure section of a shock tube containing an argon atmosphere. Spectra were recorded photographically with a 1.5 m grating spectrograph.

TABLE OF CONTENTS

I. QUANTITATIVE STUDIES OF THE NO_2-N_2O_4 SYSTEM IN THE INFRARED

A. INTRODUCTION

The qualitative features of the vibration-rotation bands of nitrogen dioxide and dinitrogen tetroxide in the infrared region of the spectrum have been investigated by a number of researchers.[1-10] Most of the work in the past has been concerned with information regarding molecular structure and interaction energy curves. Spectral locations of band centers and individual rotational lines have been determined to a high degree of accuracy and from these, estimates have been made of such quantities as molecular interaction forces, moments of inertia, atomic space configurations, and molecular sizes.

The earliest infrared work on gaseous NO_2-N_2O_4 mixtures was performed in 1909 by Warburg and Leithauser[1] who observed two bands belonging to NO_2 (3.43, 6.12 μ) and one belonging to N_2O_4 (5.70 μ). More extensive research on these gases was conducted during the following year by Eva von Bahr[2] with studies on the influence of pressurization with a foreign gas (O_2) on the amount of absorption of the same bands observed by Warburg and Leithauser. Nitrogen dioxide pressures ranged from 20 to 50 mm, while oxygen pressurization was varied between 50 mm and one atmosphere. For the 6.1-μ band, the percentage of absorption at 30 mm of NO_2 changed from 25.5 without pressurization to 43.4 at one atmosphere of oxygen. Above this pressure, the absorption remained nearly constant. Similar results, though with a somewhat weaker pressure dependence, were found for

the 5.7-μ band of N_2O_4.

Observations of the NO_2 spectrum, as well as those of other gases, in the far infrared (20-152μ) were reported by Strong and Woo[3] in 1932, but no real effort was made to identify the various bands.

The first extensive investigation of the infrared spectrum of the NO_2-N_2O_4 system at various temperatures was performed by Sutherland[4] in 1933. Eleven of the twelve fundamentals of dinitrogen tetroxide were identified along with three combination bands. In addition, seven nitrogen dioxide bands were reported. Further studies on these gases were performed in 1933 by Bailey and Cassie[5] who obtained the N-O force constant, deformation constant, and moment of inertia. In the same year, Schaffert[6] reported eight absorption bands in the gaseous state and two in the liquid state. He separated the bands belonging to NO_2 from those belonging to N_2O_4 by the usual technique of heating the gas to $150^{\circ}C$ where most of the gas decomposes to NO_2 (see Section C).

One of the most complete early studies of both gases was reported by Harris and King[7] in 1934. These authors were the first to give an upper limit estimate of 0.0003 cm^{-1}-atm^{-1} for the absorption coefficient in the infrared region below 2 microns. Absorption spectra between one and four microns were investigated thoroughly at room temperature and at $150^{\circ}C$. The NO_2 bands were identified as combination bands of two fundamentals while the N_2O_4 bands were interpreted as combinations and harmonics of known fundamentals. The bands observed by these authors were compared with those noted previously by other workers.

In more recent studies, refinements were introduced by using
isotopic species and superior instruments. Moore[8] in 1953 observed
nine combination bands and overtones belonging to NO_2 with sufficiently
high resolving power to yield the rotational fine structure. Some of his
results are presented in Table 1. Good agreement concerning the
locations of the $N_2{}^{14}O_4$ bands in the near infrared is found between the
results obtained by Snyder and Hisatsune[9] in 1957 and by Begum and
Fletcher[10] in 1960. Selected results from Begum and Fletcher are also
cited in Table 1. An infrared absorption spectrum of the gaseous mix-
ture containing NO_2 and N_2O_4 is reproduced in Fig. 1.
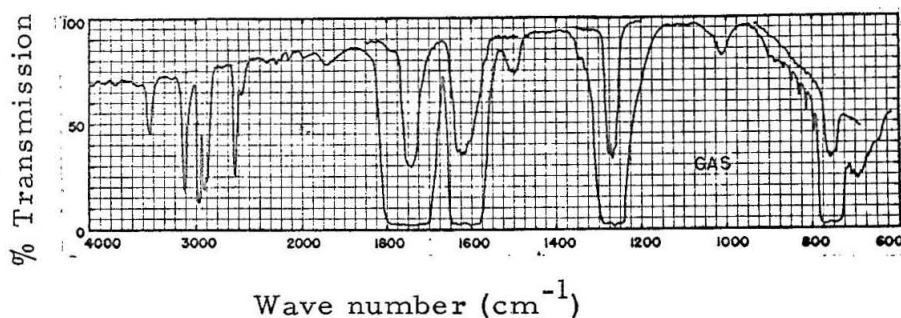
Fig. 1. Spectrum of gaseous NO_2-N_2O_4 mixtures at pressures of
approximately 40 cm and 2 cm of Hg, at $23°C$ in a 10-cm
pyrex cell (from Ref. 9).

There is a definite need for information on absolute intensities of
NO_2 and N_2O_4 bands in connection with studies on radiant-heat transfer
and concentration analysis. In particular, there is considerable interest
in atmospheric transmission of radiant energy. In addition to CO_2 and
H_2O, under certain conditions (e.g., after a nuclear bomb blast) there

Table 1. Observed infrared bands of NO_2 and N_2O_4 in the gaseous and liquid states.

Molecule	Band center observed by				Identification	$(\omega_{gas} - \omega_{liquid})$ observed by	
	us (cm^{-1})		others * (cm^{-1})			us (cm^{-1})	others (cm^{-1})
	gas	liquid	gas	liquid			
NO_2	2908	--	2905	--	$\nu_1 + \nu_3$	--	--
NO_2	1617	--	1616	--	ν_3	--	--
N_2O_4	2618	2605	2630	2616	$\nu_1 + \nu_{11}$	13	14
N_2O_4	2962	2945	2971	2956	$\nu_5 + \nu_{11}$	17	15
N_2O_4	3120	3114	3111	3107	$\nu_1 + \nu_9$	6	4
N_2O_4	3442	3429	3440	3427	$\nu_5 + \nu_9$	13	13
N_2O_4	1748	--	1748	--	ν_9	--	--
N_2O_4	1260	--	1262	--	ν_{11}	--	--
N_2O_4	750	--	750	--	ν_{12}	--	--

* NO_2 figures are from Ref. 8; N_2O_4 from Ref. 10.

may also be significant amounts of NO_2 in the atmosphere. Quantitative information in the form of spectral absorption coefficients and integrated intensities is essential for this type of study. A considerable number of experimental results are available for CO_2 and some for H_2O. To the author's knowledge, no studies of a quantitative nature on NO_2 and N_2O_4 have appeared in the open literature. There is also continuing fundamental interest in absolute intensity data since they may be used to estimate the rate of change of dipole moment with internuclear separation.

In our experiments, integrated intensities were obtained for one fundamental and one combination band of NO_2, and for three fundamentals and four combination bands of gaseous N_2O_4; integrated intensities were also measured for the four combination bands of N_2O_4 in the liquid phase. The work was performed in the spectral region between one and 15 microns. Intensities for N_2O_4 molecules in the liquid and gas phases were compared and found to be nearly equal for three of the four bands studied. From the temperature dependence of absorption in the region of the NO_2 and N_2O_4 bands, the heat of dissociation for the reaction $N_2O_4 \longrightarrow 2NO_2$ was calculated and found to agree satisfactorily with previous measurements based on other techniques.

B. EXPERIMENTAL METHOD

1. Definitions

For a gas at thermal equilibrium, a spectral absorption coefficient P_ω is defined such that the emitted radiancy, in the wave number range between ω and $\omega + d\omega$, from the center of the base of a

hemisphere of radius ℓ, filled with isothermal gas at pressure p, is

$$R_\omega d\omega = R_\omega^o \left[1 - \exp(-P_\omega p \ell) \right] d\omega, \tag{1}$$

where R_ω^o represents the blackbody radiancy at the wave number ω in any convenient set of units, and $p\ell$ is known as the optical depth. It is convenient to express pressure in atmospheres and the geometric length in centimeters, thus leaving P_ω in the units $atm^{-1}\text{-}cm^{-1}$.

The factor in brackets on the right-hand side of Eq. (1) is known as the (hemispherical) spectral emissivity and, at thermal equilibrium, is equal to the spectral absorptivity. The spectral flux density I_ω^o incident on a column of gas of length ℓ at the pressure p will be attenuated by a factor $\exp(-P_\omega p \ell)$ in passing through the gas.

For a liquid absorber it is convenient to define a linear absorption coefficient through Beer's law,

$$\frac{I_\omega}{I_\omega^o} = \exp(-k_\omega \ell), \tag{2}$$

where I_ω and I_ω^o refer to the transmitted and incident spectral flux densities, respectively, and ℓ is the geometric length of the absorbing path; k_ω is now expressed in cm^{-1}.

We define the integrated intensity a (in $cm^{-2}\text{-}atm^{-1}$), for a band located between the wave numbers ω_1 and ω_2, by

$$a = \int_{\omega_1}^{\omega_2} P_\omega d\omega \tag{3}$$

for the gas phase; for the liquid phase we define the integrated intensity a' (in cm^{-2}) similarly as

$$a' = \int_{\omega_1}^{\omega_2} k_\omega d\omega .$$

(4)

Because of instrumental limitations, it is not generally possible to perform experimental measurements without slit distortions. We define an instrumental slit function $g(\left|\omega-\omega'\right|, b', c')$ for the effective spectral width of the exit slit between $\omega-\triangle\omega^*$ and $\omega+\triangle\omega^*$. Here ω represents the actual setting of the instrument while b' and c' are parameters dependent upon the slit geometry. The slit function gives the fraction of energy at the wave number ω' to which the detector responds when the instrument is set at ω. The apparent spectral flux density I_ω^a sensed by the instrument when it is set at ω is then

$$I_\omega^a = \int_{\omega-\triangle\omega^*}^{\omega+\triangle\omega^*} I_{\omega'} \, g(\left|\omega-\omega'\right|, b', c')d\omega' ,$$

(5)

where the normalization condition

$$\int_{\omega-\triangle\omega^*}^{\omega+\triangle\omega^*} g(\left|\omega-\omega'\right|, b', c')d\omega' = 1$$

holds. Representative slit functions are triangular for prism instruments and Gaussian for grating instruments.

2. The Wilson-Wells-Penner-Weber (W_3P) Method

Experimental data from a series of absorption spectra were interpreted in accordance with the W_3P method as described by Penner.[11]

Briefly, the method entails the smearing out of the rotational fine structure of a vibration-rotation band by means of sufficient pressure broadening to yield a line half-width which is considerably greater than the spacing between lines. This may be accomplished either by maintaining a sufficiently high pressure of the absorbing gas (self broadening) or else by pressurizing with a foreign, non-absorbing gas (foreign-gas broadening). With the fine structure smeared out in this manner, it is no longer necessary to resolve details of an individual rotational line and hence one may use relatively low-resolution instruments for making quantitative measurements.

The integrated intensity is obtained by defining a quantity $\mathcal{B}$ which equals the integral of the natural logarithm of the ratio of incident apparent spectral flux density $I_\omega^{o,a}$ to the transmitted apparent spectral flux density I_ω^a and then determining the slope of a plot showing $\mathcal{B}$ as a function of the optical depth $X \equiv p\ell$.

Using previously specified notation,

$$\mathcal{B} = \int_{\omega_1}^{\omega_2} \ln\left(\frac{I_\omega^{o,a}}{I_\omega^a}\right) d\omega = \int_{\omega_1}^{\omega_2} \left[\ln \frac{\displaystyle\int_{\omega-\Delta\omega^*}^{\omega+\Delta\omega^*} I_{\omega'}^o \, g(|\omega-\omega'|, b', c')d\omega'}{\displaystyle\int_{\omega-\Delta\omega^*}^{\omega+\Delta\omega^*} I_{\omega'} \, g(|\omega-\omega'|, b', c')d\omega'} \right] d\omega. \quad (6)$$

Since $I_{\omega'} = I_{\omega'}^o \exp(-P_{\omega'}X)$, it follows, if the incident spectral flux density

$I^o_{\omega'}$ is constant over the wave number interval between $\omega - \Delta\omega^*$ and $\omega + \Delta\omega^*$, that

$$\mathcal{B} = \int_{\omega_1}^{\omega_2} \left\{ -\ln \frac{\displaystyle\int_{\omega-\Delta\omega^*}^{\omega+\Delta\omega^*} \left[\exp(-P_{\omega'}X)\right] g(\left|\omega-\omega'\right|, b', c')d\omega'}{\displaystyle\int_{\omega-\Delta\omega^*}^{\omega+\Delta\omega^*} g(\left|\omega-\omega'\right|, b', c')d\omega'} \right\} d\omega \tag{7}$$

and

$$\frac{d\mathcal{B}}{dX} = \int_{\omega_1}^{\omega_2} \left\{ \frac{\displaystyle\int_{\omega-\Delta\omega^*}^{\omega+\Delta\omega^*} P_{\omega'} \left[\exp(-P_{\omega'}X)\right] g(\left|\omega-\omega'\right|, b', c')d\omega'}{\displaystyle\int_{\omega-\Delta\omega^*}^{\omega+\Delta\omega^*} \left[\exp(-P_{\omega'}X)\right] g(\left|\omega-\omega'\right|, b', c')d\omega'} \right\} d\omega. \tag{8}$$

At this point we introduce the requirement that the fine structure of the band is sufficiently smeared out to permit $P_{\omega'}$ to be considered constant over the wave number range of the effective slit width $2\Delta\omega^*$. With this assumption, it is readily seen that the terms of Eq. (6) containing the slit function cancel out and that

$$\frac{d\mathcal{B}}{dX} = \int_{\omega_1}^{\omega_2} P_{\omega}d\omega \equiv a. \tag{9}$$

Equation (9) is the desired relation which has been used in interpreting the experimental results.

C. PROPERTIES OF NO_2 AND N_2O_4

Below -10°C, dinitrogen tetroxide exists as a crystalline solid, while from -10 to 21.64°C and at one atmosphere of pressure it is a nearly colorless liquid. Careful measurements of vapor pressure as a function of temperature have been published previously[12, 13] and selected results are reproduced in Fig. 2. These measurements were conducted in a stainless steel cell immersed in an isothermal bath. A specially-designed pressure sensor was used. Vapor pressures were obtained at intervals of approximately 30°F with a precision of better than one percent.

Because of its relatively high boiling point, N_2O_4 may be excluded from portions of the gas-handling system quite effectively with a liquid-nitrogen trap.

In the gaseous state, nitrogen dioxide and dinitrogen tetroxide exist in chemical equilibrium according to the relation

$$N_2O_4 \rightleftharpoons 2NO_2 .$$
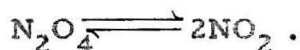
Extensive measurements of the equilibrium constant K_p at temperatures ranging from 281.82 to 403.93°K were performed by Bodenstein and Boës;[14] relevant data for K_p are plotted as a function of temperature in Fig. 3. At room temperature and one atmosphere pressure the fraction of N_2O_4 decomposed is 0.31.

The decomposition of N_2O_4 proceeds at a very rapid rate. Carrington and Davidson[15] estimated the dissociation rate constant to be $k_f = 10^{16} \exp(-11,000/RT)$ sec^{-1} in the presence of a foreign gas (N_2)
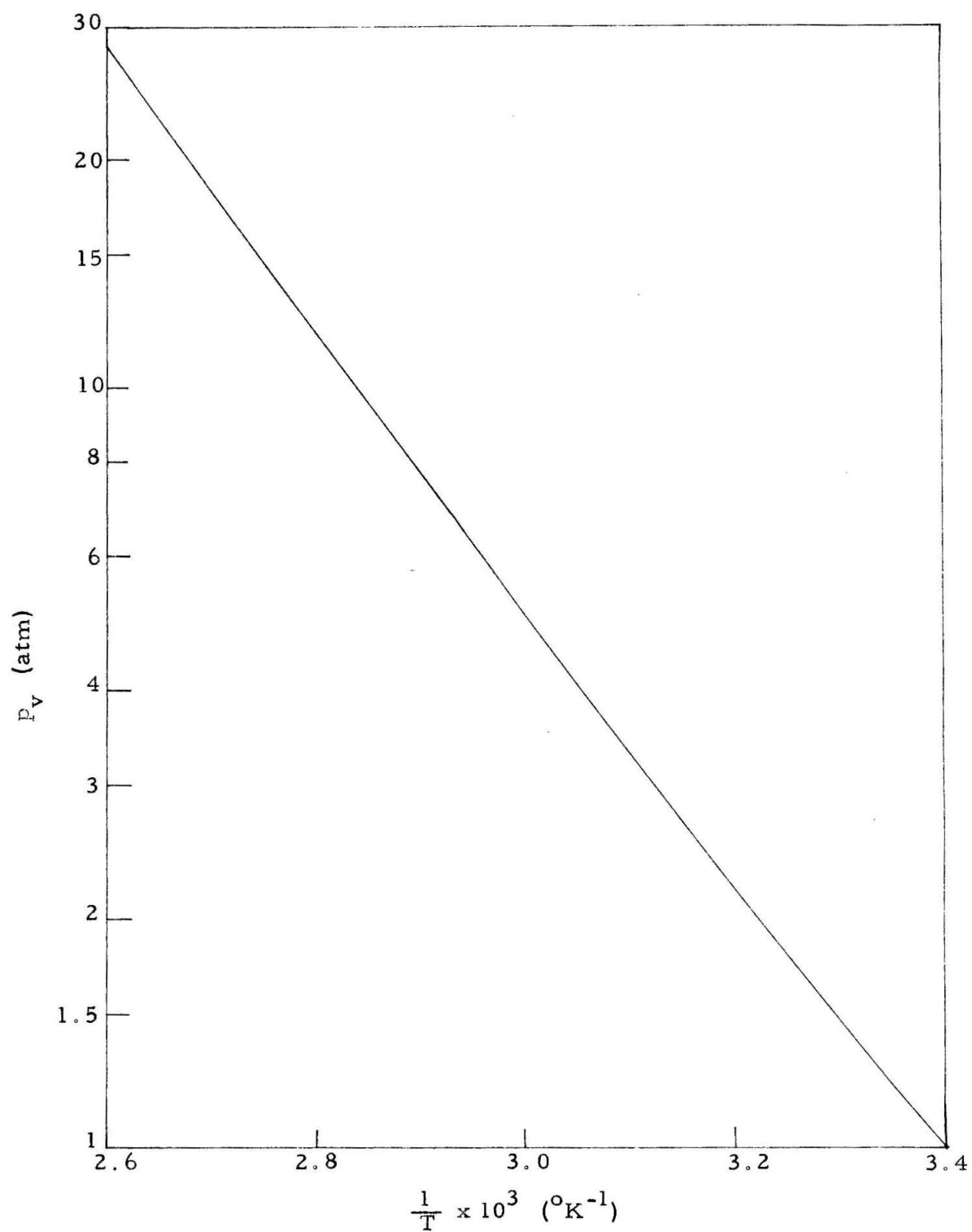
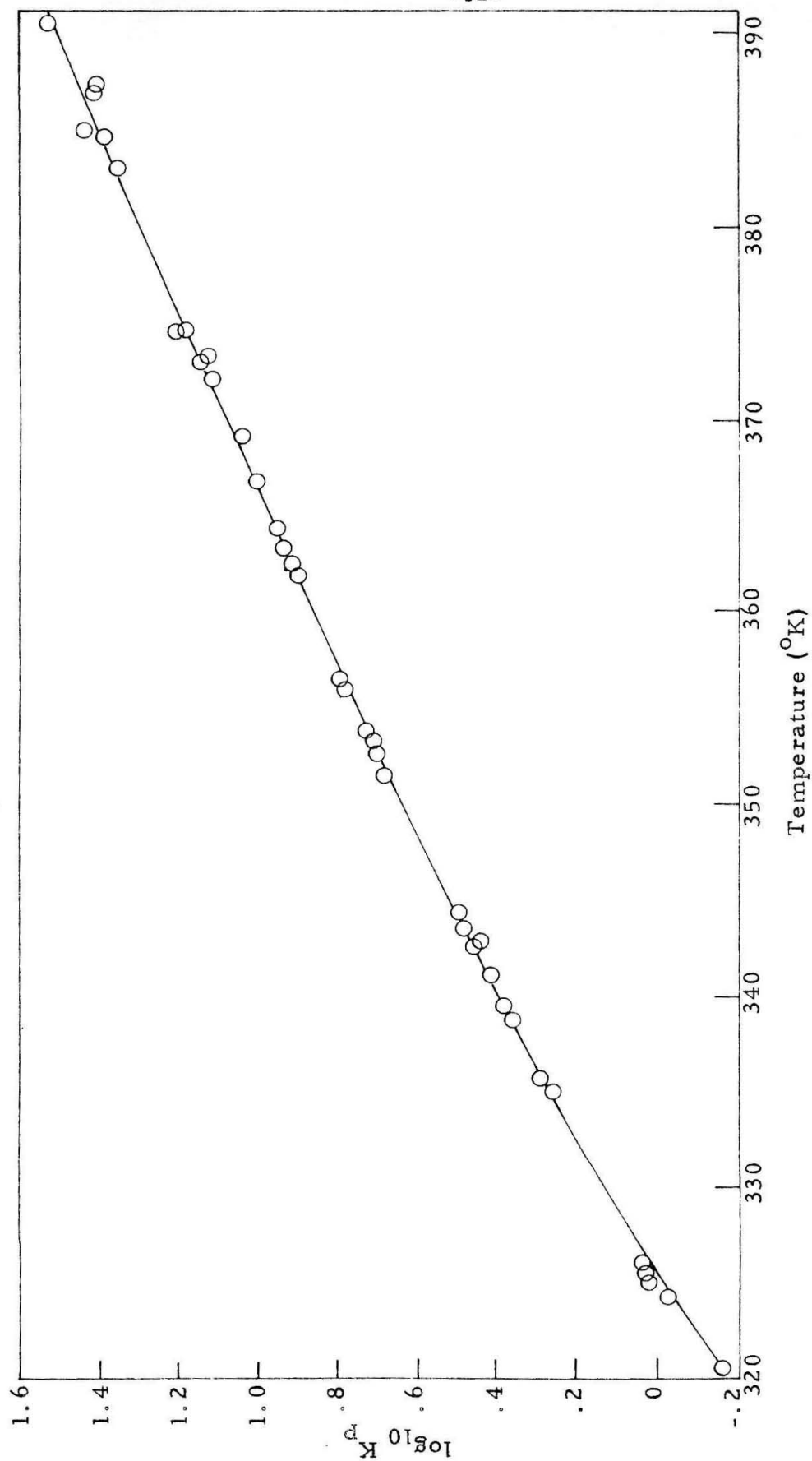Fig. 2. The vapor pressure of nitrogen dioxide as a function of temperature (from Ref. 13).

Fig. 3. Temperature dependence of the equilibrium constant (in atm) for the reaction $N_2O_4 = 2NO_2$ (from Ref. 14). The circles represent experimentally determined results.

at pressures considerably higher than one atmosphere. Under these conditions, chemical equilibrium is attained in times of the order of microseconds.

Above $400^{\circ}K$, NO_2 dissociates extensively into NO and O_2; in order to avoid this decomposition, we have not performed any experiments at temperatures above about $400^{\circ}K$.

Giauque and Kemp[16] proposed the following equation of state, which they found compatible with the data presented by Bodenstein and Boës, [14]

$$pV = \left(n_{NO_2} + n_{N_2O_4}\right) RT + \left(n_{NO_2}\beta_{NO_2} + n_{N_2O_4}\beta_{N_2O_4}\right) pRT, \qquad (10)$$

where they assumed

$$\beta_{N_2O_4} = 2\beta_{NO_2} \equiv \beta \qquad (11)$$

and, using Berthelot's equation of state, found

$$\beta = -0.01\left(\frac{294}{T}\right)^3. \qquad (12)$$

Associated with the gas mixture containing NO_2 and N_2O_4 is a characteristic brown color which becomes deeper as the temperature is raised. This color results from continuum absorption in the visible region of the spectrum by NO_2. Dinitrogen tetroxide is transparent in the visible region. As the temperature is raised, the equilibrium composition shifts toward NO_2, resulting in deepening of the brown color. Similar results occur as a result of shifts in equilibrium composition with total pressure. In preliminary studies, we utilized the visible absorption of NO_2 for the purpose of gas analysis with photoelectric recording of the absorption (see Section E).

Nitrogen dioxide is highly reactive with many substances and is extremely toxic. Exposure of the gas to small traces of moisture will result in the formation of nitric acid with subsequent corrosion of exposed metals. Rubber gaskets and O-rings are attacked, as are also most organic greases used for sealing purposes. Work done in the past was conducted entirely with glass apparatus in order to eliminate some of the corrosion problems. The experiments reported in the following sections were conducted at pressures which are too high for the use of glass apparatus and hence metallic containers had to be used.

D. EXPERIMENTAL APPARATUS[*]

1. Optical System

An overall view of the experimental apparatus appears in Fig. 4. Situated at the left of the figure is the control board on which is mounted the pressure gage used for measuring gas pressure in the absorption cell. Also mounted on this board are a thermocouple selector, the main switch box for the electric furnace, fuses, and an ammeter for measuring the current through the heating coils. The ammeter and voltmeter for the light source are mounted on the table at the extreme left; also located on this table are a thermostatic control unit and a thermocouple potentiometer. The 2-ft diameter by 5-ft long vacuum tank, which may be seen at the center of the photograph, contains the absorption cell, light source, mechanical chopper, and associated optics. Directly in front

---

[*] The apparatus used in the present studies is a modified version of equipment first assembled by D. Weber and subsequently improved by U. P. Oppenheim.
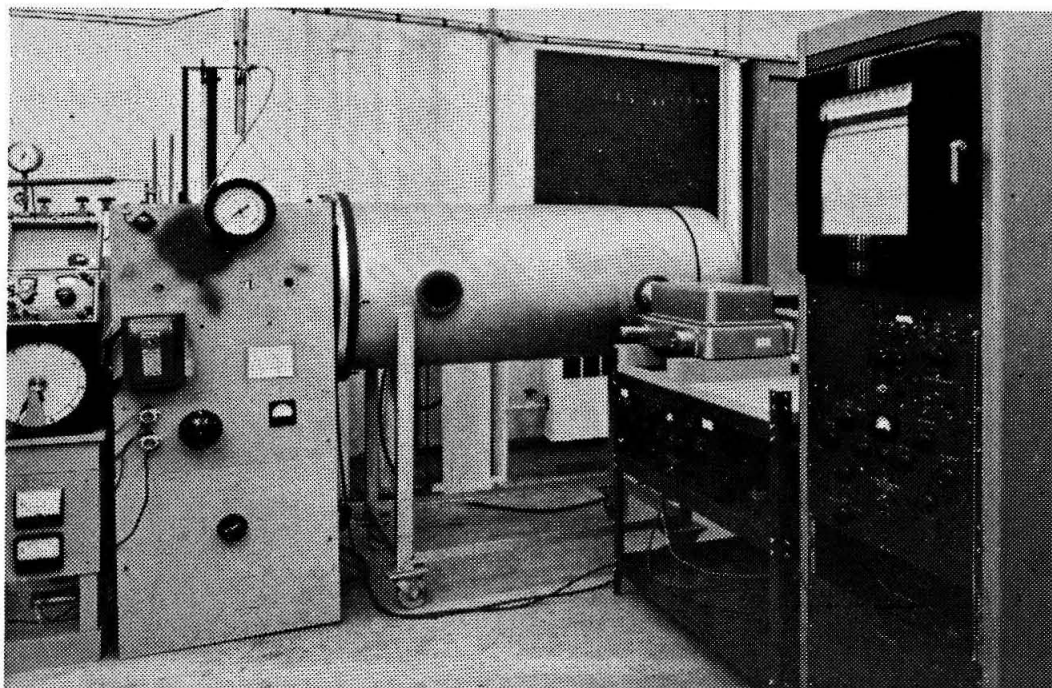
Fig. 4. Overall view of the apparatus; the vacuum tank in the center contains the absorption cell and light source with associated optics.
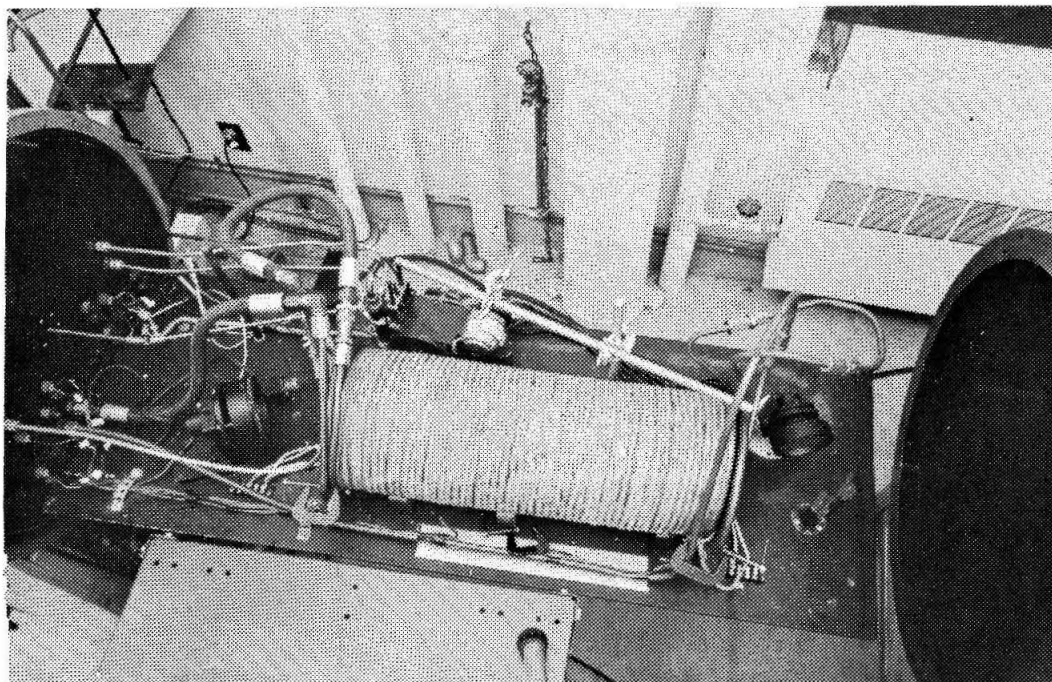

Fig. 5. Internal view of the vacuum tank; the cooling coils seen at the center surround the electric furnace which contains the absorption cell.

of the tank is located a Perkin-Elmer Model 98 spectrometer with a
13-cycle amplifier. A Leeds and Northrup Speedomax Type G recorder
is seen to the right of the spectrometer.

Figure 5 depicts the internal components of the vacuum tank,
while Fig. 6 shows a schematic diagram of the equipment. Light from
a globar source, after being chopped by a 13-cycle chopper and
collimated by a spherical mirror (M_1) is passed through the absorption
cell located in an electric furnace, and then deflected by a plane mirror
(M_2) onto an off-axis parabolic mirror (M_3) which focuses the beam on
the entrance slit of the infrared spectrometer. The light beam leaves the
vacuum tank through a 2-inch diameter by 1/4-inch thick sodium
chloride window.

As infrared light source we used a water-cooled globar which
consists of a silicon carbide rod several centimeters long and about 6
mm in diameter. It is very nearly a greybody with an emissivity of
about 0.80 in the region from 1.5 to 15 microns[17]; it is electrically
heated in air with a current of about 5 amps to a maximum temperature
of $1400^{\circ}K$. At $1400^{\circ}K$, the peak emitted radiant energy lies near 2
microns. Heating of the globar to higher temperatures will cause ex-
cessive oxidation of the silicon carbide and evaporation of the binding
material. The relatively low useful operating temperature of the globar
is its chief disadvantage. For stable radiation output, the globar re-
quires a well-regulated current. When the voltage was provided through
a variac which received its input from a Sola constant-voltage trans-
former, the radiation output varied in an irregular manner. Good
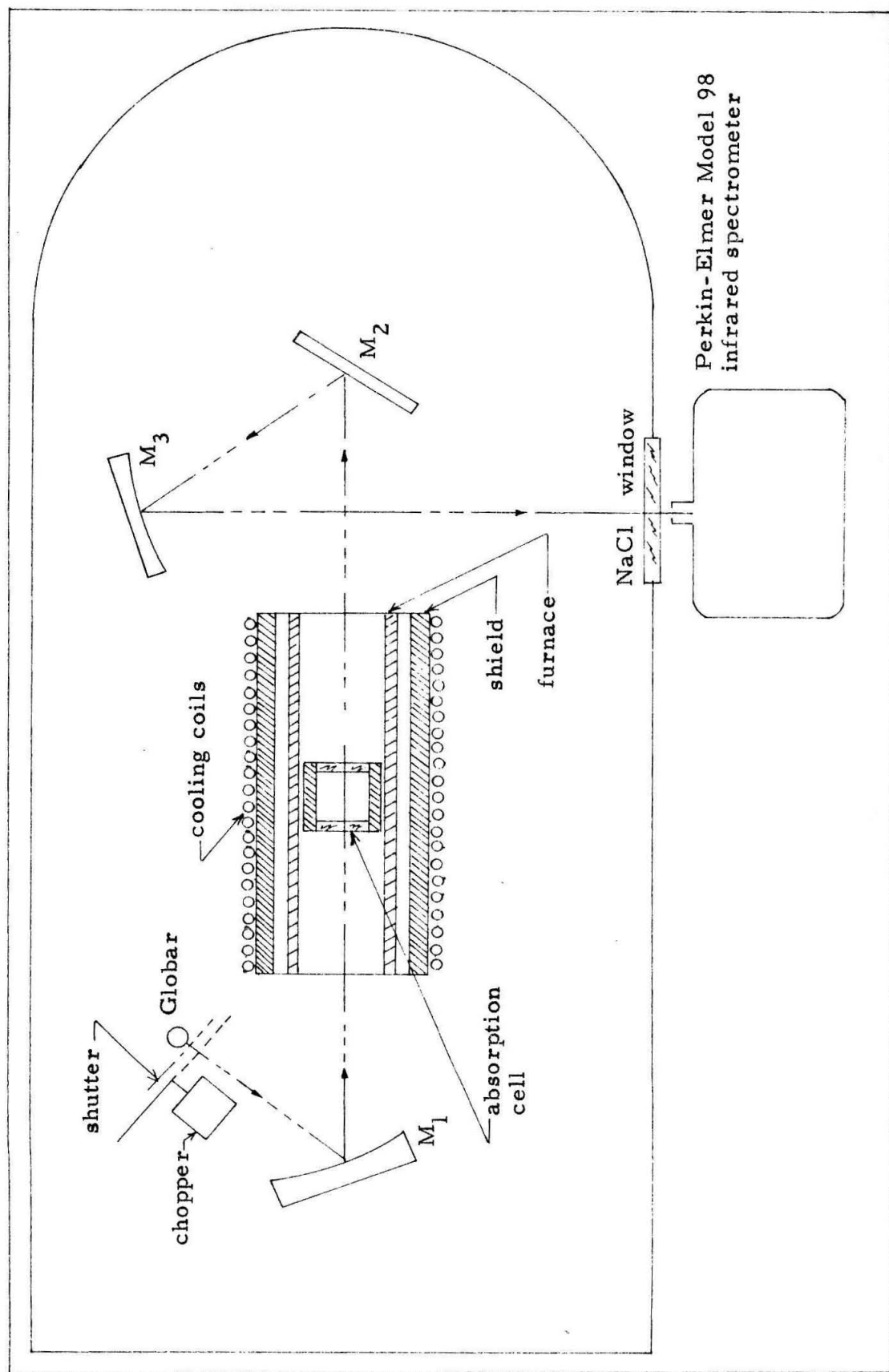stability was obtained when a number of 10-25 Amperite ballast tubes

Fig. 6. Schematic drawing of the optical layout contained in the vacuum tank; M_1: spherical illuminating mirror; M_2: plane mirror; M_3: off-axis parabolic mirror.

was put in series with the globar (see Fig. 7). The ballast tubes kept the current constant over a wide range of input voltages. A variable shunt across the globar was used to change the source temperature. The total current was kept constant while the globar current was set at any desirable level.

The radiant flux was modulated at 13 cycles/second with a standard Perkin-Elmer chopper. The chopper assembly with its rectifying contacts was placed in the vacuum tank at a short distance from the light source. A shutter, which was operated from outside the vacuum chamber, could be raised into the beam in a position between the light source and the chopper.

After dispersing the light by means of a lithium fluoride (LiF) prism, it was received by a thermocouple detector located in the spectrometer, and the resulting electrical signal was amplified by a 13-cycle, Perkin-Elmer model 13 amplifier which was electrically coupled with the rectifying points of the light chopper to prevent amplification of any light other than that which passed through the chopper.

Standard procedures were used to calibrate the monochromator with the LiF prism. In addition to known atmospheric absorption lines, we used some CO rotational lines near 4.5 microns. The resulting plot of instrument drum reading against wavelength is shown in Fig. 8.

Amplifier output was recorded on logarithmic chart paper No. 578 supplied by Technical Charts Incorporated. The labor of data reduction was thereby considerably reduced.
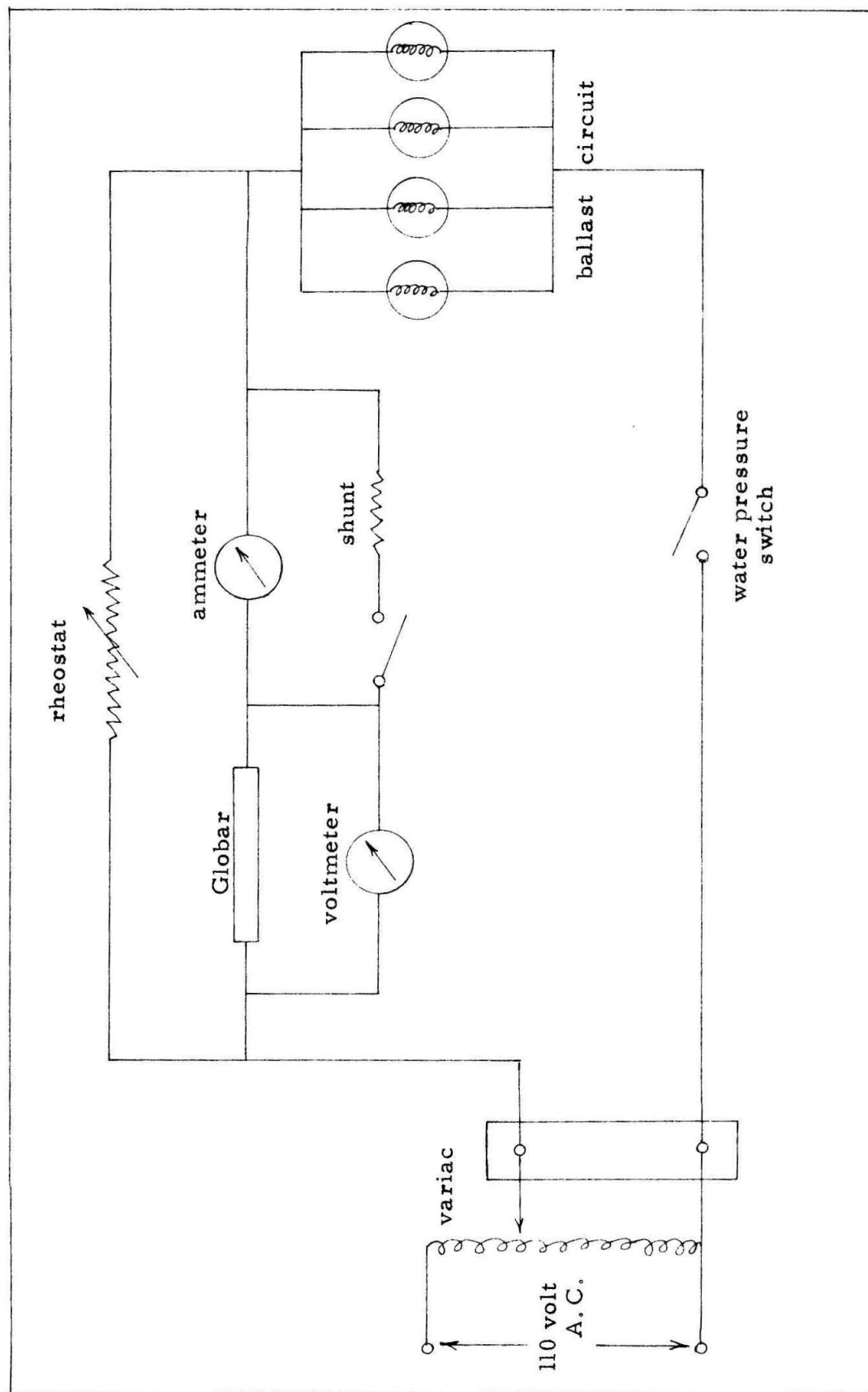
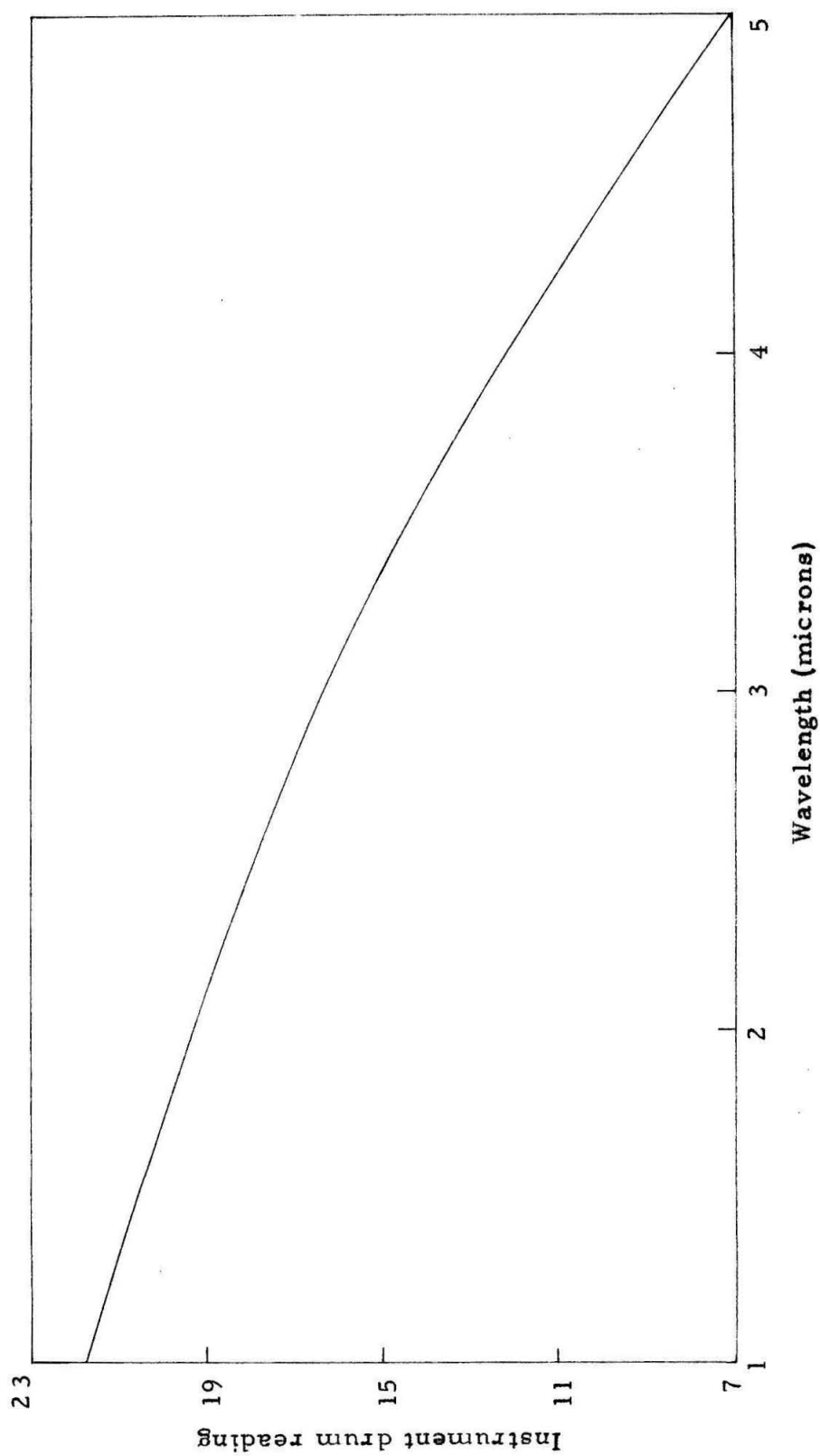Fig. 7. Circuit diagram of the current-regulated light source.

Fig. 8. Calibration curve for the Perkin-Elmer Model 98 infrared spectrometer with lithium fluoride prism.

2. Temperature Measurement and Control

The absorption cell was situated in a closely fitting electric furnace of cylindrical shape which was 61 cm long, 7.6 cm in diameter and wound with 20 gauge nichrome wire. The furnace was surrounded by a cylindrical shield of zirconium oxide which was provided with a water-cooled jacket. A maximum current of 10 amps was passed through the heating coils from a 220-volt A.C. source controlled by a variac. The wall temperature of the absorption cell was monitored by two chromel-alumel thermocouples which were firmly secured to the cell wall by spring clamps (see Fig. 10) or by a bolt and washer. The output of one thermocouple was fed into a Leeds and Northrup Speedomax Type H temperature control unit which controlled the main heating circuit and provided a continuous temperature record. The other thermocouple was used to obtain more accurate readings of temperature from a Leeds and Northrup No. 8657-C Double Range Potentiometer Indicator. With a capability of reading thermocouple output to $\pm .01$ mV, temperatures were obtained with an accuracy of $\pm 0.1^\circ$C. The actual gas temperature, however, was not established to this accuracy, since conditions could not be maintained absolutely constant during the 20 minutes that it took to scan the spectrum. Because the cell was situated in a vacuum and the temperatures involved were relatively low, the heat losses to the surroundings were quite small and the temperature could be maintained constant within $\pm 0.5^\circ$C during any given run. This result was established by continuous monitoring with the potentiometer. Isothermal conditions were very nearly maintained in the cell because of the very large ratio of thermal conductivity inside the cell walls to that of the surroundings.

3. Gas and Liquid Supply and Handling

For self-broadening experiments, commercial grade NO_2 with a minimum purity of 98% was obtained from the Matheson Company and used without further purifications. An examination of the infrared spectrum indicated no significant impurities. It should be noted that impurities such as homonuclear diatomic molecules (e.g., N_2, O_2) are infrared-inactive and would not produce impurity absorption. The commercial cylinder used contained 10 pounds of liquid N_2O_4.

Foreign-gas broadening was accomplished with an NO_2-argon mixture containing about 1.5% NO_2 and supplied by the Matheson Company. The argon in this mixture had a nominal purity of 99.998%.

The infrared cell with associated apparatus used for self-broadening experiments is illustrated in Fig. 9 and shown schematically in Fig. 10. In order to minimize chemical attack, all metallic parts were made of stainless steel and teflon O-rings were used for seals. The cell was designed to accommodate spacers ranging in thickness from 0.001 inch to several inches. One-inch diameter by 1/4-inch thick sapphire (Al_2O_3) windows were used for the spectral region from one to five microns. The needle valve at the left of Fig. 10 served to introduce liquid N_2O_4 into the base of the annular space surrounding the windows (see filling details below). At a given temperature, the previously measured vapor pressure (see Fig. 2) was utilized, and the optical depth was varied by introducing a series of spacers of varying thickness. With the liquid-vapor equilibrium thus established, problems of surface adsorption were completely eliminated.
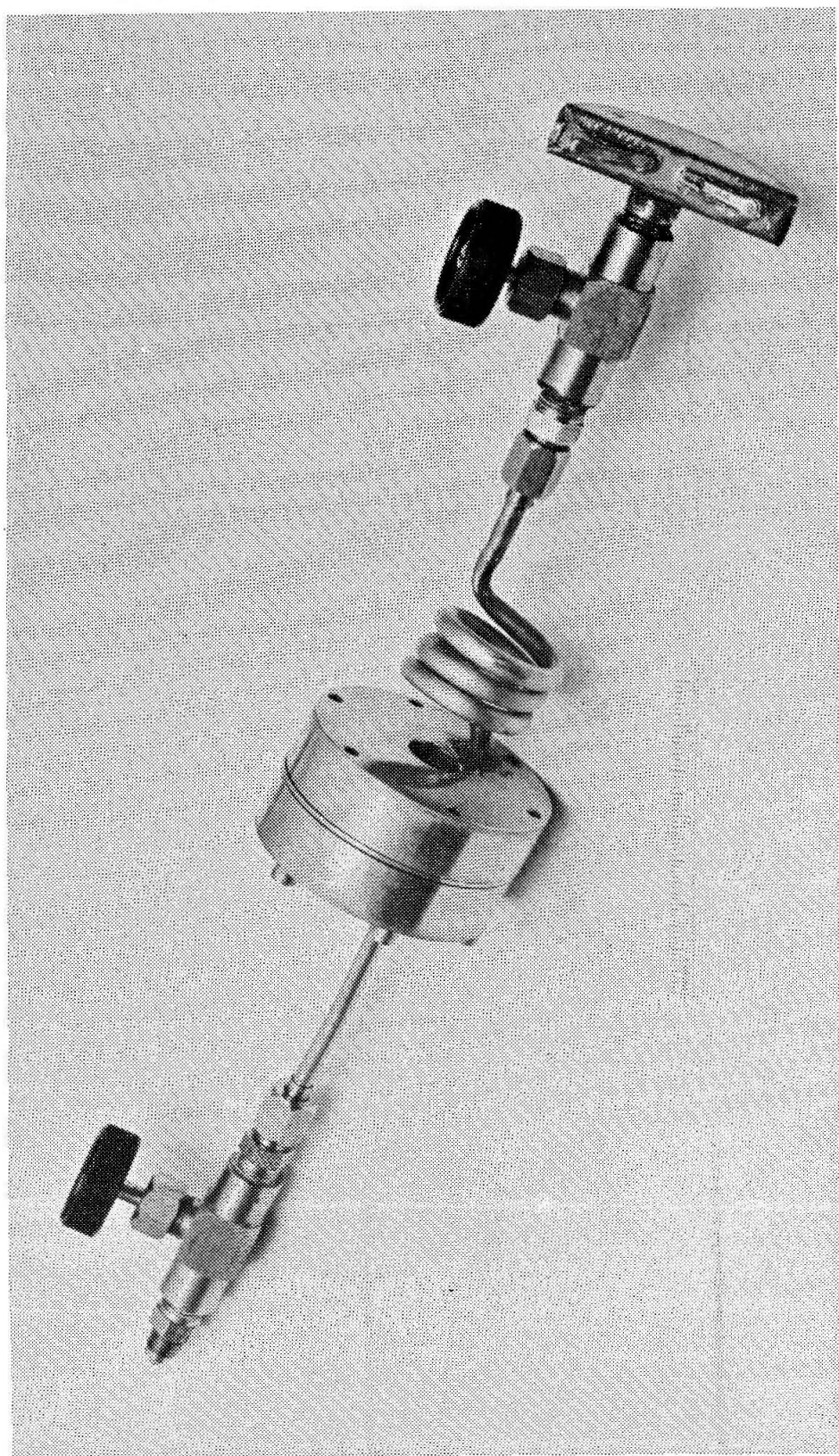
Fig. 9. Infrared cell and associated apparatus used in self-broadening experiments. The container on the right is a liquid N_2O_4 reservoir.
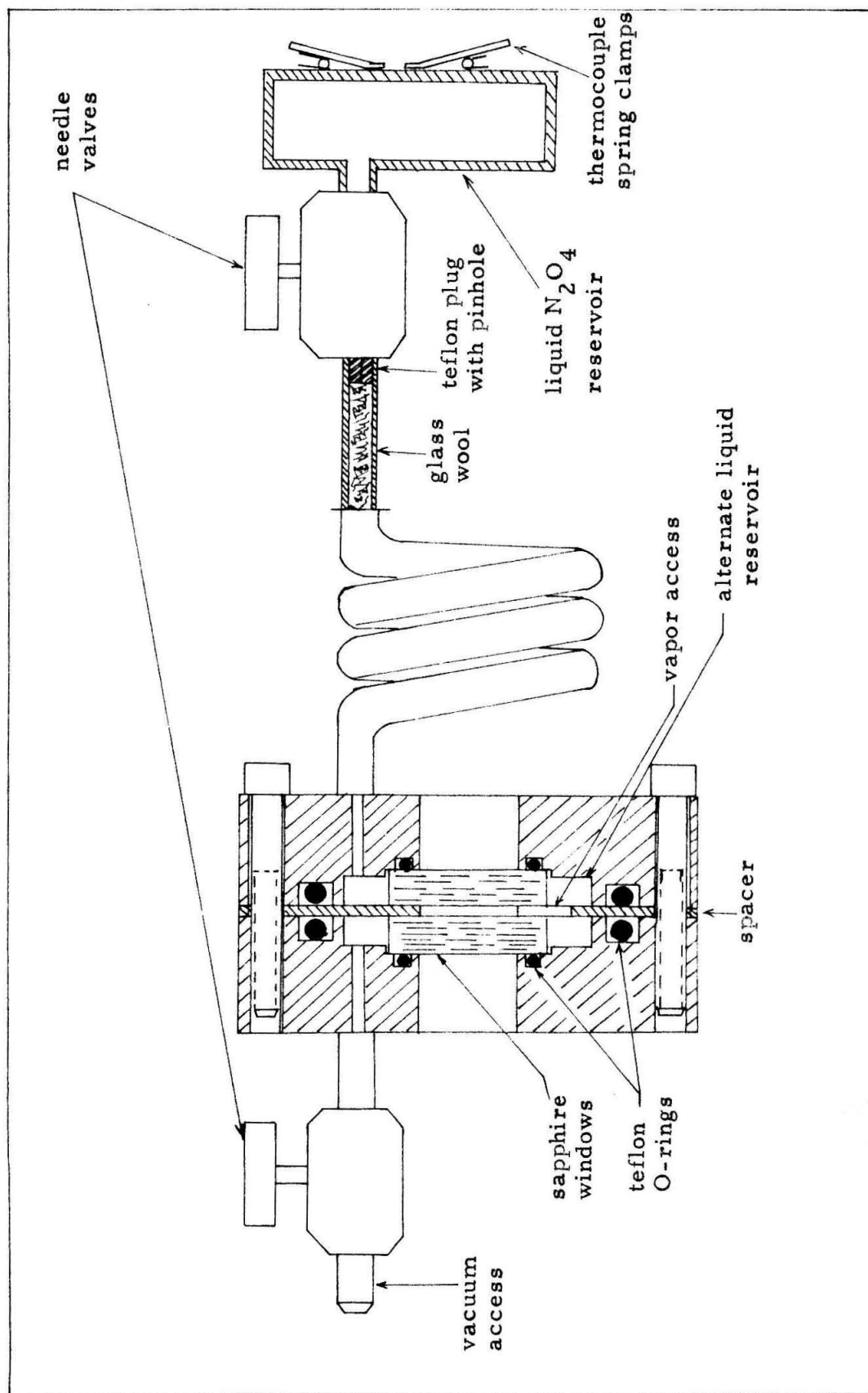
Fig. 10. Cross-sectional view of the infrared cell assembly and associated apparatus used for measurements with self-broadening. The cell is drawn to full scale.

During the early parts of the experiments it was suspected that, with the liquid located in the main cell, some of it might enter the space between the windows, either in the form of small droplets or as a thin surface film. The liquid would produce much greater absorption by the N_2O_4 bands than the vapor. In order to determine the extent of falsification of data by liquid N_2O_4, we placed the liquid in a chamber separated from the main cell by a coil of 1/4-inch tubing filled with tightly-packed glass wool and a teflon plug with a pinhole at its center (see Fig. 10). This device served to prevent any liquid N_2O_4 from entering into the absorption cell while permitting the vapor to pass. A check of the porous filter with about 30 atm of nitrogen at one end showed a very substantial pressure drop across the filter, thus making it appear unlikely that any liquid could pass under the conditions encountered in the experiments. Comparison of gaseous absorption spectra with the liquid in the two alternate positions showed no significant differences.

The needle valve at the right of Fig. 10 served to isolate the liquid reservoir for purposes of changing the spacer in the absorption cell. Two thermocouples were firmly attached to the liquid reservoir by means of spring clamps soldered to the wall.

Preliminary studies involving foreign-gas broadening were performed in the cell shown in Fig. 11. This cell had a fixed length and was designed with two ideas in mind, namely, to assure pressure tightness and minimize selective surface adsorption. Both of these factors would lead to errors in the assumed concentrations of NO_2 during the course of a run. The amount of adsorption depends linearly on the surface area
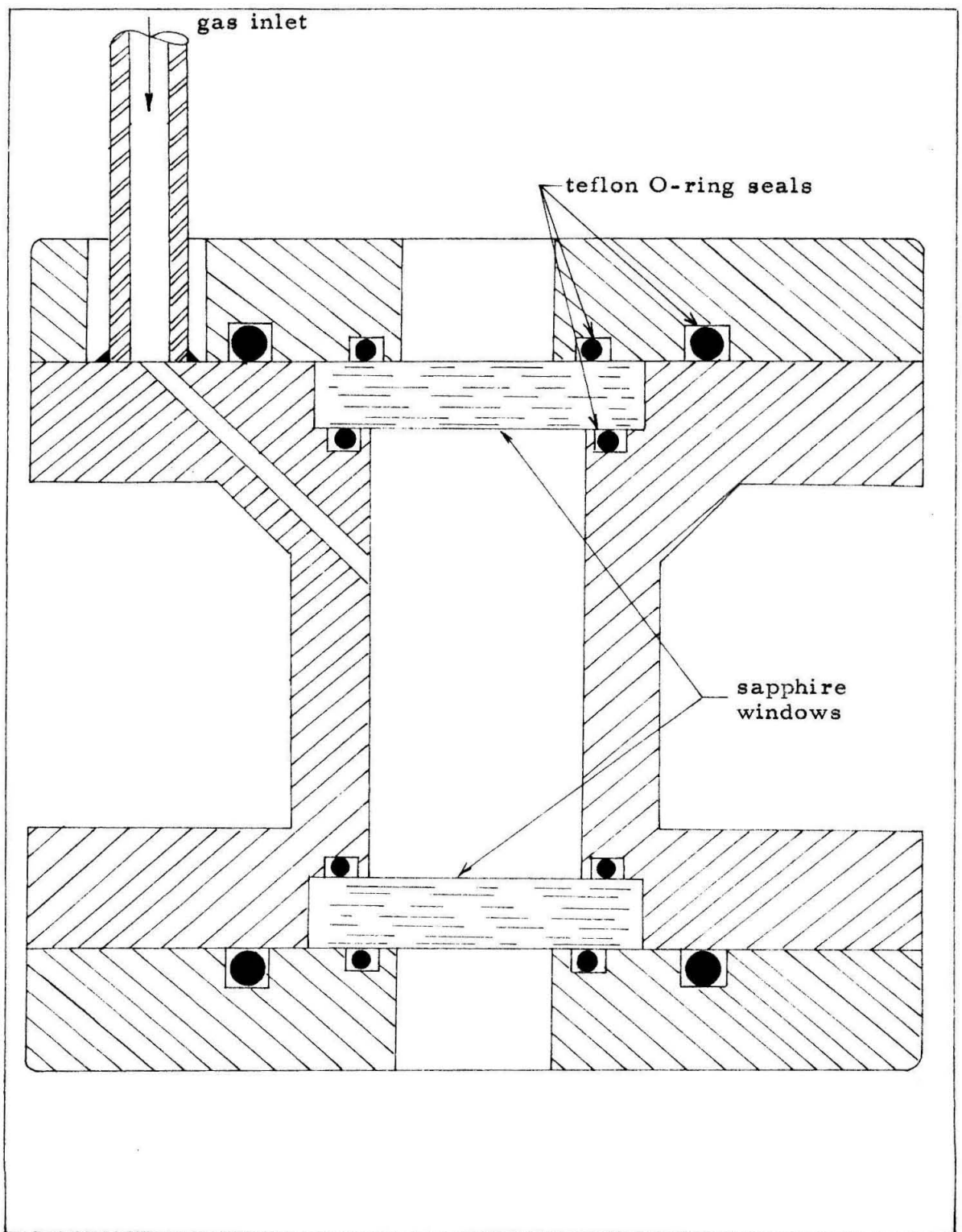
Fig. 11. Cross-sectional view of the infrared cell assembly used to obtain foreign-gas broadening (drawn to double scale).

exposed to the gas. We have therefore tried to minimize the internal surface area by eliminating all unnecessary spacers inside the cell. Instead, the O-ring shoulders were used directly for spacing the one-inch diameter by 1/4-inch thick sapphire windows at a distance of 3.81 cm apart. Chemical attack of the walls was minimized by the use of 304 stainless steel and teflon O-rings. Gas leakage was prevented by the use of double O-ring seals, one on each side of the window. The cell was found to hold 500 psi of gas for over a week with no detectable pressure loss. Selective surface adsorption was, however, found to be excessive (see Section E).

Evacuation of the system was accomplished with a CEC Type MCF-60 oil diffusion pump backed up by a Kinney Model KC-8 mechanical pump as shown in Fig. 12. Gases containing NO_2 were first passed through a liquid-nitrogen trap to avoid contamination of the pump oil. The pressure was read on a CEC Pirani vacuum gage with 0-2000 and 0-50 micron scales. The entire gas-handling system could be evacuated to less than 10^{-3} mm of pressure, with a leak rate of about 10^{-2} mm/ minute. The tank containing the optical system was evacuated to a pressure of 50×10^{-3} mm with a negligible leak rate. In addition, the tank was flushed several times with H. P. dry nitrogen in order to eliminate the infrared-active impurities in the relatively long (several meters) geometric path length of the light beam. Outside the tank, the optical path was also purged of undesired impurities by continuous flushing with dry nitrogen of the monochromator and of a short tube leading from the monochromator slit to the exit window of the tank.

Valve Designations

p = Circle Seal plug valve
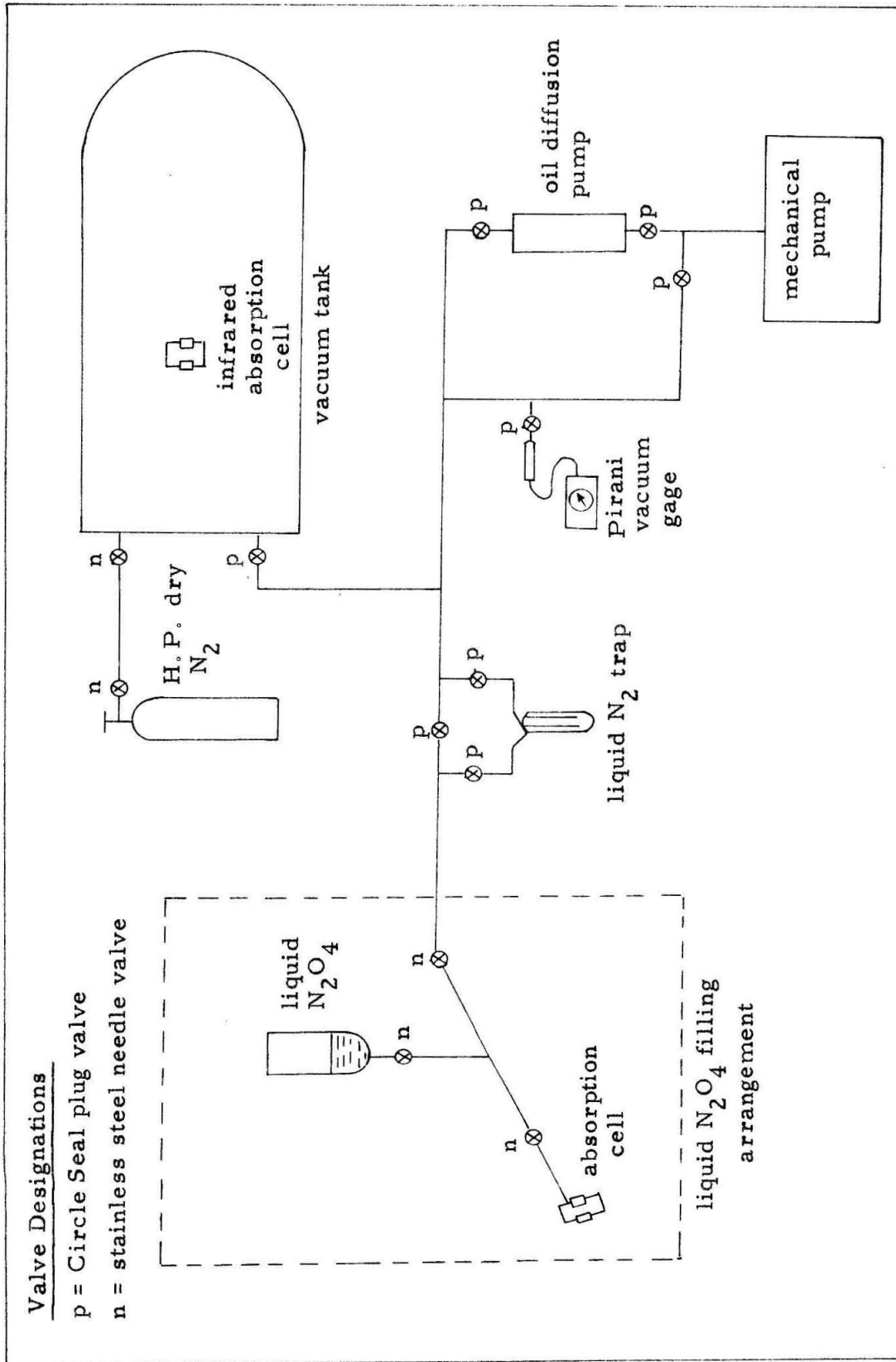
n = stainless steel needle valve

Fig. 12. System for handling gases and liquid.

Standard 304 stainless steel, 1/4-inch tubing with flare fittings was utilized for all lines carrying nitrogen dioxide; for vacuum lines we used standard 1/2-inch copper tubing which was soft-soldered at all joints. Stainless steel Circle Seal plug valves were found to be best suited for systems subjected to both high pressure and vacuum. Where metering or throttling of the gas was required, standard needle valves were used.

Liquid N_2O_4 was transferred from a commercial cylinder to the absorption cell reservoir by gravity feed. We found condensation techniques to be much too slow and inefficient in transferring several grams of N_2O_4, even when the condensing surface was at dry-ice temperatures. The filling arrangement is shown in Fig. 12. The liquid N_2O_4 cylinder was positioned, with its valve pointing toward the ground, at the highest point in the system while the absorption cell was attached to the system in such a manner that the liquid reservoir would occupy the lowest point. The entire system up to the main cylinder valve was then evacuated to less than 10^{-3} mm of Hg. With the vacuum valve shut, N_2O_4 was forced into the cell by gravity until the liquid level could be seen through the cell windows. Excess liquid was pumped out to clear the window area. The cell was then isolated by means of a needle valve and removed from the filling position. Cell weights were measured before and after filling to determine the quantity of liquid transferred.

E. PRELIMINARY STUDIES

Initial experiments were performed with foreign-gas broadening, using argon as a pressurizing agent. The optical depth was varied by

changing the NO_2-N_2O_4 concentration in gas mixtures at total pressures of about 30 atm.

It was hoped that selective surface adsorption would be unimportant. For analytical purposes, we designed and constructed a double-beam, photoelectric gas analyzer in order to measure NO_2 concentrations of gas samples drawn from the main apparatus before and after each run. The instrument was similar to a single-beam device described previously by Smith.[18]

Figures 13 and 14 illustrate the gas analyzer. The light source consisted of an air-cooled, 500 watt, tungsten-filament, G.E. projector lamp, masked off to approximate a point source. After passing the light through a 2.45-mm Corning glass filter (No. 3387), it was split into two beams by a plane mirror (M_1). One of these beams was deflected by another plane mirror (M_2) to a collimating lens (L_1). The beam diameter was then adjusted to that of the absorption tube by an iris-shutter assembly taken from a camera. The glass absorption tubes were 56.5 cm long between the inside edges of the pyrex windows, which were cemented to the tubes with Epibond resin. The light beam emerging from the absorption tube was condensed by the lens L_2 and then deflected with a plane mirror (M_3) onto a 1P37 phototube whose output was read on a Simpson VTVM (see Fig. 13 for circuit diagram). The other beam followed a parallel path.

The analyzer was capable of measuring partial pressures of NO_2-N_2O_4 mixtures at room temperature down to pressures of several millimeters of mercury. With a total pressure of about one atmosphere in the absorption tube, it was possible to analyze concentrations of less than 0.1%.
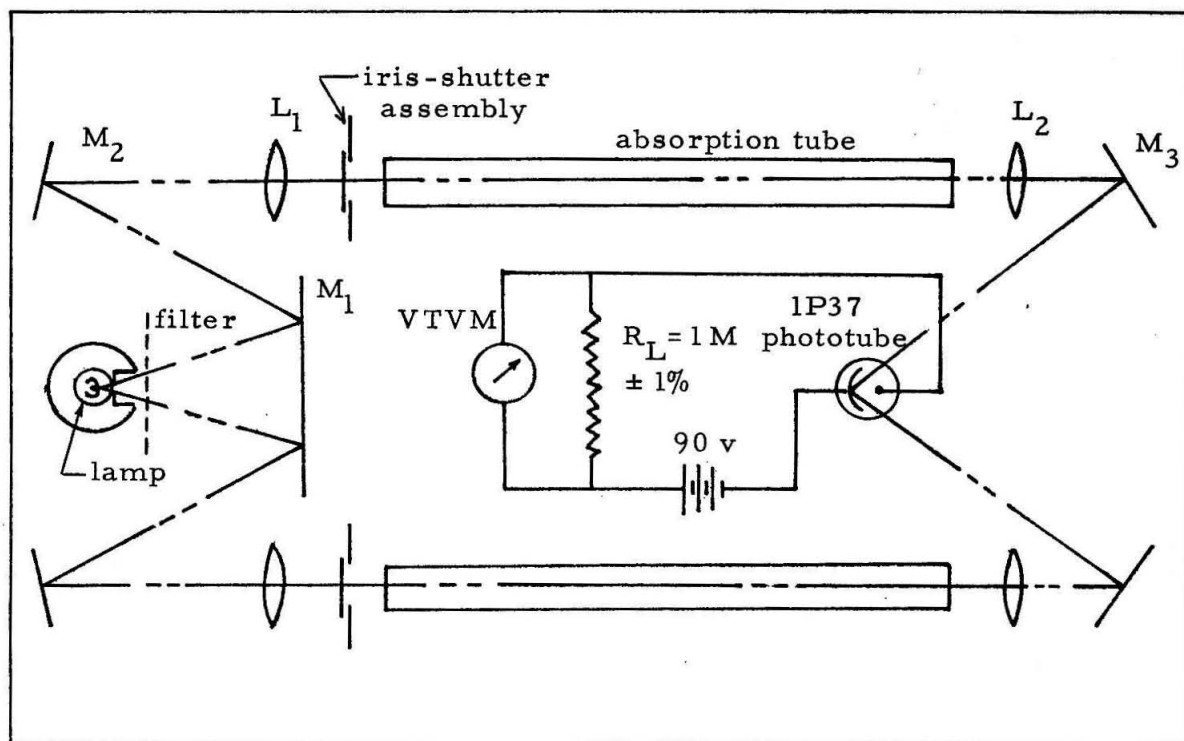
Fig. 13. Schematic diagram of the double-beam, photoelectric gas analyzer for measuring NO_2 concentrations; M_1, M_2, M_3: plane mirrors; L_1: collimating lens; L_2: condensing lens.
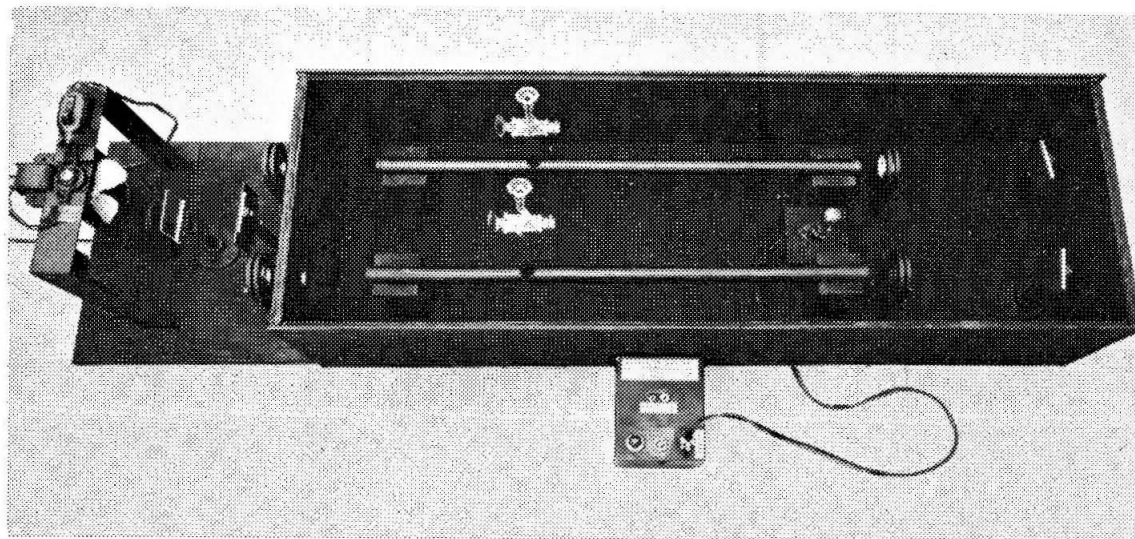

Fig. 14. Internal view of the gas analyzer showing absorption tubes and optical path.

The phototube linearity was checked by reading successively each beam intensity separately (this was accomplished by using the shutter arrangement), then superimposing both beams on the same portion of the phototube plate, and finally making another reading of the intensity. In particular, the intensity of each of the beams was adjusted with the irises to read 0.5 volts; with both shutters open, the reading obtained was 0.995 volts, which is 0.5% off linearity.

We calibrated the instrument by two different procedures. One method involved a volumetric chemical analysis performed on mixture samples drawn from the standard NO_2-argon mixture; in the other method we measured the pressures of pure NO_2-N_2O_4 samples with a dibutyl phthalate manometer. The calibration curve provided us with a plot of the partial pressures of NO_2-N_2O_4 mixtures as a function of the percentage of transmission through the gas in the tube.

A series of experiments was performed at room temperature utilizing this method of gas analysis before and after each run. Unfortunately, we found that the NO_2 concentrations at the end of a run were considerably lower than the initial concentrations, indicating significant adsorption during the course of the experiment. For example, during one test, the percentage of transmission changed from an initial value of 24% to a final value of 35%, which corresponds to an apparent decrease in the partial pressure in the sample gas from 15 to 9 mm at a total pressure of 730 mm. Thus variations of approximately a factor of 2 occurred in the gas composition during a given run. Integrated intensities obtained by this procedure, utilizing only the final analysis

of each test, differed from "best estimates" (see below) by approximately a factor of two.

F. OPERATING PROCEDURE FOR SELF-BROADENING EXPERIMENTS

1. An appropriate spacer was selected and the absorption cell assembled and pressure tested with about 30 atm of N_2 for approximately 24 hrs. The empty cell was then weighed.

2. Liquid N_2O_4 was admitted to the cell. Calculations showed that approximately 2 grams was sufficient to yield the intended highest vapor pressure (19.8 atm) without consuming all of the liquid in the cell reservoir.

3. The cell was next isolated and removed from the filling station, and, after weighing, was placed at the center of the electric furnace in a position such that the light beam could pass through the cell windows. Thermocouples were attached with spring clamps.

4. After aligning the mirrors, the vacuum tank was closed and evacuated to about 50×10^{-3} mm, flushed with H. P. dry nitrogen, and reevacuated. The spectrum of the light source was recorded and continuously examined in the region of atmospheric absorption. The 2.7 micron band of H_2O and the 4.3 micron band of CO_2 were gradually eliminated as the optical path was purged of H_2O and CO_2, respectively.

5. With the shutter placed in the light path, the amplifier was adjusted to give zero reading on the recorder.

6. The monochromator slit width, amplifier gain and response, and light source intensity were next adjusted to the desired level.

7. The cell was then heated to the desired temperature. In addition to the automatic control in the system, we found it necessary to

use manual adjustment of the heating current in order to maintain nearly constant temperature during a run.

8. The transmission spectrum was automatically scanned and recorded. During the 20 minutes of this operation, we monitored the cell temperature constantly and made appropriate adjustments.

9. Leaving the cell unchanged, the temperature was raised to a new level and step 8 repeated.

10. After completing a series of runs at different temperatures, the cell was removed from the furnace and purged of all NO_2 and N_2O_4.

11. The entire procedure was repeated for various spacers.

G. DISCUSSION OF RESULTS AND SOURCES OF ERROR

1. Qualitative Analysis of Spectrum

A representative record of the absorption spectrum (of a gas mixture containing NO_2 and N_2O_4) in the near infrared is reproduced in Fig. 15. The temperature was $80^{\circ}C$ with a corresponding vapor pressure of 10.3 atm; a spacer of 0.124 cm thickness was used. Five distinct bands are clearly identifiable, two of which overlap partially.

Since both NO_2 and N_2O_4 have bands in this region of the spectrum, the question arises how the observed bands are to be assigned to the proper gas component. This problem may be resolved readily by raising the temperature of a gas sample to about $150^{\circ}C$ when most of the gas has dissociated into NO_2; consequently, the N_2O_4 bands disappear while the NO_2 bands appear stronger. In this manner, one may identify the 2908 cm^{-1} band as belonging to NO_2, while all of the other bands shown in Fig. 15 belong to N_2O_4. Reference to Table 1 shows
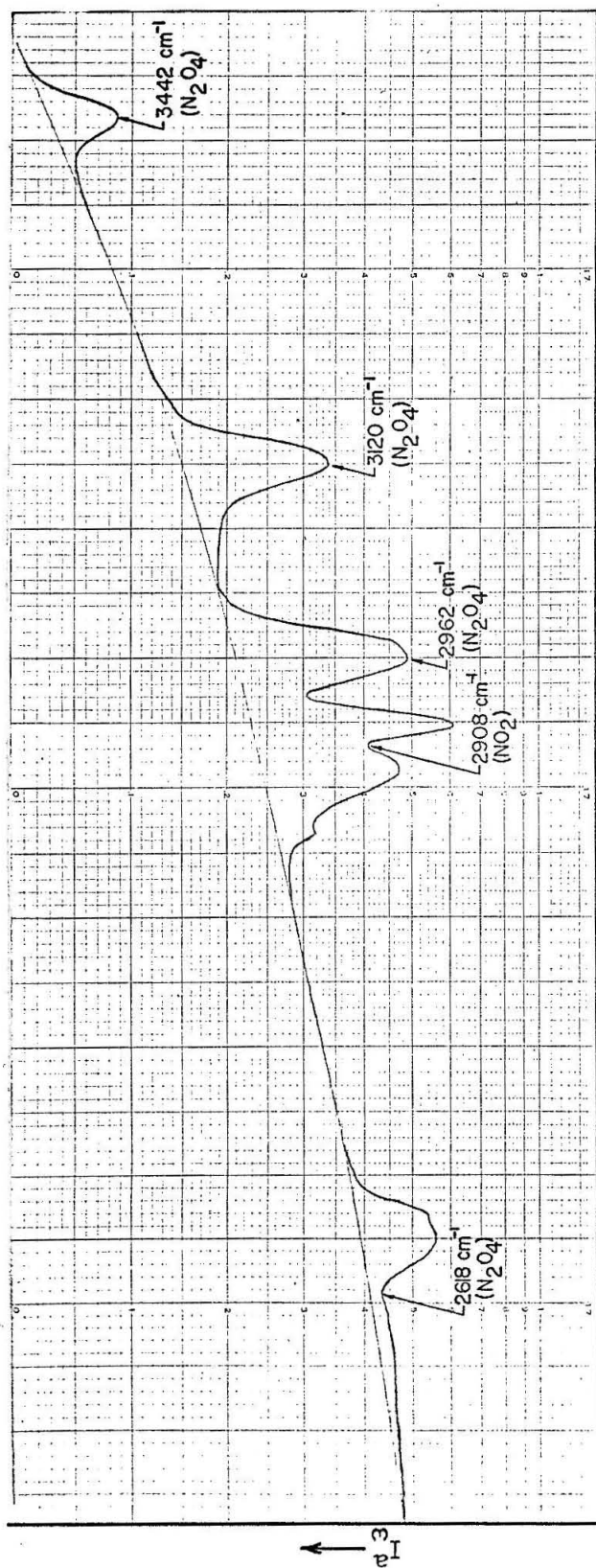
Fig. 15. Infrared absorption spectrum of gaseous NO_2-N_2O_4 at 10.3 atm, 80°C, and a geometric path length of 0.124 cm.

that our observed band centers agree quite well with those measured by other investigators. The random differences of less than 12 cm^{-1} may be attributed to the limited spectral resolution of approximately 5 cm^{-1} obtainable with our apparatus. However, the wave number differences between gaseous and liquid N_2O_4 band centers agree to within 2 cm^{-1} with previously published estimates. For the quantitative work reported here, we are not actually concerned with band locations except in so far as they serve to identify the vibrational modes.

The occurrence of slight overlapping between bands (NO_2 at 2908 cm^{-1} and N_2O_4 at 2962 cm^{-1}) did not introduce serious errors since less than 5% of the areas under the $\log(I_\omega^o/I_\omega)$ curves correspond to overlapping regions. We tried to resolve these two bands graphically by using an obvious plotting procedure on the original records. This method gave an estimated error in the quantity β of less than one percent as established by applying varying degrees of artistic skill to the problem and comparing the resulting values of β .

Two weak impurity bands appeared in the spectrum. One may be seen in Fig. 15 just to the short-wave number side of, and partly overlapping with, the 2908 cm^{-1} band of NO_2; the other band overlaps with the R-branch of the same band. These small dips were present even when the absorption cell was completely removed from the optical path. The strengths of the dips were found to be independent of the amount of atmospheric gas in the path. The undesired dip in the P-branch was again corrected for graphically; the effect of the other dip is discussed in Part 2b below.

The shapes of all five combination bands at various optical depths and temperatures are shown in Figs. 25 to 54 of Appendix I, where we have plotted $\log_{10}(I_\omega^{o,\,a}/I_\omega^a)$ as a function of wave number. Assuming that the rotational fine structure has been completely smeared out by pressure broadening, the ordinates of these curves are equal to $P_\omega X/2.303$.

The P- and R-branches are clearly noticeable in the 2908 cm^{-1} band of NO_2 and the 2618 cm^{-1} band of N_2O_4, although the latter has its P-branch considerably suppressed (see Fig. 31).

2. Quantitative Analysis of Bands

a. Gas Composition

Because of the relatively high vapor pressures used in the experiments (up to 19.8 atm), real-gas effects must be considered in calculating the equilibrium composition of gaseous NO_2 and N_2O_4. The total pressure in each case was assumed to be the equilibrium vapor pressure at the measured temperature.

A general expression for the equilibrium constant at any pressure has been shown[19] to be

$$\ell n \frac{K_p}{K_p^*} = -\frac{1}{RT} \sum_i \left\{ \nu_i \left[\int_0^p \left[\left(\frac{\partial V}{\partial n_i} \right)_{pTn} - \frac{RT}{P} \right] dp \right] \right\} . \tag{13}$$

where K_p^* refers to the equilibrium constant at zero pressure, V is the gas volume, ν_i is the stoichiometric coefficient of the ith species, and the other symbols have their usual meaning.

If we let the subscript 1 refer to NO_2 and the subscript 2 to N_2O_4, then $\nu_1 = 2$ and $\nu_2 = -1$. From Eqs. (10) and (11) it follows that

$$\frac{\partial V}{\partial n_1}\bigg)_{pTn_2} = \frac{RT}{p}\left(1 + \frac{\beta}{2}p\right)$$

and

$$\frac{\partial V}{\partial n_2}\bigg)_{pTn_1} = \frac{RT}{p}\left(1 + \beta p\right).$$

Substituting these relations into Eq. (13) gives

$$\ell n \frac{K_p}{K_p^*} = -\frac{1}{RT}\left\{2\int_0^p \left[\frac{RT}{p} + \frac{\beta}{2}RT - \frac{RT}{p}\right]dp - \int_0^p \left[\frac{RT}{p} + \beta RT - \frac{RT}{p}\right]dp\right\} = 0,$$

or

$$K_p = K_p^*.$$

It is thus apparent that, assuming the validity of the equations of state presented by Giauque and Kemp, real-gas effects cancel out in calculating the equilibrium composition.

The actual computations of partial pressures were performed by defining the decomposed fraction as

$$a \equiv \frac{p_{NO_2}}{p}$$

whence

$$K_p = \frac{a^2 p}{1-a}.$$

(14)

For the quantity p, we used the previously measured vapor pressure $p_v(T)$, (see Fig. 2).

b. Estimate of Rotational Line Spacing

Because of the limited spectral resolution of our instrument, it was impossible to measure directly the spacing between rotational lines of the NO_2 and N_2O_4 molecules. However, one can make a crude estimate of the spacing from a knowledge of the wave number interval between the maxima of the P- and R-branches of a band or by the use of the effective band width at a known temperature.

Let $\Delta\omega$ be the measured wave number interval between the maxima of the P- and R-branches of a band. For diatomic or spherical top polyatomic molecules, the value for the rotational quantum number $J = J^*$ at which the initial (lower) state population is a maximum is, approximately,

$$J^* = \left(\frac{kT}{2hcB_e}\right)^{1/2} - \frac{1}{2}.$$ (15)

The peak of the R-branch corresponds to the rotational transition $J^* \longrightarrow J^* +1$, while for the P-branch it coincides with the frequency for the transition $J^* \longrightarrow J^* -1$. These transitions, superimposed on the vibrational transition, correspond to wave numbers for the maxima of the P- and R-branches of

$$\omega_P^* = \omega_o - 2B_e J^*$$

and

$$\omega_R^* = \omega_o + 2B_e(J^* +1),$$

respectively, where ω_o refers to the wave number of the pure vibrational transition. Thus,

$$\Delta\omega = \omega_R^* - \omega_P^* = B_e(4J^* +2).$$ (16)

Combining Eqs. (15) and (16) gives the desired relation, viz.,

$$B_e = \frac{hc(\triangle\omega)^2}{8kT} .$$

(17)

To test the validity of Eq. (17), we apply it to the fundamental band of HCl at about 300°K where $\triangle\omega$ was found[20] to be approximately 140 cm^{-1}. Using these results, Eq. (17) yields a value for B_e of 11.7 cm^{-1}, whereas the exact value is known to be 10.59 cm^{-1}. The discrepancy in B_e results from the fact that we have neglected vibration-rotation interactions and that both branches of the band display rather flat maxima, and hence $\triangle\omega$ cannot be obtained with great accuracy.

Applying Eq. (17) to the 2908 cm^{-1} band of NO$_2$, for which the measured value of $\triangle\omega$ is about 20 cm^{-1} at 298°K, we find the rotational constant for NO$_2$ to be about 0.24 cm^{-1}, which gives an approximate line spacing of 0.48 cm^{-1}. Moore[8] found the rotational constant $\overline{B}'' = 0.429 \pm 0.002$ cm^{-1} and $\overline{A}''-\overline{B}'' = 7.62 \pm 0.05$ cm^{-1}. The discrepancy between our estimate and the value obtained from the results of Moore are not surprising in view of the fact that the NO$_2$ molecule is not a spherical top as was assumed in the derivation of Eq. (17). The actual line spacing for an asymmetrical molecule is probably smaller than that predicted by Eq. (17).

To estimate the line spacing of the N$_2$O$_4$ molecule, we consider the effective band width at a known temperature. An approximate relation for the effective band width $\triangle\omega'$ is given in Eq. (11-25) of Ref. 11, viz.,

$$\Delta\omega' \approx 11.9 \left(\frac{hcB_e}{kT} \right)^{1/2} \frac{kT}{hc} \quad .$$

The measured effective band width for the 3120 cm^{-1} band of gaseous N_2O_4 at 298°K is approximately 70 cm^{-1} which yields an estimated value for the rotational constant of 0.17 cm^{-1} and a corresponding line spacing of 0.34 cm^{-1}.

Results for other polyatomic molecules (e.g., CO_2) indicate that a line spacing of the order of 0.5 cm^{-1} will give effectively complete overlapping at total pressures of one to three atmospheres. It is therefore reasonable to assume that, at the total pressures encountered in our experiments (3 to 20 atm), the rotational fine structure was sufficiently smeared out to yield smooth functions for the spectral absorption coefficients of the various bands.

c. Integrated Intensities

Measurements were performed in the temperature range between 40 and 100°C at 10 degree intervals. The optical depth was varied by introducing a series of five spacers in the absorption cell, giving geometric path lengths of 0.0394, 0.0495, 0.0749, 0.106, and 0.124 cm.

In Figs. 16 to 20 we have plotted the measured quantity β as a function of spacer thickness at various temperatures and corresponding vapor pressures. The parameter β was obtained by graphical integration of the function $\log(I_\omega^{o,\,a}/I_\omega^a)$, which was taken from the original records. No significant deviation from linearity is observed in these curves. Least-square fits to the experimental points are also shown in Figs. 16 to 20. Most of the curves corresponding to the N_2O_4 bands pass through the origin or close to it. Deviations from the origin seem to vary in a random manner for these bands. The curves corresponding to the
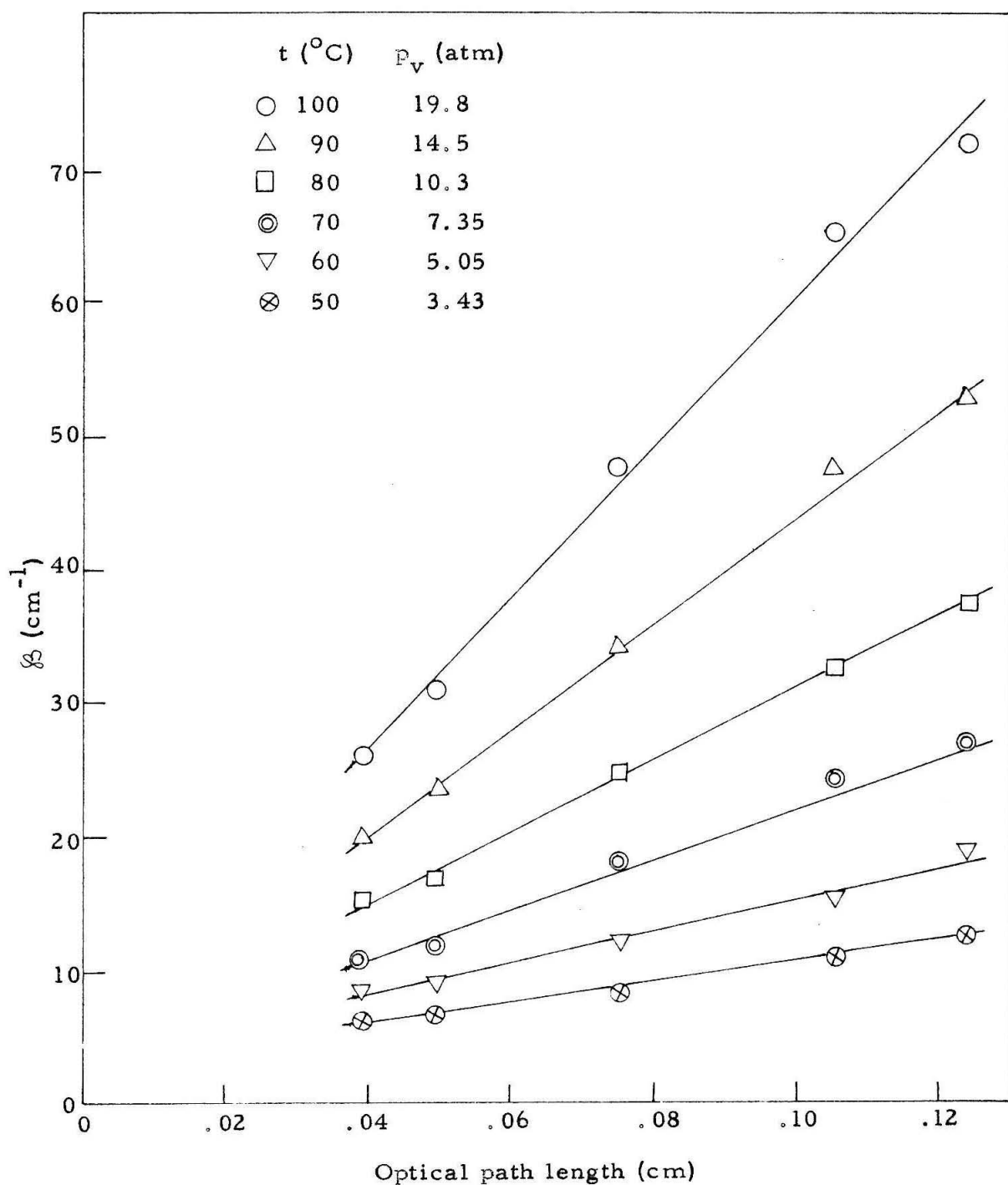
Fig. 16. Dependence of β on optical path length at various temperatures and vapor pressures for the 2908 cm^{-1} band of NO$_2$.

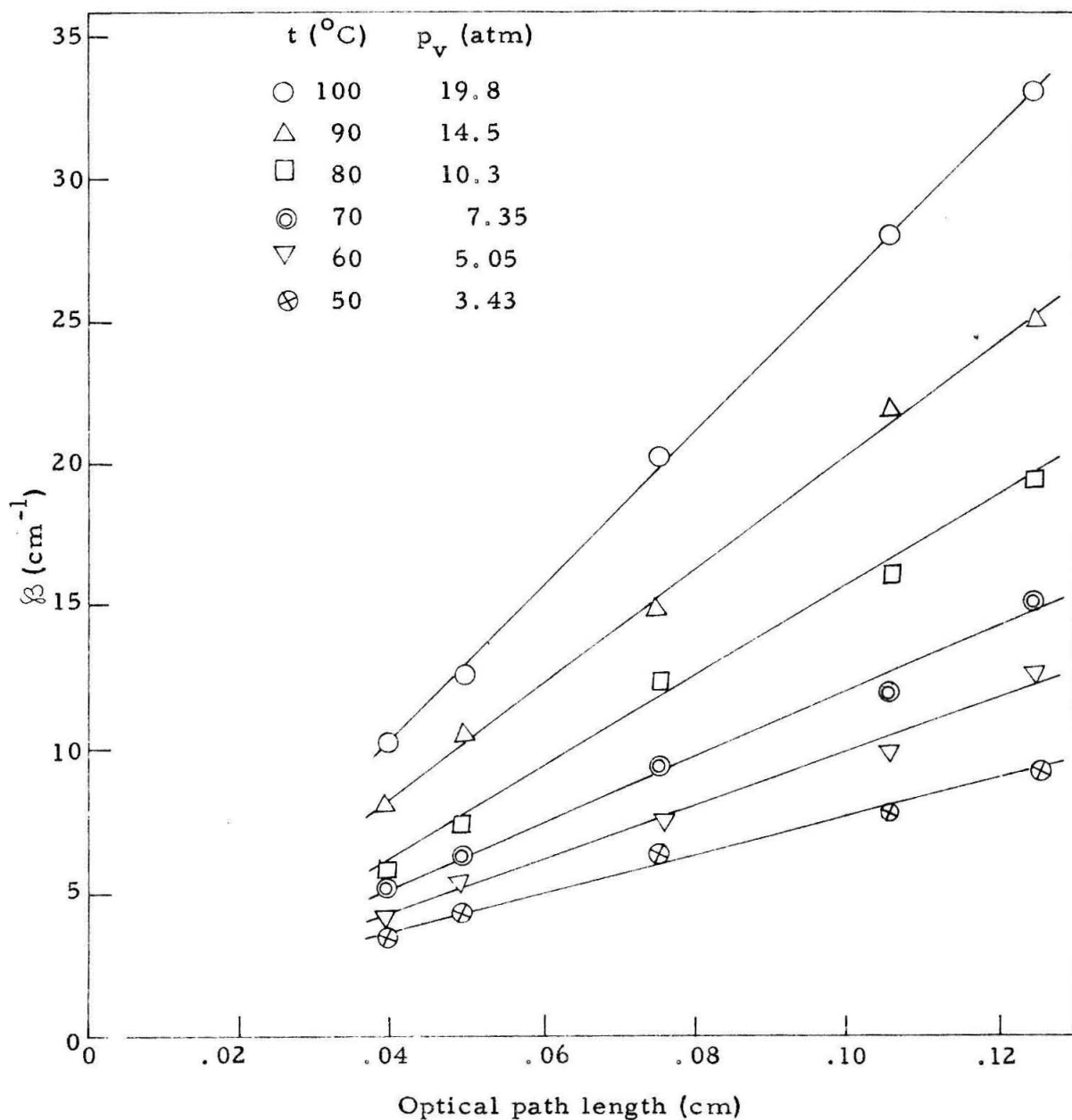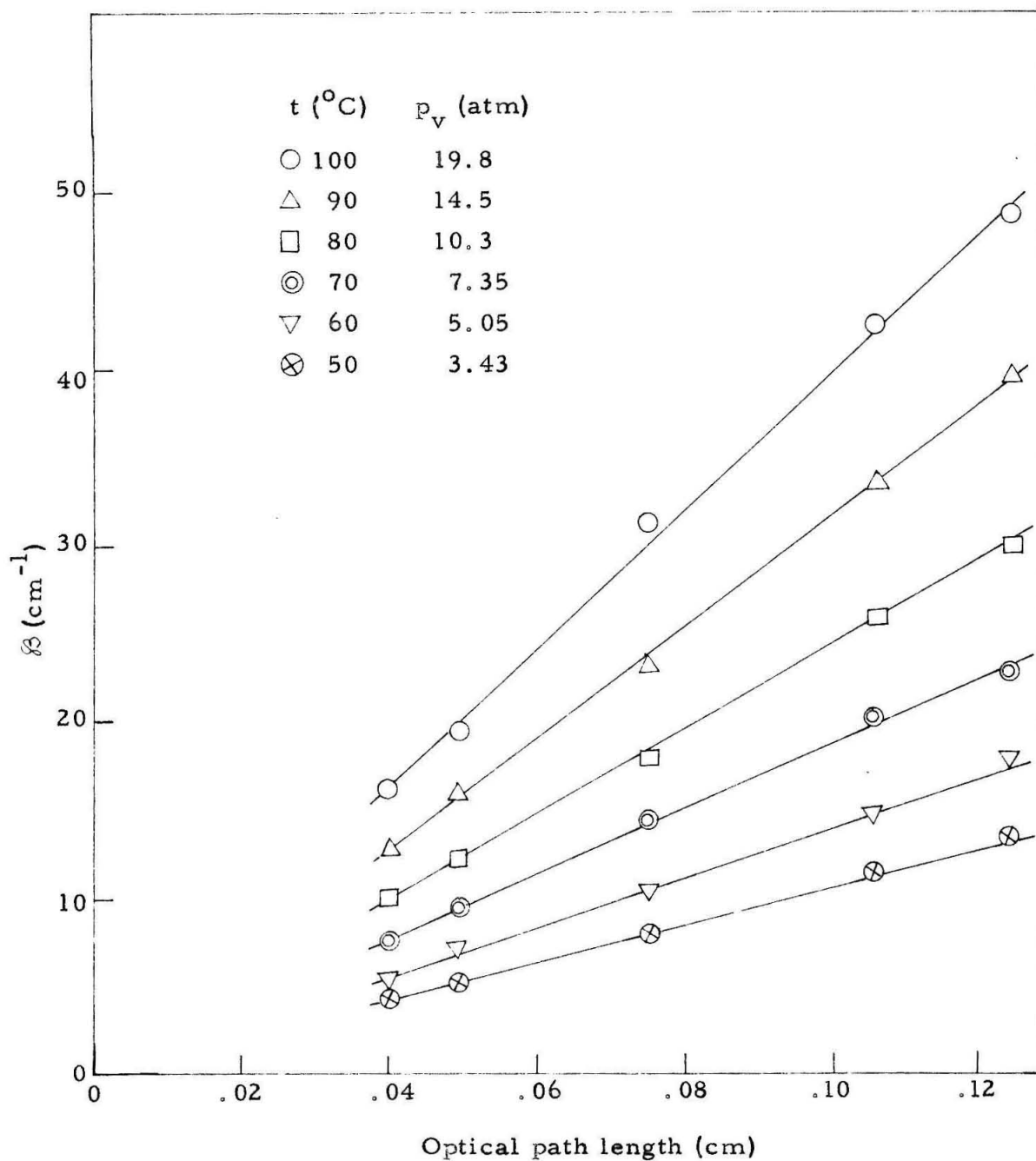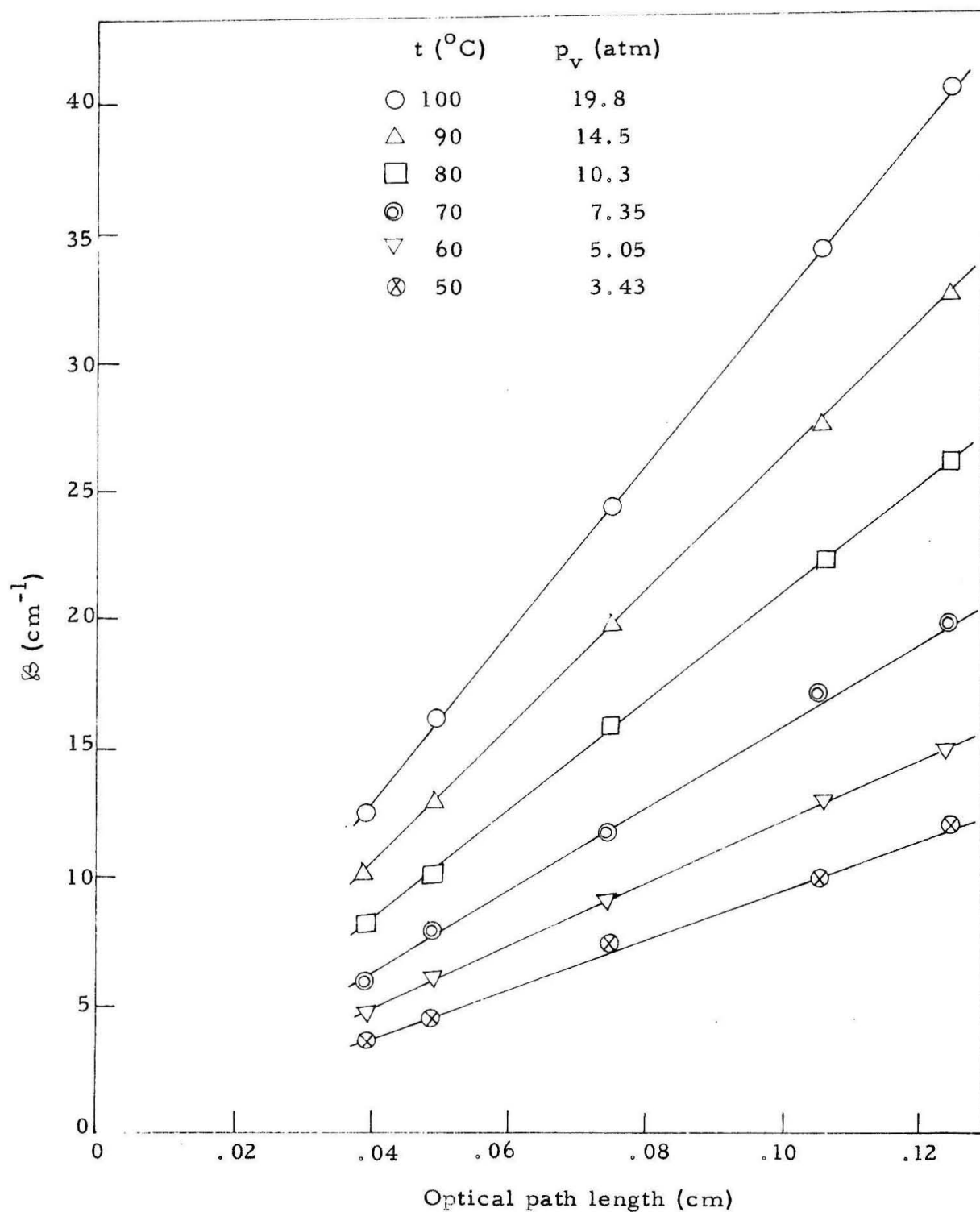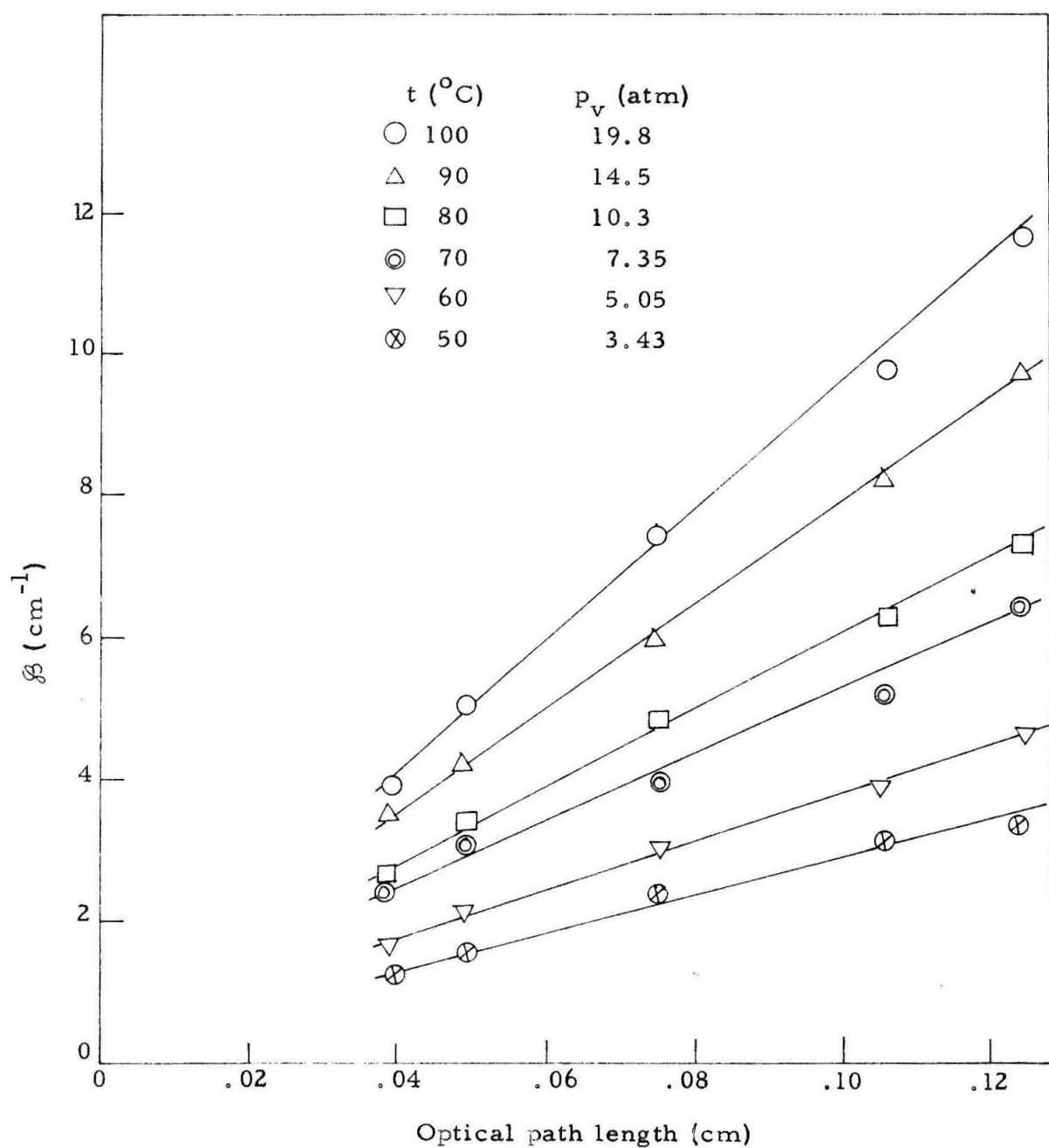Fig. 17 . Dependence of β on optical path length at various temperatures and vapor pressures for the 2618 cm^{-1} band of gaseous N_2O_4.

Fig. 18. Dependence of β on optical path length at various temperatures and vapor pressures for the 2962 cm^{-1} band of gaseous N_2O_4.

Fig. 19. Dependence of ℬ on optical path length at various tempera-
tures and vapor pressures for the 3120 cm^{-1} band of gaseous
N_2O_4.

Fig. 20. Dependence of β on optical path length at various temperatures and vapor pressures for the 3442 cm^{-1} band of gaseous N_2O_4.

2908 cm^{-1} band of NO_2, however, display a systematic deviation from the origin. All five curves intercept the ordinate at approximately 4 cm^{-1}, which equals very nearly the measured quantity $\mathscr{B}$ for the impurity absorption coinciding with the R-branch of this band. Since the amount of absorption produced by the impurity was independent of the optical depth of NO_2, the slopes of the $\mathscr{B}$ vs. X curves were not affected and should yield true values for integrated intensity.[*]

Integrated intensity estimates for one NO_2 and four N_2O_4 combination bands are summarized in Table 2 and their temperature dependance is shown in Fig. 21. The linear dotted curves were fitted to the experimental points by assuming that the intensities are inversely proportional to the absolute temperature. It is seen that the results show very nearly a 1/T dependance for the temperature range under consideration.

3. Composition Error Analysis

A major source of random errors results from uncertainties in the determination of partial pressures. The parameter that limits our experimental precision is the temperature, since it is the only measured quantity.

For a quantitative determination of the expected scatter in partial pressures as obtained from the measured temperatures, we begin with Eq. (14). From this relation it follows that

---

[*] The question of the origin of small deviations of $\mathscr{B}$ from zero at zero optical depth has been discussed extensively in connection with early studies of absolute intensity measurements. In most of the published papers, deviations larger than those noted in Figs. 17 to 20 have been observed. Furthermore, these deviations are not usually accounted for as satisfactorily as they are in Fig. 16 by the presence of impurity absorption bands in the gas. It is well known to workers in the field that small deviations of the extrapolated curves from the origin, whether they are produced by an imperfect optical system involving some scattered light or by other effects, do not influence significantly the measured values of the slopes $a = d\mathscr{B}/dX$.

Table 2. Integrated intensities for gaseous NO_2 and N_2O_4 bands in the near infrared region of the spectrum.

Molecule	Band center (cm^{-1})	Integrated intensity (cm^{-2}-atm^{-1})					
		Temperature (°C)					
		50	60	70	80	90	100
NO_2	2908	56.9	55.5	56.0	53.2	52.7	50.7
N_2O_4	2618	32.7	33.4	29.5	30.9	29.2	30.9
N_2O_4	2962	52.7	50.7	47.2	46.8	46.3	44.9
N_2O_4	3120	47.4	42.1	41.9	41.7	38.7	38.0
N_2O_4	3442	12.9	11.9	11.6	10.6	10.7	10.3
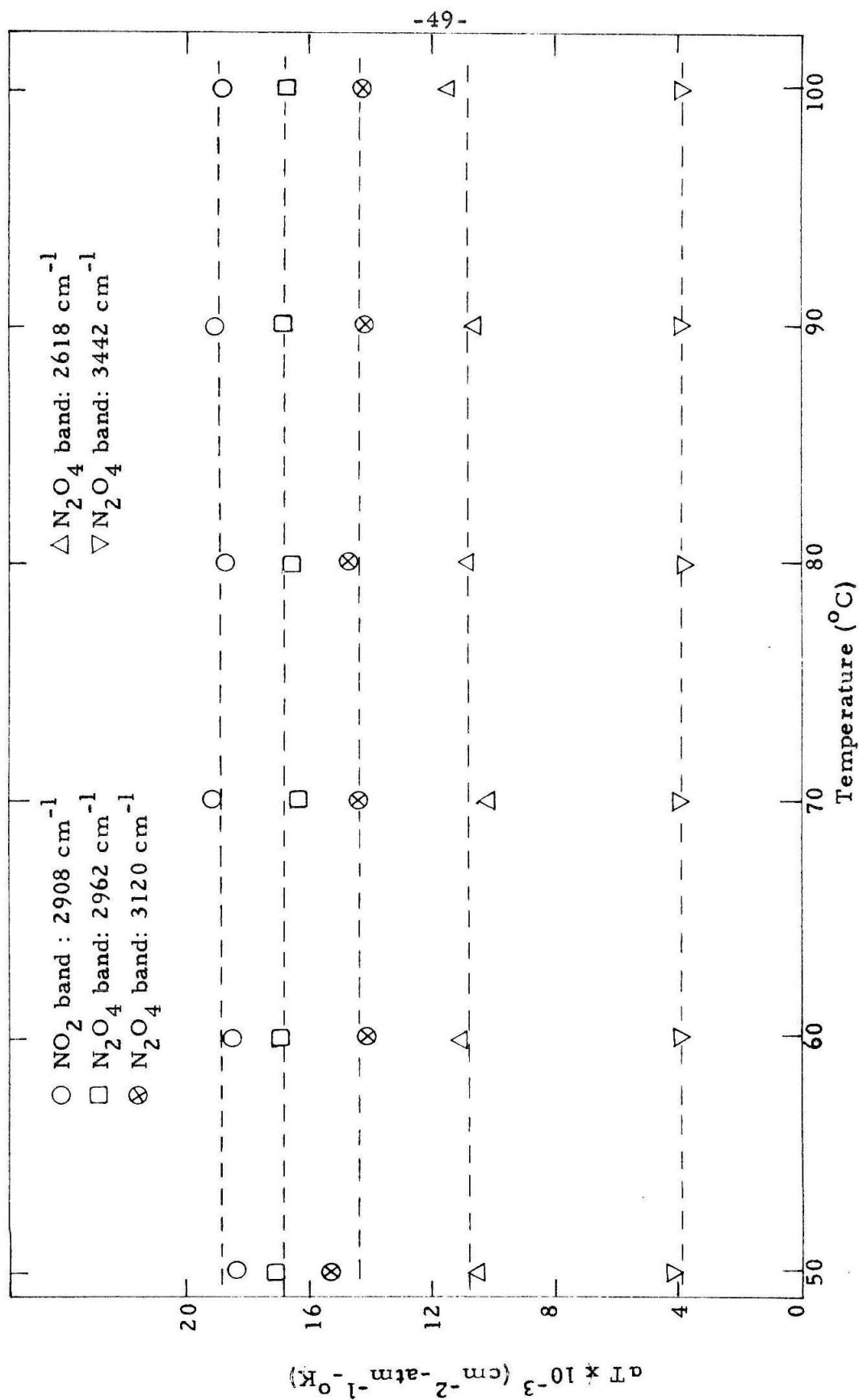
Fig. 21. Temperature dependence of the quantity αT for the combination bands of gaseous NO_2 and N_2O_4. The dotted lines represent the integrated intensities that vary as $1/T$.

$$\frac{da}{a} = \left(\frac{dK_p}{K_p} - \frac{dp}{p}\right)\left(\frac{1-a}{2-a}\right) \tag{18}$$

and

$$\frac{d(1-a)}{1-a} = -\left(\frac{dK_p}{K_p} - \frac{dp}{p}\right)\left(\frac{a}{2-a}\right) . \tag{19}$$

From our definition of a,

$$p_{NO_2} = ap \qquad \text{and} \qquad p_{N_2O_4} = (1-a)p ;$$

thus

$$\frac{dp_{NO_2}}{p_{NO_2}} = \frac{da}{a} + \frac{dp}{p} \tag{20}$$

and

$$\frac{dp_{N_2O_4}}{p_{N_2O_4}} = \frac{d(1-a)}{1-a} + \frac{dp}{p} . \tag{21}$$

Substituting Eqs. (18) and (19) into Eqs. (20) and (21), respectively, yields

$$\frac{dp_{NO_2}}{p_{NO_2}} = \left(\frac{1}{2-a}\right)\frac{dp}{p} + \left(\frac{1-a}{2-a}\right)\frac{dK_p}{K_p} \tag{22}$$

and

$$\frac{dp_{N_2O_4}}{p_{N_2O_4}} = \left(\frac{2}{2-a}\right)\frac{dp}{p} - \left(\frac{a}{2-a}\right)\frac{dK_p}{K_p} . \tag{23}$$

From the data presented in Figs. 2 and 3, we find, for the temperature range encountered in our experiments,

$$\frac{1}{K_p}\frac{dK_p}{dT} \approx 0.046 \ ^\circ K^{-1};$$

$$\frac{1}{p} \frac{dp}{dT} \approx 0.036 \ {}^{o}K^{-1};$$

$$a \approx 0.5.$$

Here we have utilized the experimental condition that the total pressure p corresponds to the vapor pressure p_v at a particular temperature. With an experimental scatter in temperature of $\pm 0.5 {}^{o}K$, we thus find

$$\frac{\Delta K_p}{K_p} \approx \pm 0.023 \quad \text{and} \quad \frac{\Delta p}{p} \approx \pm 0.018,$$

where we have approximated differential quantities by finite differences. Substituting these numerical values into Eqs. (22) and (23) gives

$$\frac{dp_{NO_2}}{p_{NO_2}} \approx \pm 0.020$$

$$\frac{dp_{N_2O_4}}{p_{N_2O_4}} \approx \pm 0.016.$$

Hence, we conclude that the scatter in partial pressures, resulting from inaccuracies in temperature measurement of $\pm 0.5 {}^{o}K$, is $\pm 2.0\%$ for NO_2 and $\pm 1.6\%$ for N_2O_4.

4. Light Scattering in the Spectrometer

Short-wavelength scattering in the spectrometer can be a source of serious error. The following procedure was used to demonstrate that light scattering in the instrument was not a serious source of error. A glass plate of 0.2 inch thickness was inserted in the light path to the spectrometer. The glass was found to transmit about 86% at wave-

lengths below 2.8μ . At longer wavelengths, the recorder indicated that a very small energy flux (about 2%) reached the detector. We next superimposed on the glass an interference filter which was completely opaque to visible light up to 1.7μ and transmitted about 95% above this wavelength. Above 2.8μ , the recorder again indicated the same flux on the detector as was found with the glass alone. Since in the last case all short wavelength radiation below 1.7μ had been eliminated, the observed flux must have been either scattered light at wavelengths greater than 1.7μ or else a small amount of transmission through the glass at a wavelength corresponding to the instrument setting. As light source we used a Nernst glower which operates at $1900^{\circ}K$; at $1900^{\circ}K$, the peak emitted energy lies near 1.5μ . Hence, with the interference filter in the light path, the energy peak and light of all wavelengths below it were eliminated from the spectrometer. The small flux on the detector, therefore, is probably due to transmission through the glass at a wavelength corresponding to the instrument setting.

H. QUANTITATIVE STUDIES ON LIQUID N_2O_4 BANDS

1. Experimental Apparatus

The optical system used for measuring liquid N_2O_4 absorption was identical with that described in Section D. The absorption cell shown in Fig. 10 was now completely filled with liquid N_2O_4. Extreme care was exercised to eliminate all bubbles from the space between the windows, as this would introduce serious errors into the interpretation of experimental results.

Spectra were obtained with two spacers in the cell corresponding to optical path lengths of 0.0127 and 0.00508 cm. The use of these thin spacers required measurements of actual spacing between the windows when the cell was subjected to internal pressures corresponding to those encountered in the experiments. The actual window spacing under pressure may change as a result of two possible causes: (a) with the windows supported on the periphery by O-rings, bulging out of the center portions may be of significance; (b) the supporting O-rings themselves may be sufficiently compressed to increase the spacing appreciably. The effect of these factors at various pressures was determined with the aid of a dial gage indicator capable of measuring differences in position as small as 0.0001 inch. The gage was fixed to the cell body in such a way that the moving rod was in contact with and normal to the outside surface of a window. We were thus able to read the outward deflection of the window center as a function of pressure. Results indicated no detectable deflection up to a pressure of 25 atm. At 37 atm, the deflection for one window was 0.0013 cm, which corresponds to a 50% increase in window separation for the 0.00508 cm spacer. We may conclude from these results that the actual spacing between windows during the experiments (at a maximum pressure of 19.8 atm) corresponded to the spacer thickness.

2. Results

Transmission spectra were obtained in the temperature range from 25 to 100°C at intervals of approximately 20 degrees. Final results are based on measurements with the 0.00508 cm spacer. For the

0. 0127 cm spacer, the liquid was opaque in the region of the stronger bands. However, results for the weakest band (3429 cm^{-1}) followed Beer's law according to which the quantity $\mathcal{B}$ is directly proportional to the optical path length $\left[\text{see Eqs. (2) and (6)}\right]$. For the ratio of path lengths $l_2/l_1 = 2.5$ we found $\mathcal{B}_2/\mathcal{B}_1$ to be 2.46, 2.52, and 2.48 at temperatures of 25, 40, and 60°C, respectively. Assuming that Beer's law is valid, we may consider these results to provide an additional check on the actual window spacing.

Spectral absorption coefficients for four liquid-N_2O_4 combination bands at various temperatures are plotted in Figs. 55 to 58 of Appendix II. All bands are shifted by 6 to 17 cm^{-1} toward the lower frequencies (see Table 1) relative to the bands observed for the gas.

Integrated intensity estimates are summarized in Table 3 and plotted, per unit mass density, as a function of temperature in Fig. 22. We conclude from the observed results that the integrated intensity per unit mass density is approximately constant over the indicated temperature range.

I. COMPARISON OF INTEGRATED INTENSITIES FOR N_2O_4 IN THE GASEOUS AND LIQUID STATES

Reference to Table 1 shows that the shifts in band locations in going from the gaseous to the liquid state are of the order of 10 cm^{-1}. These results suggest that the wave functions corresponding to the upper and lower vibrational states are not greatly changed in going from the vapor to the liquid phase. One might therefore expect the vibrational matrix elements for the N_2O_4 molecule to be approximately equal

-55-

Table 3. Integrated intensities for liquid N_2O_4 bands in the near infrared region of the spectrum.

Band center (cm^{-1})	Integrated intensity ($cm^{-2} \times 10^3$)					
	Temperature (°C)					
	25	40	60	80	100	
2605	13.7	13.2	12.5	11.9	11.2	
2945	22.7	22.1	21.2	20.2	19.2	
3114	21.5	20.6	19.7	18.8	18.2	
3429	7.78	7.50	7.18	6.93	6.67	
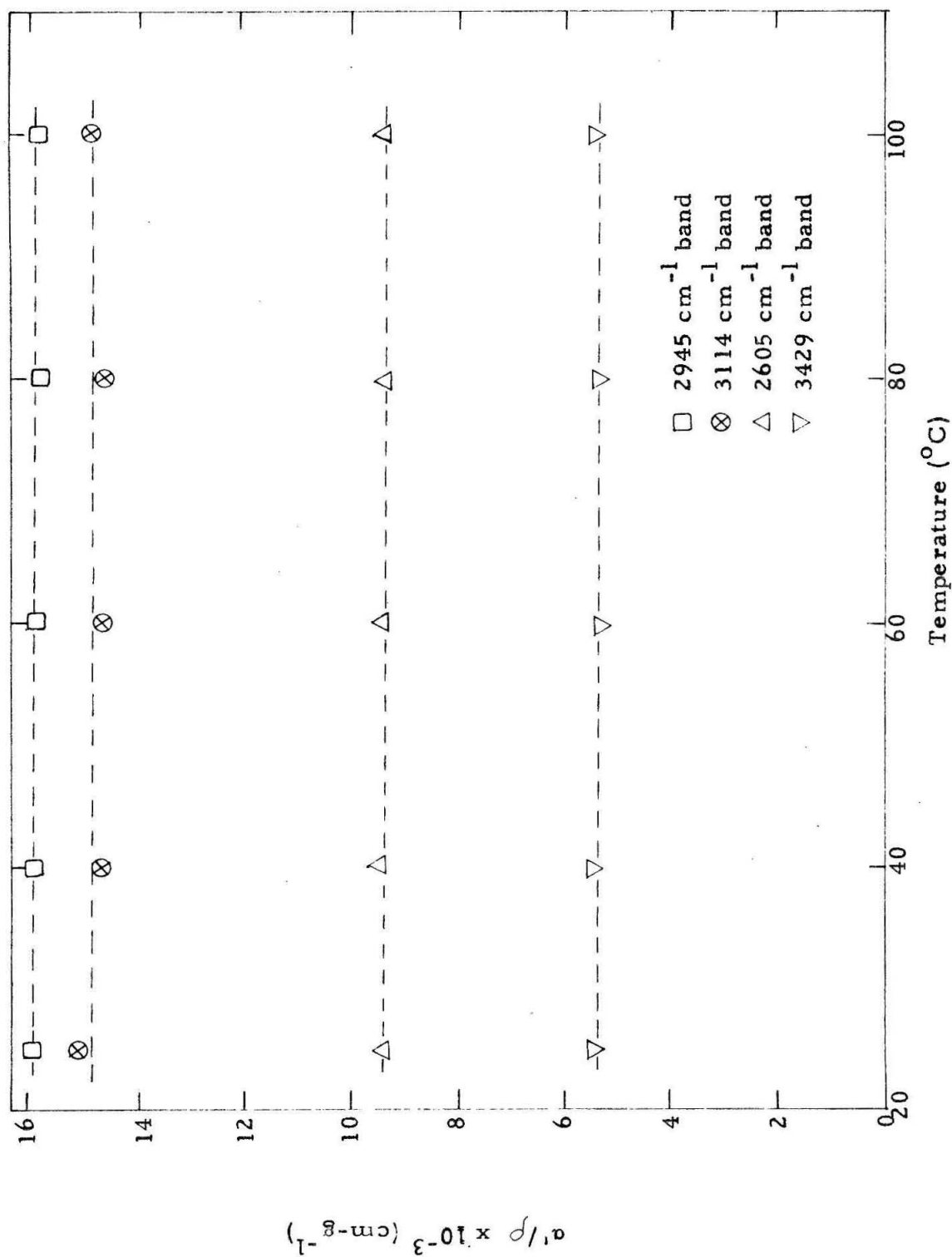
Fig. 22. Temperature dependence of integrated intensities for the combination bands of liquid N_2O_4. The quantity ρ represents the mass density of liquid N_2O_4.

in the liquid and gas phases. The integrated intensity is directly proportional to the square of the matrix element. Hence, the intensities of liquid and gaseous N_2O_4 bands should be approximately equal if expressed in the same units.

In Table 4 we compare the integrated intensities, expressed per unit mass density, for the gaseous and liquid states of N_2O_4. Good agreement in intensities is noted for the 2618, 2962, and 3120 cm^{-1} bands, with the percentage differences at the three temperatures being less than 16%. For three of the four bands studied, the integrated intensity in the liquid phase is larger than in the vapor phase. The weakest band (3442 cm^{-1}) shows a percentage difference between the intensities of the gaseous and liquid states of about 50%. It should perhaps be noted that the absolute accuracy of intensity measurements is usually smallest for the weakest bands (compare Figs. 17 to 20). It is not clear that any particular physical significance, in terms of liquid structure, may be attached to the observed results.

J. DETERMINATION OF ΔH^o FOR THE REACTION $N_2O_4 \rightleftharpoons 2NO_2$ FROM INFRARED MEASUREMENTS

One of the more interesting applications of experimental infrared measurements on systems in chemical equilibrium is the determination of equilibrium constants and chemical heats of reaction. Optical techniques would be particularly useful on complicated systems containing more than two species, for it is relatively easy to follow the concentrations of each species by monitoring the absorption in the region

Table 4. Comparison of integrated intensities for gaseous and liquid N_2O_4 bands in the near infrared region of the spectrum.

Band center (cm^{-1})		Integrated intensity per unit mass density (cm-gm^{-1} × 10^3) Temperature (°C)					
		60		80		100	
gas	liquid	gas	liquid	gas	liquid	gas	liquid
2618	2605	9.92	9.27	9.73	9.24	10.3	9.20
2962	2945	15.1	15.8	14.7	15.7	15.0	15.7
3120	3114	12.5	14.6	13.1	14.6	12.7	14.8
3442	3429	3.53	5.34	3.34	5.37	3.43	5.47

of a characteristic vibration-rotation band. In particular, we shall
demonstrate the feasibility of this technique by applying it to the system

$$N_2O_4 \rightleftharpoons 2NO_2,$$

for which we have measured infrared absorption data as a function of
temperature. With suitable assumptions, these measurements yield
the variation of the equilibrium constant with temperature, from which
we obtain the heat of reaction ΔH^O. It should be noted that, in order to
obtain these results, it is not necessary to know the absolute values for
the integrated intensities. A knowledge of their temperature dependence
is sufficient.

Let us assume that, for the results presented in Figs. 16 to 20,
the total pressures were sufficiently high to smear out the rotational
fine structure completely. Then, by Eq. (9), provided adequate broaden-
ing has been obtained,

$$p_{NO_2} = \frac{\mathcal{B}_{NO_2}}{a_{NO_2}\ell}$$

and

$$p_{N_2O_4} = \frac{\mathcal{B}_{N_2O_4}}{a_{N_2O_4}\ell} \tag{24}$$

where $\mathcal{B}_{NO_2}$ and a_{NO_2} refer to any given band of NO_2 and a similar
notation is used for N_2O_4. Now we assume that the integrated intensities
vary inversely with the absolute temperature, an assumption which is
well justified for the relatively small temperature range under con-
sideration (see Fig. 21). Thus

$$a_{NO_2} = a_{o,NO_2} \frac{T_o}{T}$$

and

$$a_{N_2O_4} = a_{o,N_2O_4} \frac{T_o}{T}.$$

(25)

Here a_o is the value of the integrated intensity at the temperature T_o. Substituting Eqs. (25) into Eqs. (24) yields

$$P_{NO_2} = \frac{\mathcal{B}_{NO_2} T}{a_{o,NO_2} T_o \ell}$$

and

$$P_{N_2O_4} = \frac{\mathcal{B}_{N_2O_4} T}{a_{o,N_2O_4} T_o \ell}$$

which, when substituted into the relation for chemical equilibrium, gives

$$K_p = \left(\frac{a_{o,N_2O_4}}{a^2_{o,NO_2} T_o \ell} \right) \left(\frac{\mathcal{B}^2_{NO_2} T}{\mathcal{B}_{N_2O_4}} \right) \quad.$$

(26)

The factor in the first set of parentheses of Eq. (26) is a constant independent of temperature.

Reference to Eq. (26) shows that in order to obtain absolute values for the equilibrium constant, it is necessary to know the absolute intensities at an arbitrary temperature T_o for one band of NO_2 and one of N_2O_4. Absolute intensities for NO_2 may be obtained by establishing a sufficiently high temperature to yield a condition of nearly complete dissociation, thus making the total pressure approximately equal to the

partial pressure of NO_2. Unfortunately, under the saturated vapor conditions of our experiments, this procedure would require the use of extremely high vapor pressures, and was therefore not feasible with the available equipment. It is hardly feasible to obtain pure N_2O_4 at reasonably high pressures (greater than one atm) in the vapor phase. However, one may estimate absolute intensities for N_2O_4 from the liquid phase (see Table 4). Once the intensities for two bands at any arbitrary temperature are determined, thermochemical data such as ΔF^O and ΔS^O may be computed from spectroscopic measurements by the use of Eq. (26).

The equilibrium constant for a reaction at constant pressure and temperature can be expressed in terms of the difference between the standard free energies of the products and reactants ΔF^O, i.e.,

$$K_p = \exp\left(-\frac{\Delta F^O}{RT}\right)$$

from which it can easily be shown[21, 22] that

$$\frac{d \ln K_p}{d\left(\frac{1}{T}\right)} = -\frac{\Delta H^O}{R} \ , \tag{27}$$

which is known as van't Hoff's equation. The quantity ΔH^O represents the difference in enthalpy between the products and reactants evaluated at a pressure of one atmosphere and at the temperature T.

Combining Eqs. (26) and (27) gives

$$\frac{d \ln \left(\frac{\mathscr{B}^2_{NO_2} T}{\mathscr{B}_{N_2O_4}}\right)}{d\left(\frac{1}{T}\right)} = -\frac{\Delta H^O}{R} \tag{28}$$

Hence, a plot of the experimentally determined function $\ln(\mathcal{B}^2_{NO_2} T/\mathcal{B}_{N_2O_4})$ against $1/T$ will yield a straight line with slope equal to $-\Delta H^o/R$.

In Fig. 23 we have plotted the function appearing on the left-hand side of Eq. (28) for a spacer thickness of 0.124 cm. We used the 2908 cm^{-1} band of NO_2 in conjunction with the three strongest bands of N_2O_4 in the region from 1 to 5 microns. Corrections were made for the impurity band coinciding with the 2908 cm^{-1} band of NO_2 by subtracting 3.7 cm^{-1} from each measured value for $\mathcal{B}_{NO_2}$ (see Fig. 16).

The experimental points shown in Fig. 23 yield nicely linear plots, indicating that ΔH^o is nearly constant in the specified temperature range. Least-square fits yield values for ΔH^o of 13,070, 12,980, and 13,160 cal/(mole N_2O_4) for the curves corresponding to the 2618, 2962, and 3120 cm^{-1} bands of N_2O_4, respectively. Thus, we obtain a mean value of 13,070 $\pm$ 90 cal/(mole N_2O_4) which is in good agreement with the value at 298°K of 13,693 $\pm$ 14 cal/(mole N_2O_4) reported by Giauque and Kemp.[16]

The preceding results provide an important check on the self consistency of our absolute infrared intensity measurements.

K. INTEGRATED INTENSITIES FOR FUNDAMENTAL BANDS OF GASEOUS NO_2 AND N_2O_4 IN THE 5 TO 15μ REGION

1. Optics

For the spectral region from 5 to 15 microns, we used silver chloride (AgCl) windows in the absorption cell. A 5-mm AgCl window transmits about 80 percent in the region from 5 to 20μ.[26] Silver chloride was chosen primarily for its resistance to chemical attack by nitrogen dioxide;[9] another important consideration was the fact that it
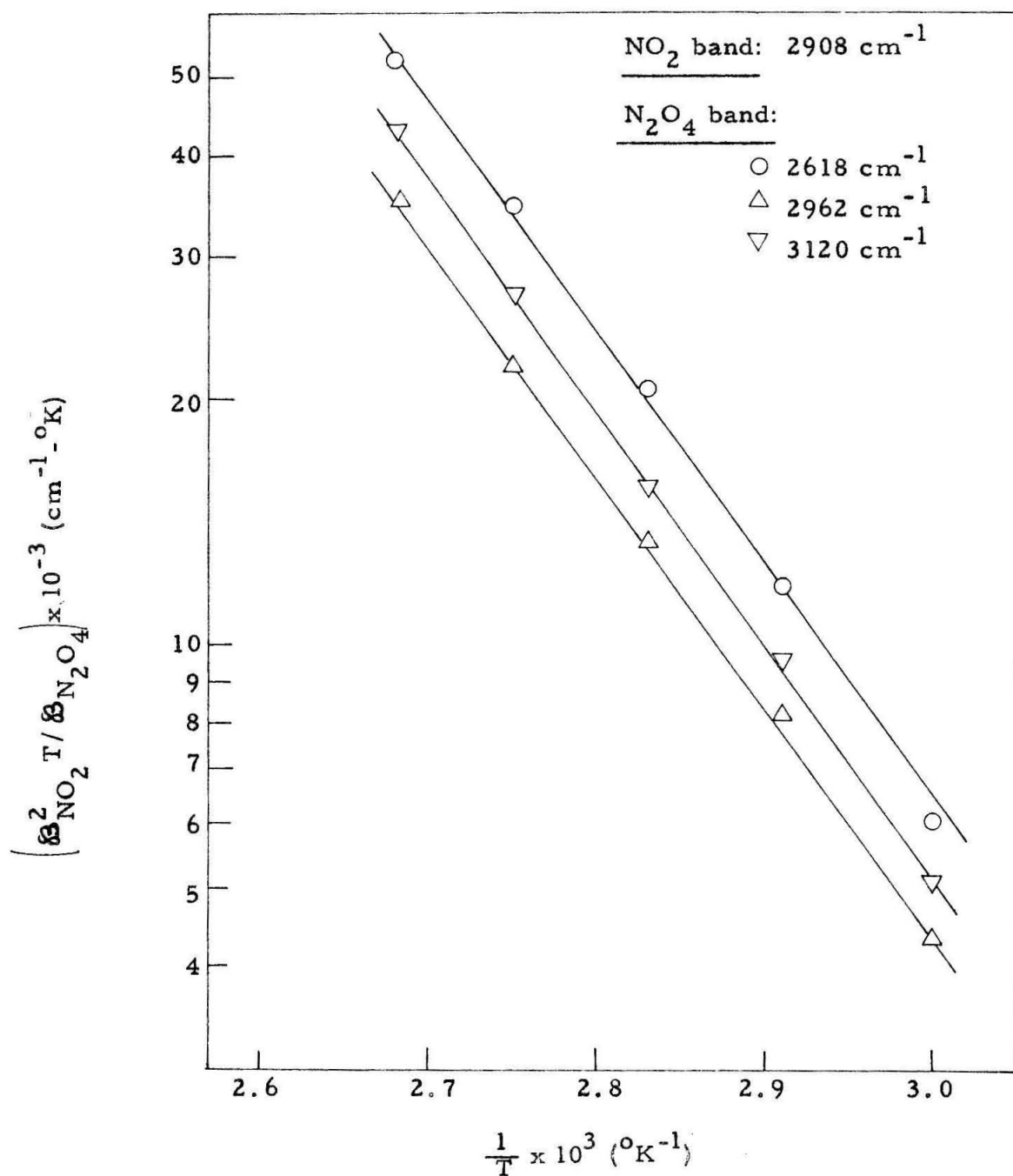
Fig. 23. Plots used for determining ΔH^o for the reaction $N_2O_4 =$ $2NO_2$ from experimental values of the parameters $\mathcal{B}$. The three curves were obtained using the strongest N_2O_4 bands in the region from 1 to 5 microns.

does not cleave easily, as does sodium chloride, and hence will not crack upon being pressed against the cell spacer (see Fig. 10).

We used a rocksalt (NaCl) prism for studies above 5μ ; sodium chloride is nearly opaque above 15μ . Standard procedures were utilized to obtain a wavelength calibration of the spectrometer. Atmospheric and polystyrene bands gave calibration points up to about 10μ . In addition, known lines belonging to the $950\ cm^{-1}$ fundamental band of NH_3 were used. For the region near 15μ , we used the $668\ cm^{-1}$ fundamental of CO_2.

The spectrometer slit width was varied in such a manner that the resolution for the entire spectral range was between 5 and $10\ cm^{-1}$.

2. Results

Since the conditions for complete overlapping of the rotational lines had been studied extensively for the work in the near infrared region (1 to 5μ), we assumed that it was not necessary to plot the parameter δ as a function of optical depth for the fundamentals in the 5 to 15μ region. Measurements were made at $25°C$ corresponding to a vapor pressure of 1.18 atm. This pressure should be sufficiently high to smear out the rotational fine structure, particularly since we are dealing with very strong bands. Only one spacer (0.0495 cm thick) was used. Integrated intensities were obtained for one NO_2 and three N_2O_4 fundamental bands, which are the strongest bands in the region from 5 to 15μ .

Light scattering in the spectrometer was measured and corrected for in the following manner. If the optical depth is made sufficiently high,

the gas becomes practically opaque in the region of the strongest

absorption of bands (see Fig. 24). This condition may be detected
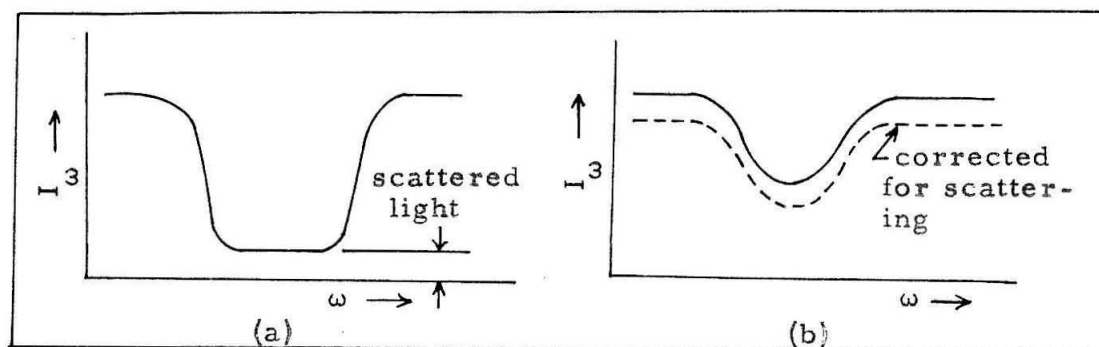
Fig. 24. Effect of scattered light on an absorption band.

easily by noting that the transmitted radiancy is constant for a wide

wavenumber range near the band center, as in Fig. 24(a). Hence,

if the transmitted radiancy is not zero, the observed flux must be

scattered light. Corrections for scattering may be made by simply

increasing the optical depth, without altering the light intensity, slit

width and amplifier gain, and then subtracting the scattered light from

the transmission spectrum, as in Fig. 24(b). This procedure is easily

accomplished in our experimental setup, since the optical depth may be

raised by raising the cell temperature, thereby increasing the vapor

pressure. In this manner, we made corrections for scattering near the

750 cm^{-1} fundamental of N_2O_4. The scattered light in the vicinity of

this band was found to be about 5% of the incident light and about 30% of

the transmitted light at the band maximum. In the vicinity of the other

bands, scattered light was found to be negligibly strong.

Shapes of the four fundamental bands are shown in Figs. 59 to 62 of Appendix III, where we have plotted $\log_{10}(I_\omega^{o,\,a}/I_\omega^a)$ as a function of wave number. Final estimates for the integrated intensities are presented in Table 5.

Table 5. Integrated intensities at 25°C for the strongest fundamental bands of NO_2 and N_2O_4 in the spectral region from 5 to 15 microns.

Molecule	Band center (cm^{-1})	Integrated intensity $(cm^{-2}\text{-atm}^{-1})$
NO_2	1617	2059
N_2O_4	1748	2940
N_2O_4	1260	1803
N_2O_4	750	1104

L. SPECTRAL AND TOTAL EMISSIVITY ESTIMATES FOR NO_2

Radiant energy emission from the atmosphere of the earth is an important problem that is being studied actively by a number of investigators. For example, the emission from OH in the upper atmosphere has been estimated both experimentally[23] and theoretically.[24, 25] The species NO_2 is also believed to be present in the upper atmosphere, although no unambiguous spectroscopic detection has been made so far. In this connection, quantitative values of spectral absorption coefficients for NO_2 from laboratory experiments are of considerable interest. These data should facilitate estimates of the contribution by NO_2 to the "night

glow" of the earth's atmosphere.

The spectral emissivity $\mathcal{E}_\omega$ of a gas with optical depth $p\ell$ is related to the absorption coefficient by

$$\mathcal{E}_\omega = 1 - \exp(-P_\omega p\ell). \tag{29}$$

In Figs. 25 to 30 and Fig. 59, we have plotted $\log_{10}(I_\omega^{o,\,a}/I_\omega^a)$, for the strongest bands of NO_2 in the region from 1 to 15 μ . The ordinates of these curves represent $P_\omega p\ell/2.303$ since we have shown that, during the experiments, the rotational fine structure was completely smeared out (see Section G, Part 2b). For temperatures other than those for which measurements are available, it is a simple matter to estimate the appropriate value of the spectral absorption coefficients provided the rotational fine structure is again smeared out. We would expect that this condition is satisfied, in good approximation, for total pressures greater than about one atmosphere in the temperature range in which NO_2 and N_2O_4 are stable.

At altitudes greater than 100,000 ft, the local pressure is less than 0.01 atm; under these conditions, the rotational lines of NO_2 are not expected to overlap appreciably. Because of the complex band structure of asymmetric polyatomic molecules such as NO_2, it may be convenient to use the statistical model developed by Mayer[27] and Goody.[28] According to this model, the mean emissivity $\overline{\mathcal{E}}$ for a band, with randomly distributed lines having the same integrated intensity ($\overline{S}$) and a resonance contour with a half-width b, is given by

$$\overline{\mathcal{E}} = 1 - \exp\left[-\frac{2\pi b}{\delta^*} \ f(\overline{x})\right] \tag{30}$$

where

$$f(\overline{x}) = \overline{x} \left[\exp(-\overline{x}) \right] \left[J_0(i\overline{x}) - i \, J_1(i\overline{x}) \right]$$

and $\overline{x} = \overline{S}X/2\pi b$. The parameter δ^* refers to the mean spacing between lines. For $\overline{S}X/2\pi b \ll 1$, the mean emissivity reduces to

$$\overline{\varepsilon} \approx 1 - \exp(- \frac{\overline{S}}{\delta^*} X) \simeq \frac{\overline{S}X}{\delta^*} \tag{31}$$

since $2\pi b/\delta^*$ for the specified altitude $\gtrsim 10^{-1}$.

We shall now apply Eq. (31) to the emission from NO_2 in the upper atmosphere. The results are considerably simplified by identifying $\overline{S}_i$ in the usual manner, viz.,

$$\overline{S}_i = \frac{a_i}{(\Delta\omega_i / \delta_i^*)} \tag{32}$$

where $\Delta\omega_i$ is the effective band width for the ith band. Substituting Eq. (32) into Eq. (31) gives[*]

$$\overline{\varepsilon}_i = \frac{a_i X}{\Delta\omega_i} \, . \tag{33}$$

All of the parameters on the right-hand side of Eq. (33) have been measured or can be estimated for the two strongest infrared bands of NO_2, and hence the mean emissivities for these bands may be calculated at arbitrary optical depths. Let us now examine under what conditions the basic inequality

$$\frac{\overline{S}X}{2\pi b} \ll 1$$

holds for NO_2. Replacing $\overline{S}_i$ according to Eq. (32), we obtain

---

[*] Equation (33) may be obtained directly from Eq. (29) by assuming that the emitter radiates like a transparent gas.

$$\frac{a_i}{\Delta\omega_i} \frac{\delta_i^*}{b_i} \frac{X}{2\pi} << 1 \tag{34}$$

For the bands under consideration, $a_i/\Delta\omega_i \gtrsim 10$, and $\delta_i^*/2\pi b_i \simeq 10$ at high altitudes. Hence we find the inequality to be satisfied for optical depths $X \ll 10^{-2}$ cm-atm. Because of the very low concentrations of NO_2 in the upper atmosphere, this last condition may well be satisfied, particularly since the NO_2 has not been observed spectroscopically. If NO_2 constitutes less than one part in 10^7 of the atmosphere at a total pressure of 10^{-2} atm, then the NO_2 will emit like a transparent gas for path lengths as long as 100 km.

For temperatures other than those at which measurements are available, one may extrapolate a_i and $\Delta\omega_i$ by using the relations (see Ref. 11, p. 322)

$$\Delta\omega_i(T) = \Delta\omega(T_o)(\frac{T}{T^o})^{1/2} ; \qquad a_i(T) = a_i(T^o)\frac{T^o}{T} .$$

The engineering emissivity may be calculated from the relation

$$\varepsilon = \frac{1}{\sigma T^4} \sum_i \overline{\varepsilon}_i R^o_{\omega_i} \Delta\omega_i, \tag{35}$$

where we sum over all bands belonging to NO_2. In Eq. (35) the parameter σ is the Stefan-Boltzman constant and $R^o_{\omega_i}$ is the spectral blackbody radiancy evaluated at the center of the ith band.

REFERENCES

1. Warburg, E., and Leithauser, G., Ann. der Phys. 28, 313-325 (1909).

2. Von Bahr, E., Ann. der Phys. 33, 585-594 (1910).

3. Strong, J., and Woo, S.C., Phys. Rev. 42, 267-278 (1932).

4. Sutherland, G.B.B.M., Proc. Roy. Soc. 141, 342-362 (1933).

5. Bailey, C.R., and Cassie, A.B.D., Nature 131, 239 (1933).

6. Schaffert, R., J. Chem. Phys. 1, 507-511 (1933).

7. Harris, L., and King, G.W., J. Chem. Phys. 2, 51-57 (1934).

8. Moore, G.E., J. Opt. Soc. Am. 43, 1045-1050 (1953).

9. Snyder, R.G., and Hisatsune, I.C., J. Molec. Spect. 1, 139-150 (1957).

10. Begum, G.M., and Fletcher, W.H., J. Molec. Spect. 4, 388-397 (1960).

11. Penner, S.S., Quantitative Molecular Spectroscopy and Gas Emissivities, pp. 73-74, Addison-Wesley Publishing Company, Inc., Reading, Mass., 1959.

12. Schlinger, W.G., and Sage, B.H., Ind. Eng. Chem. 42, 2158-2163 (1950).

13. Reamer, H.H., and Sage, B.H., Ind. Eng. Chem. 44, 185-187 (1952).

14. Bodenstein, M., and Boës, F., Z. Physik. Chem. 100, 75-96 (1922).

15. Carrington, T., and Davidson, N., J. Phys. Chem. 57, 418-427 (1953).

16. Giauque, W.F., and Kemp, J.D., J. Chem. Phys. 6, 40-52 (1938).

17. Smith, R.A., Jones, F.E., and Chasmar, R.P., The Detection and Measurement of Infra-Red Radiation, p. 313, Oxford University Press, Amen House, London, 1957.

18. Smith, J.H., Ph.D. Thesis, p. 13, University of Wisconsin, 1941.

19. Beattie, J.A., Chem. Revs. 44, 141-192 (1949).

20. Imes, E.S., Astrophys. J., $\underline{50}$, 251-262 (1919).

21. Denbigh, K., The Principles of Chemical Equilibrium, p. 141, Cambridge University Press, Cambridge, 1957.

22. Penner, S. S., Chemistry Problems in Jet Propulsion, pp. 124-125, Pergamon Press, New York, 1957.

23. Meinel, A.B., Astrophys. J. $\underline{111}$, 555-564 (1950); $\underline{112}$, 120-130 (1950).

24. Heaps, H.S., and Herzberg, G., Z. Physik $\underline{133}$, 48-64 (1952).

25. Bates, D.R., and Nicolet, M.J., Geophys. Res. $\underline{55}$, 301-312 (1950).

26. Ballard, S.S., McCarthy, K.A., and Wolfe, W.L., Optical Materials for Infrared Instrumentation, p. 39, Report Number 2389-11-S, The University of Michigan, Willow Run Laboratories, 1959.

27. Mayer, H., Los Alamos Scientific Laboratory Report LA-647, 1947.

28. Goody, R.M., Quart. J. Roy. Met. Soc. $\underline{78}$, 165-172 (1952).

II. EMISSION OF DIFFUSE BANDS OF SODIUM BEHIND SHOCK FRONTS

by H. Takeyama and A. Guttman

Emission of Diffuse Bands of Sodium behind Shock Fronts*

H. TAKEYAMA† AND A. GUTTMAN‡

*Daniel and Florence Guggenheim Jet Propulsion Center,
California Institute of Technology, Pasadena, California*

(Received October 14, 1959)

WURM[1] has described a continuous emission band extending from 5490 A to the D lines and inferred the existence of van der Waals states of Na_2. Hamada[2] has classified sodium bands in the red and yellow regions into three groups, *viz.*, (1) red bands ($\lambda\lambda8150$–5500), (2) cathode ray fluorescence band, and (3) the continuous band ($\lambda\lambda5470$–7200). Recently, wide diffuse bands have been observed and discussed qualitatively for rubidium-rare gas mixtures.[3,4]

By utilizing the shock tube, we have observed the emission of a continuous band corresponding to Hamada's type (3) band. We used finely ground salts as a source of sodium in a one-inch diameter tube; the low-pressure section was 51 in. long and the high-pressure section had a length of 24 in. Mylar diaphragms (0.003 and 0.005 in. thick) separated the two sections. Observations were made through a lucite block at the end of the low pressure section. Spectrograms were taken with a 1.5-m ARL spectrograph with a dispersion of 6.8 A/mm. Kodak Royal-X panchromatic sheet film and Kodak Tri-X panchromatic roll film were used. Intensity measurements were made with an ARL 2250 densitometer.

Measured quantities (from 5 to 300 mg) of finely ground sodium salts (e.g., NaCl, NaBr, and Na_2CO_3) were placed in the Lucite block and spread evenly. Argon, at pressures from 5 to 100 mm Hg, was admitted to the low-pressure section. The high-pressure section was filled with helium and a magnetic breaker used to burst the diaphragm.

We observed atomic lines of Na and a continuous band under various shock conditions. As the amount of sodium salt is increased at constant shock conditions, the D lines become stronger, wider and self-reversed; also the diffuse series lines ($\lambda\lambda5682$, 5688) and sharp series lines ($\lambda\lambda6154$, 6160) appear. When the quantity of sodium chloride exceeds about 10 mg, the diffuse band becomes superimposed on the atomic lines. Further increases in the amount of sodium chloride up to 300 mg did not change the general features of the spectrum. A typical intensity profile (Fig. 1) shows a continuous band starting at about 5490 A and extending beyond 6200 A. The quantities T_5 and p_5 were estimated by using ideal, one-dimensional shock theory.[5] An intermediate maximum occurs at about 5500 A; on the long-wavelength side the intensity decreases continuously without distinct cutoff.

There is little doubt that the continuous band $\lambda\lambda5490$–6200 is identical with Hamada's (3) band and Wurm's band. The discrepancy in the long-wavelength
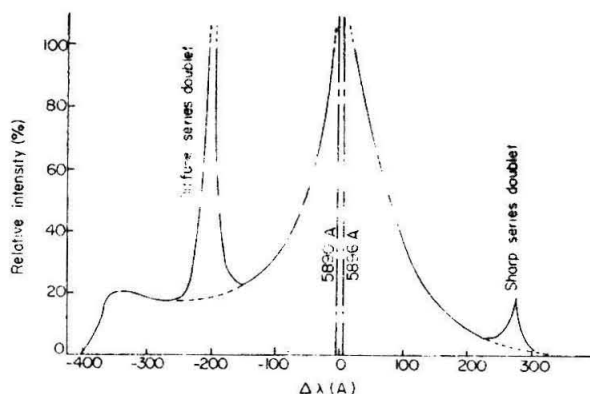
FIG. 1. Intensity distribution of band accompanying D lines; $p_1 = 50$ mm Hg, $p_4 = 395$ psi, $p_5 = 12$ atmos, $T_5 = 6300$ K. NaCl = 50 mg.

extent of the band between Hamada's results and ours may be attributed·to the extreme difference of excitation conditions. The principal support for the assertion that the band belongs to Na_2 molecular states comes from the observation that the emission spectrum is independent of the nature of the foreign gas. Wurm considered the structure in the long-wavelength region of the D lines to result from absorption of the red band of Na_2, the background being the broadening of the D lines. On the other hand, Hamada interpreted the entire continuum (both sides of the D lines) to constitute a single band caused by the same mechanism described by Wurm. Recently, Ch'en, Bennett, and Jefimenko[3] have presented potential curves that are consistent with both the red and violet bands. It appears reasonable to conclude that the continuous band results from a transition between a molecular state composed of ^2S and ^2P Na atoms and a similar molecule composed of two ground state Na atoms. It should be noted that Na_2 molecules should be formed behind shock fronts after interaction between the incident or reflected shocks and the rarefaction wave.

Further research of a more quantitative nature is now in progress and will be reported in the near future.

[1] K. Wurm, Z. Physik **79**, 736 (1932).

[2] H. Hamada, Phil. Mag. **15**, (7), 574 (1933).

[3] Ch'en, Bennett, and Jefimenko, J. Opt. Soc. Am. **46**, 182 (1956).

[4] O. Jefimenko and W. Curtis, J. Chem. Phys. **27**, 953 (1957).

[5] Ressler, Lin, and Kantrowitz, J. Appl. Phys. **23**, 1390 (1952).

APPENDIX I

Plots of $Log_{10}(I_\omega^{o,a}/I_\omega^a)$ as a Function of Wave Number for Gaseous NO_2 and N_2O_4 Combination Bands at Various Optical Depths and in the Temperature Range 50 to 100^oC.
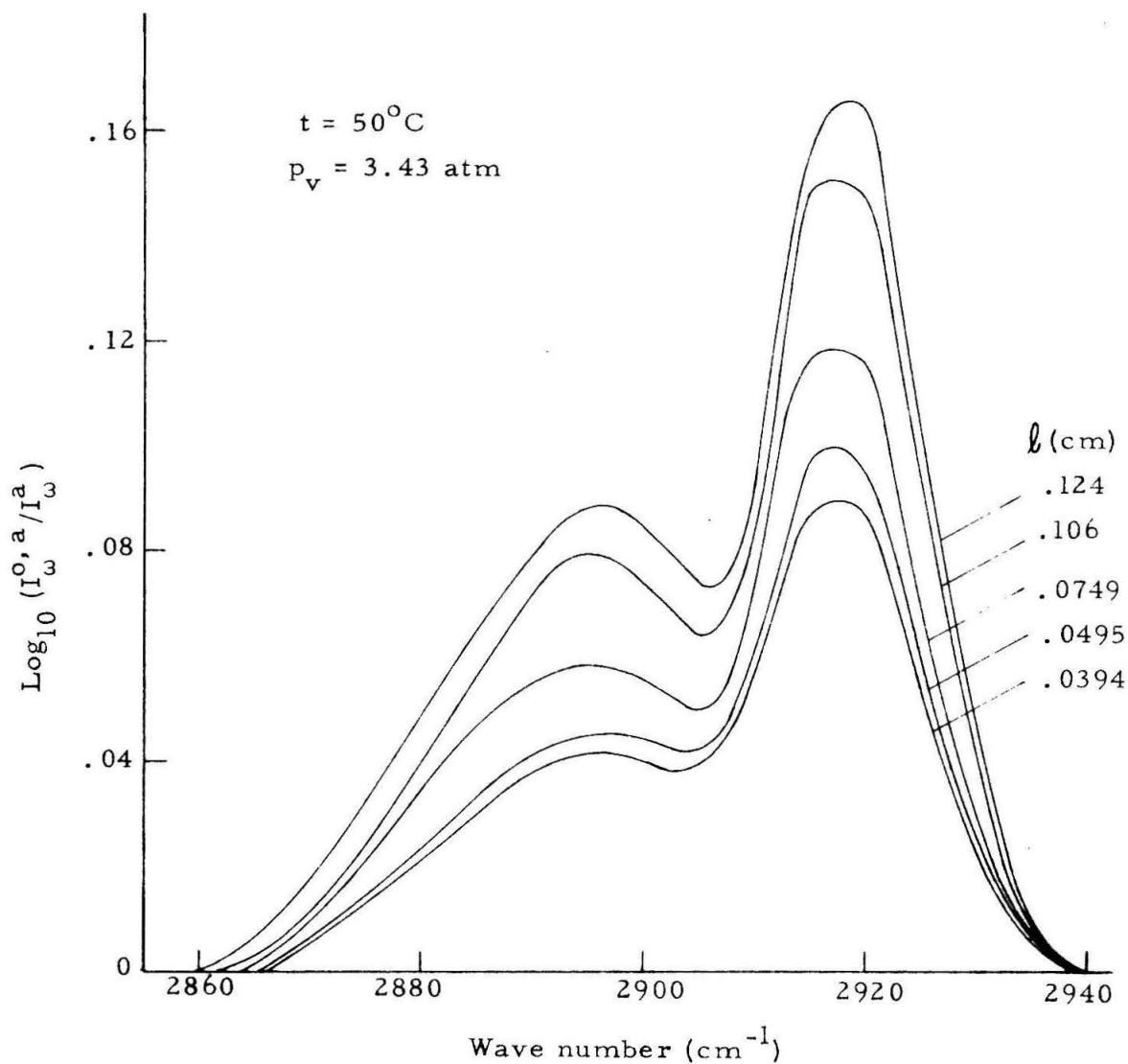
Fig. 25. Logarithm of the reciprocal of apparent spectral trans-
mission for the 2908 cm^{-1} band of NO_2 at various optical
depths.
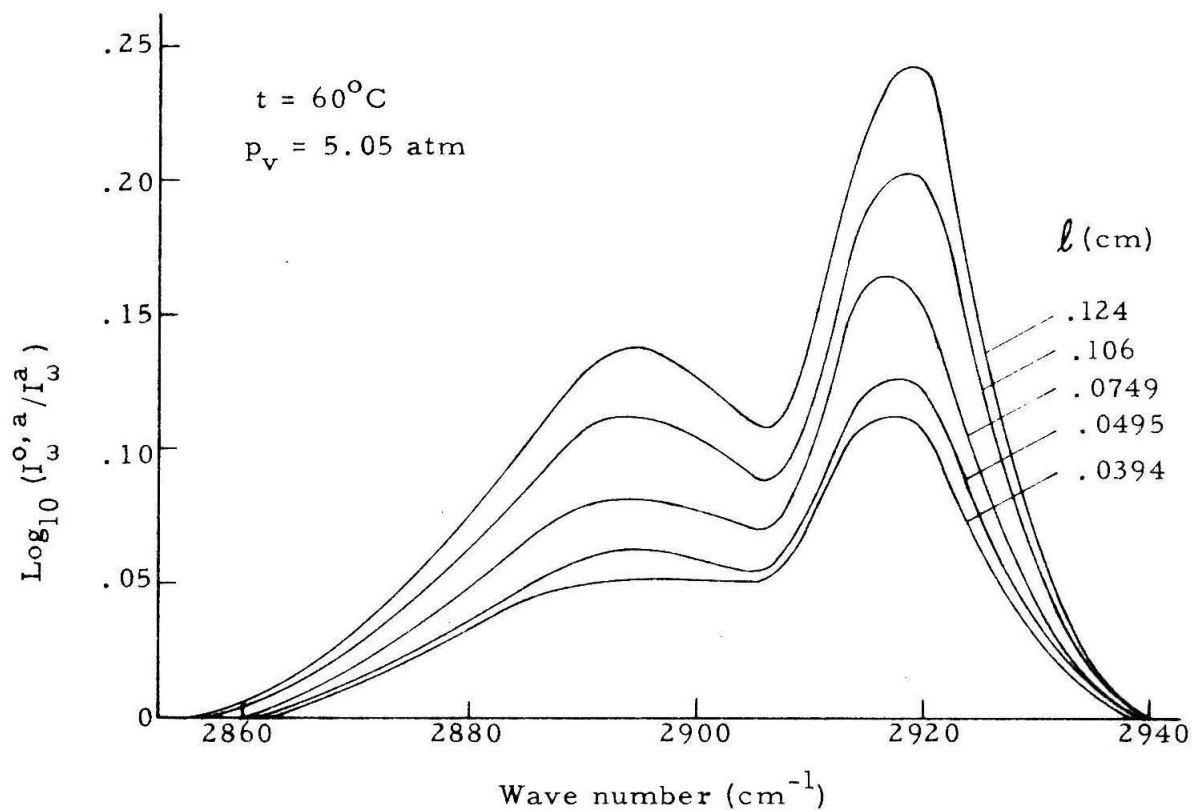
Fig. 26. Logarithm of the reciprocal of apparent spectral trans-
mission for the 2908 cm^{-1} band of NO_2 at various optical
depths.
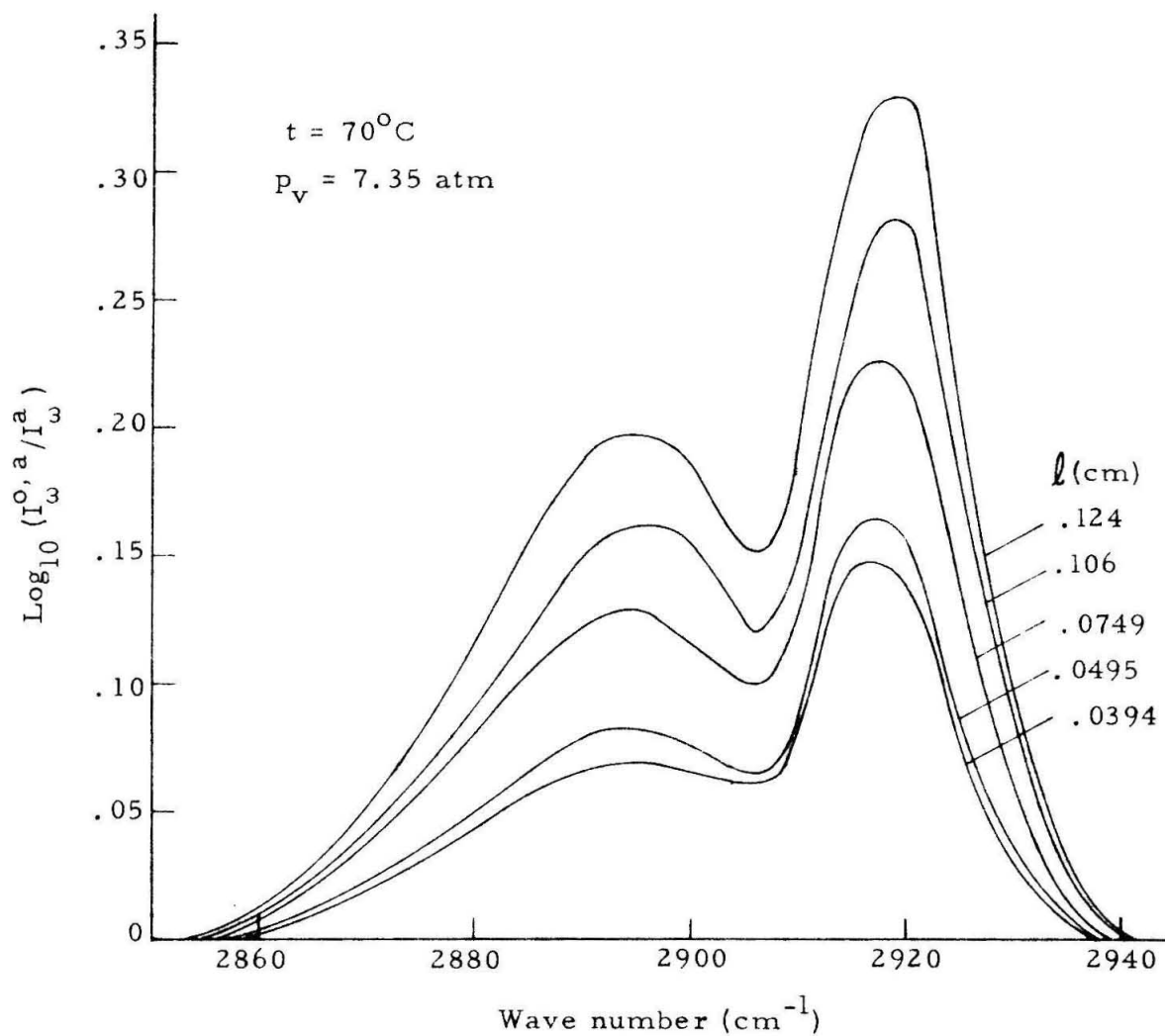
Fig. 27. Logarithm of the reciprocal of apparent spectral trans-
mission for the 2908 cm^{-1} band of NO_2 at various optical
depths.
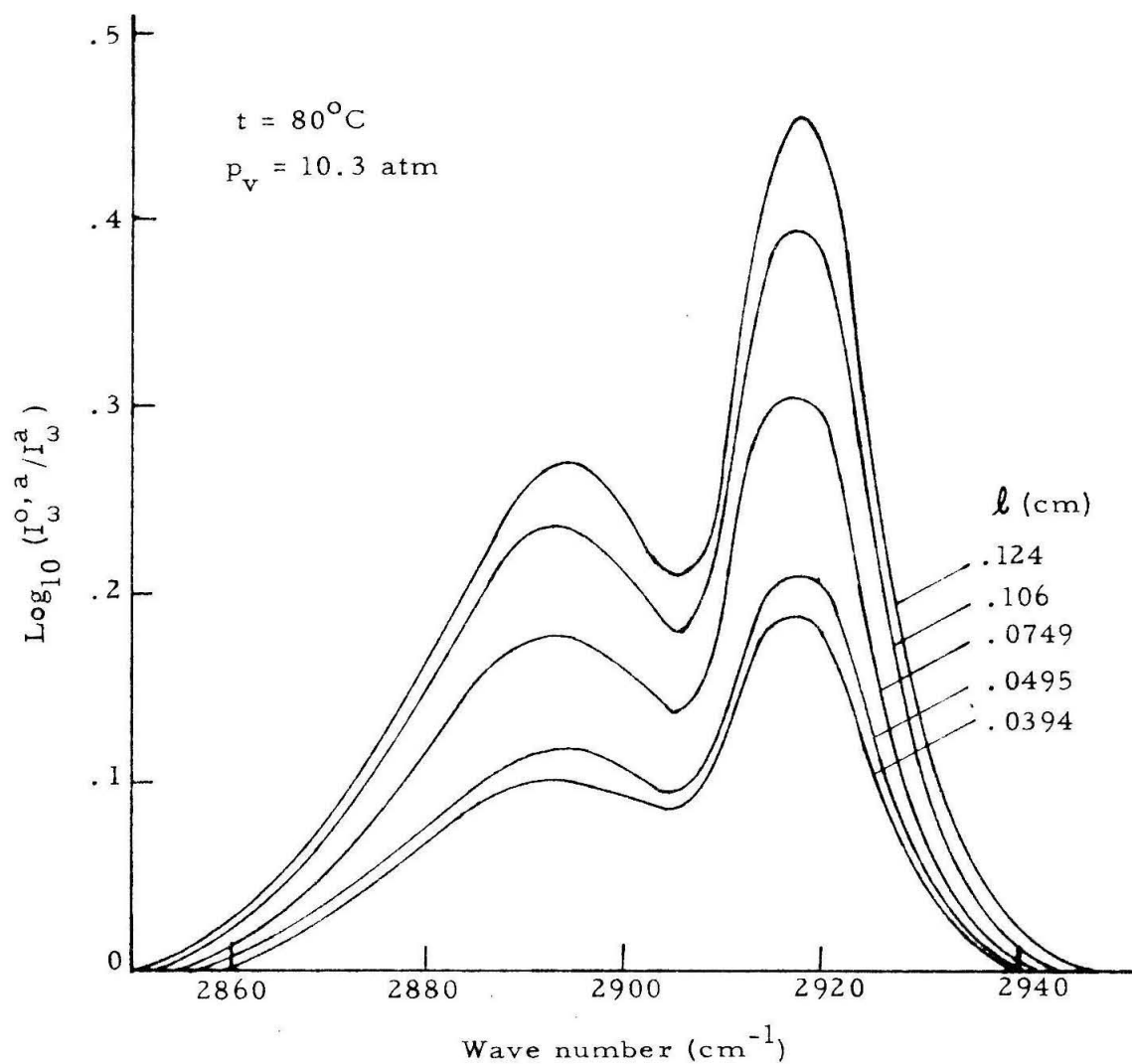
Fig. 28. Logarithm of the reciprocal of apparent spectral trans-
mission for the 2908 cm^{-1} band of NO_2 at various optical
depths.
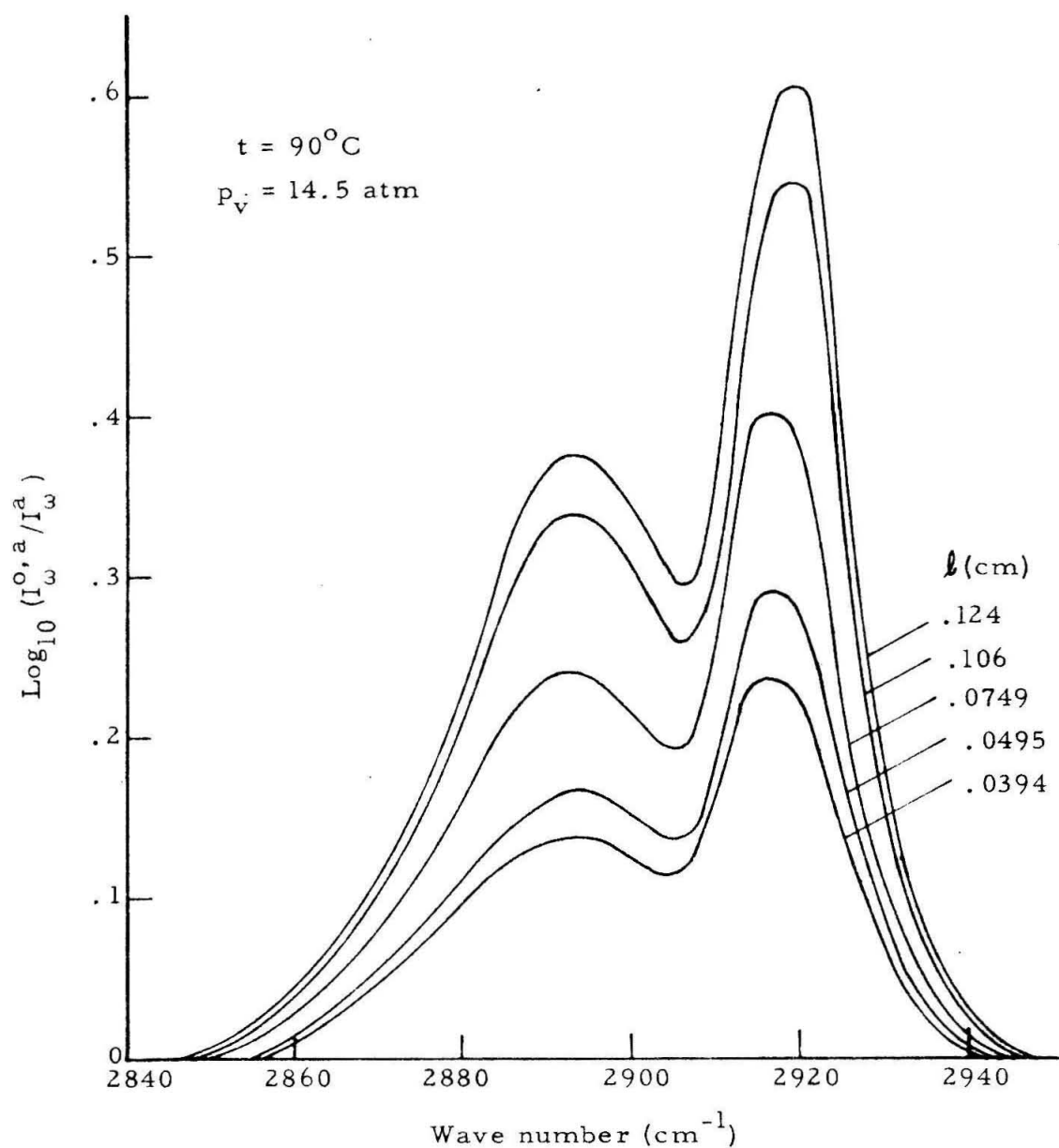
Fig. 29. Logarithm of the reciprocal of apparent spectral trans-
mission for the 2908 cm^{-1} band of NO_2 at various optical
depths.
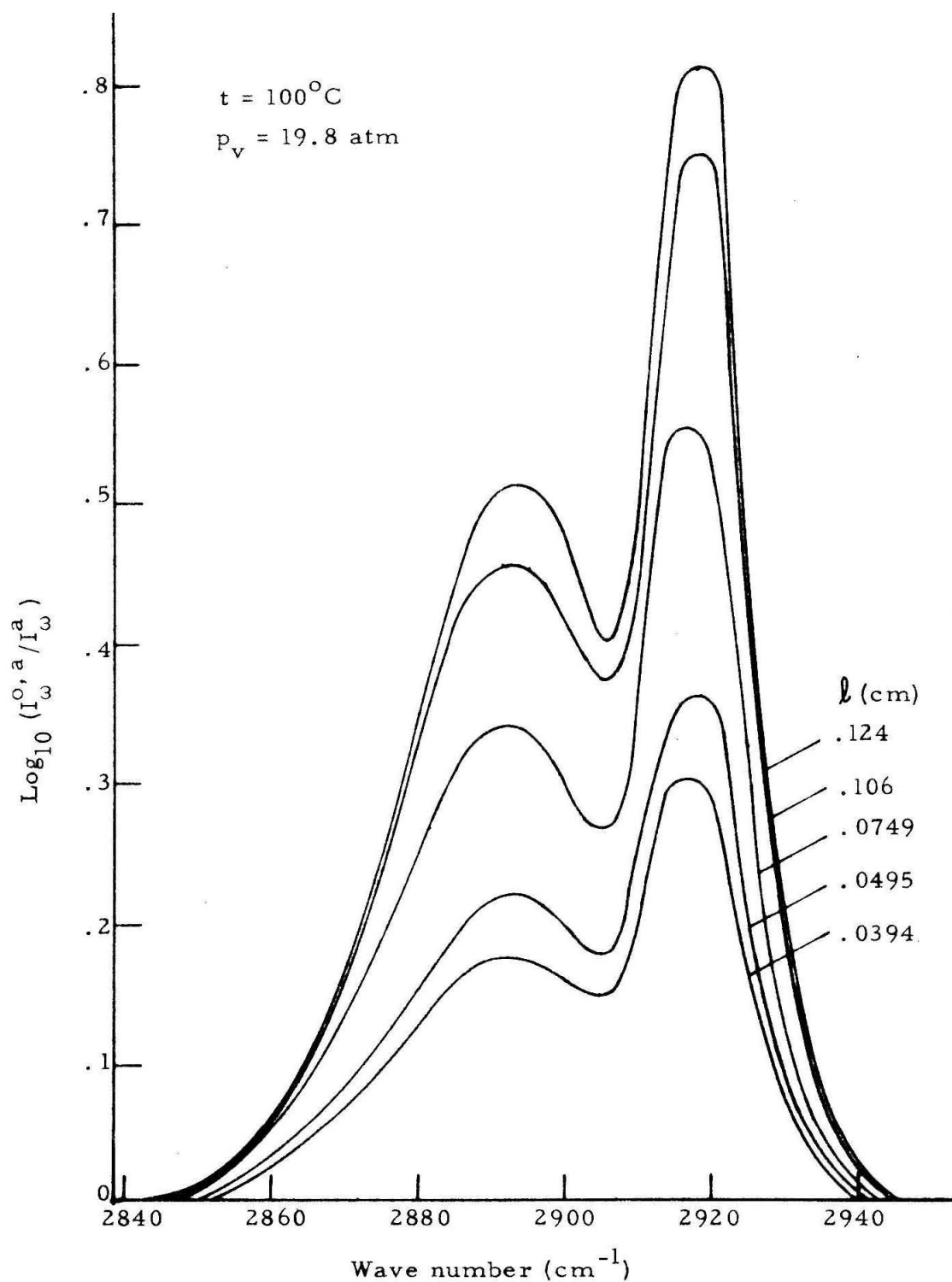
Fig. 30. Logarithm of the reciprocal of apparent spectral trans-
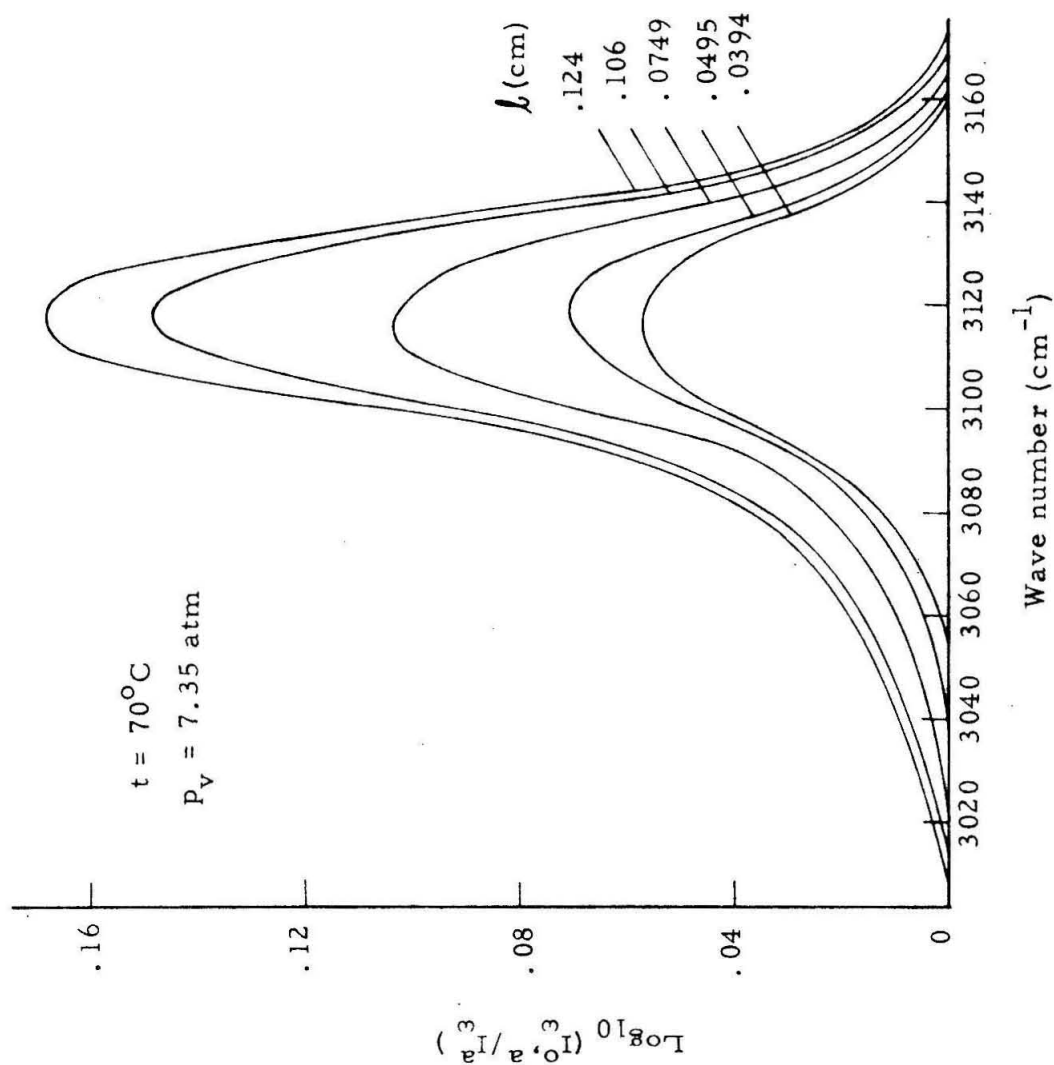mission for the 2908 cm^{-1} band of NO_2 at various optical
depths.
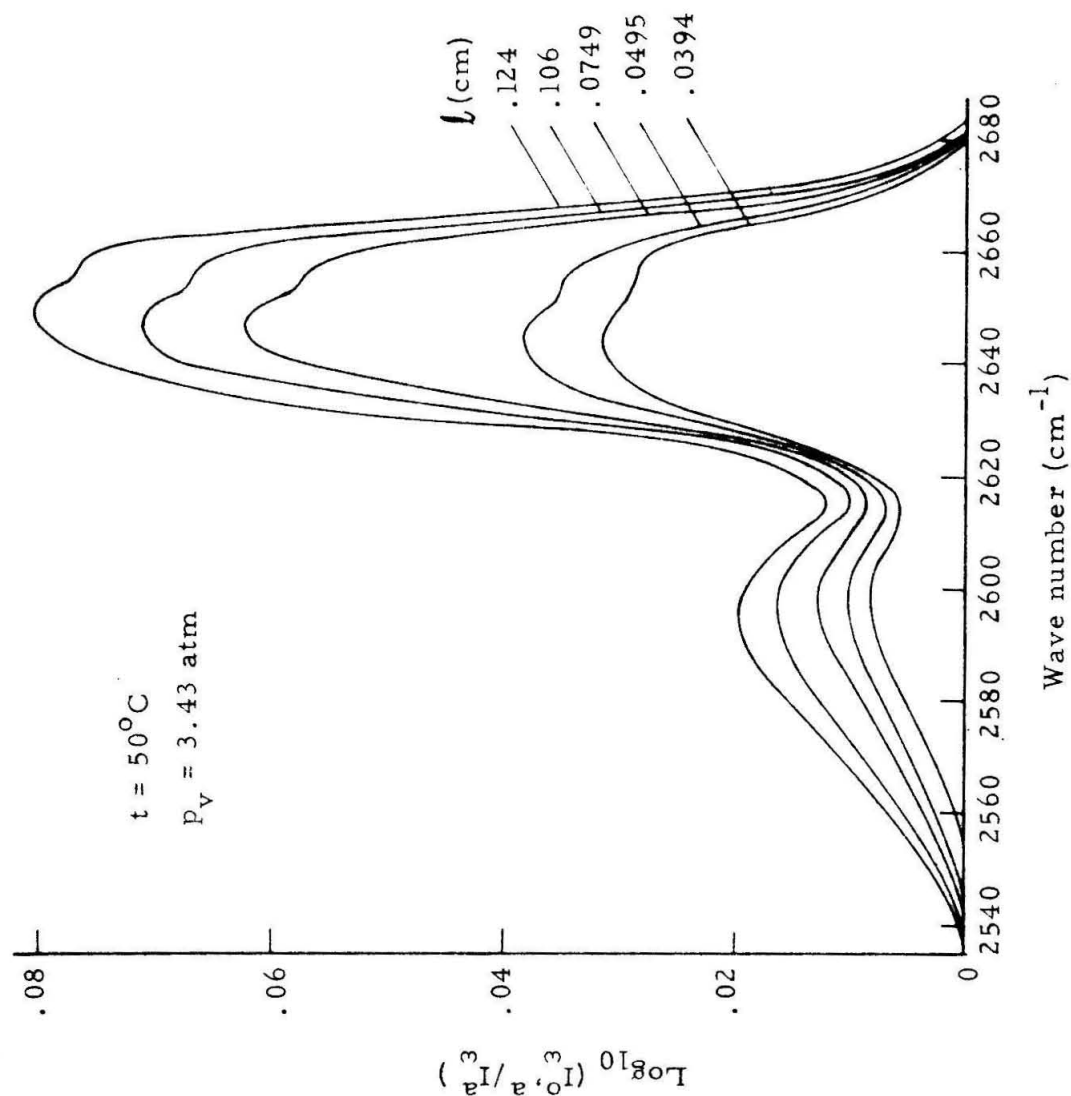
Fig. 31. Logarithm of the reciprocal of apparent spectral transmission for the 2618 cm^{-1} band of gaseous N_2O_4 at various optical depths.
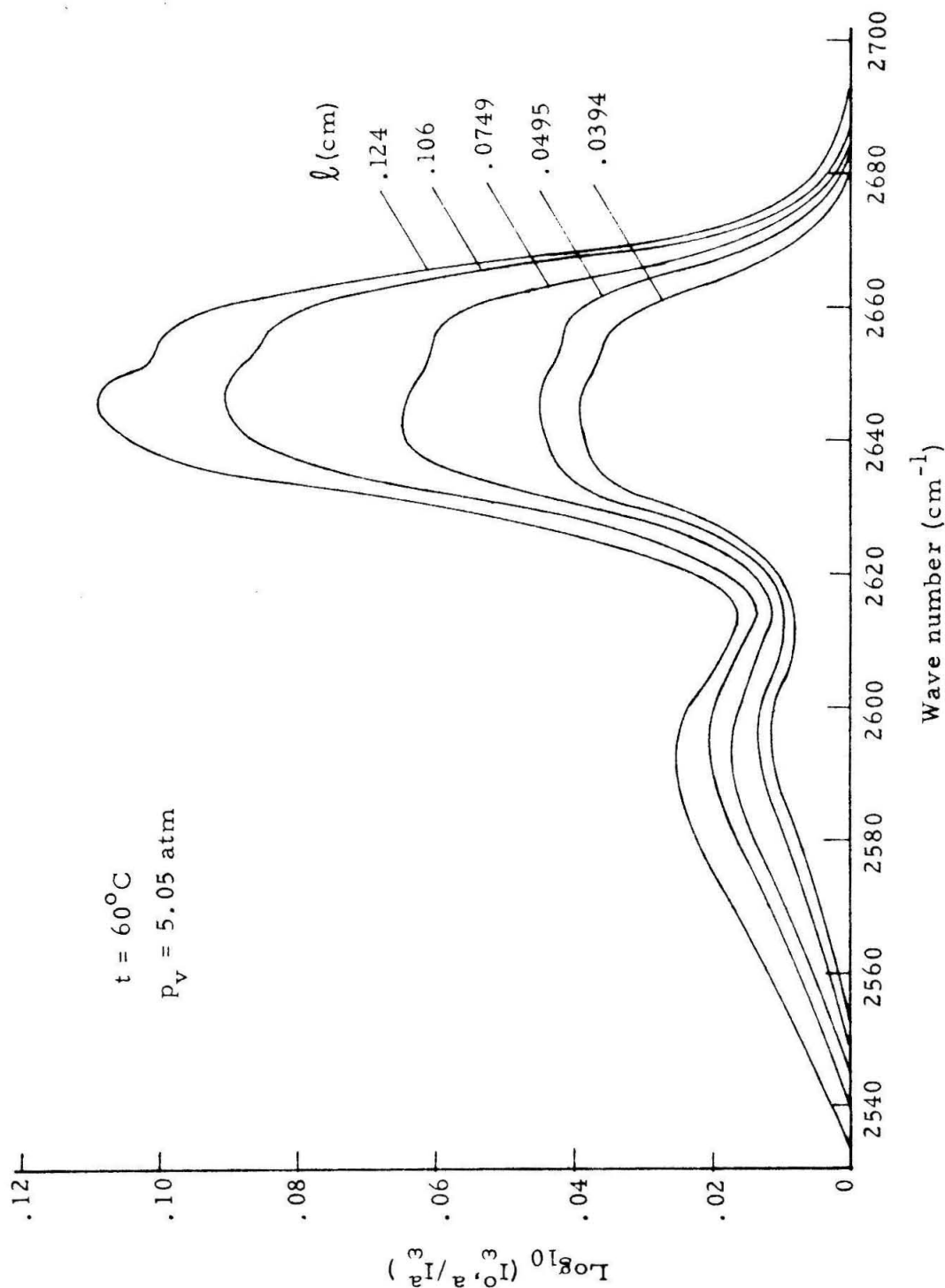
Fig. 32. Logarithm of the reciprocal of apparent spectral transmission for the 2618 cm^{-1} band of gaseous N_2O_4 at various optical depths.
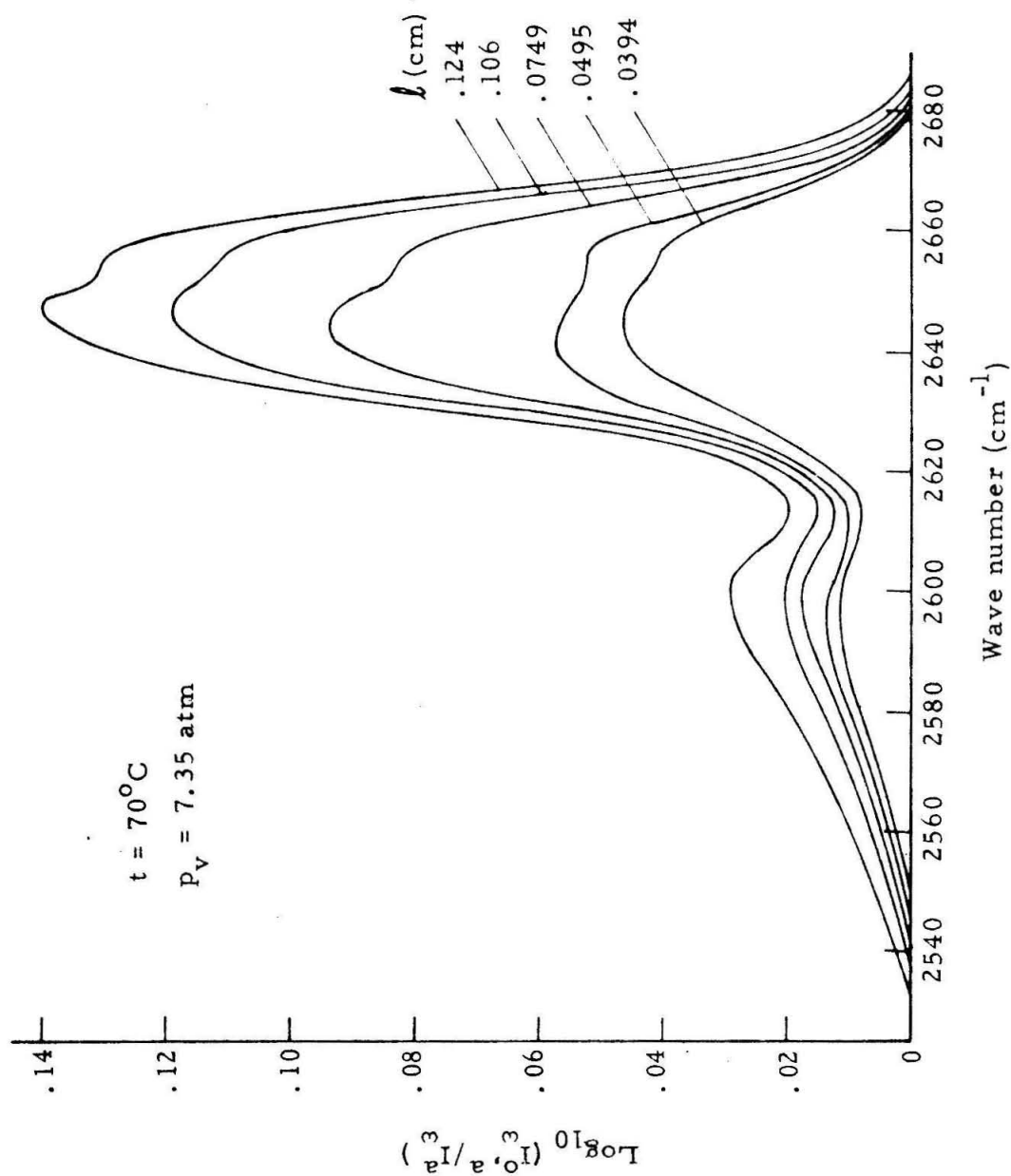
Fig. 33. Logarithm of the reciprocal of apparent spectral transmission for the 2618 cm^{-1} band of gaseous N_2O_4 at various optical depths.
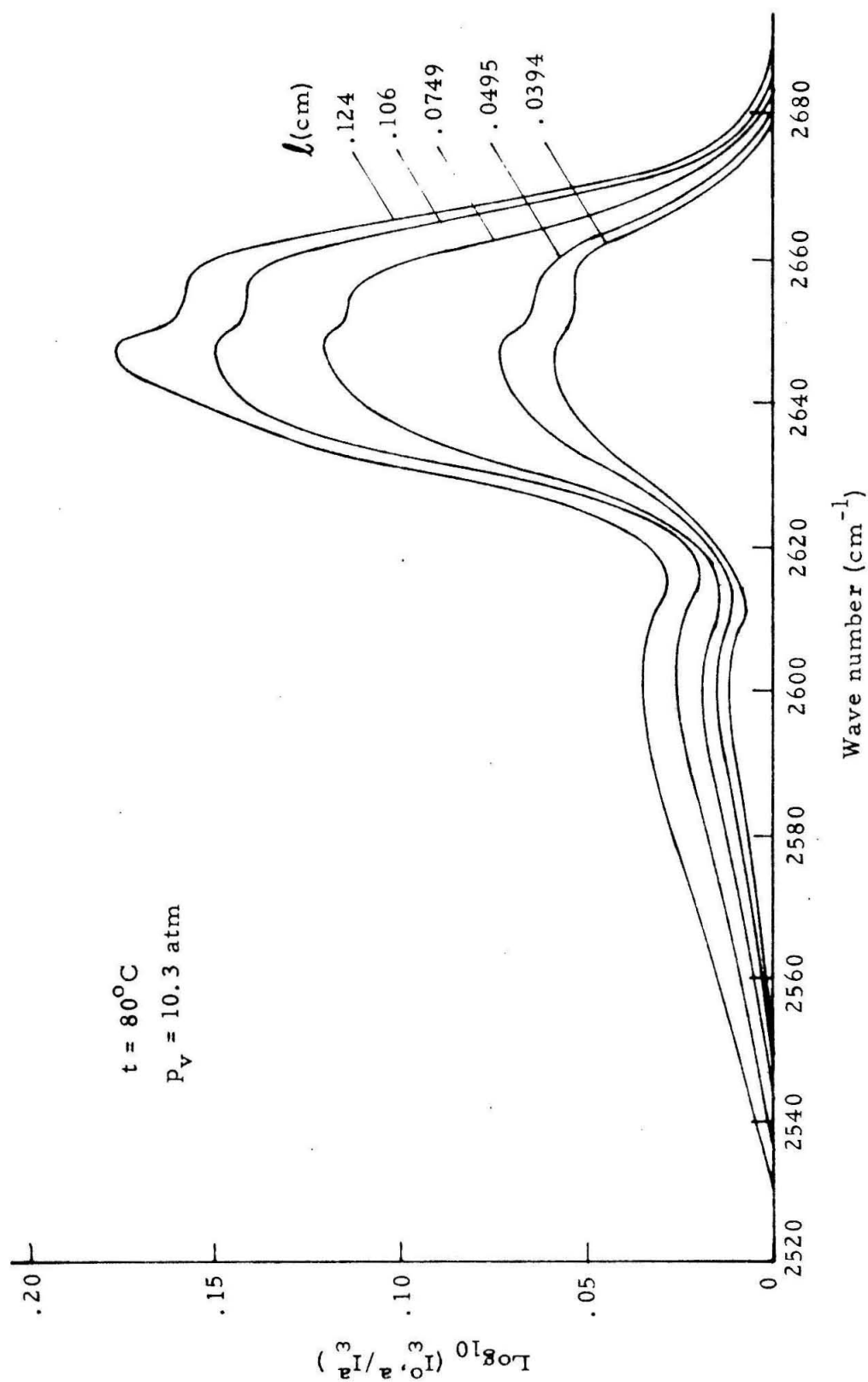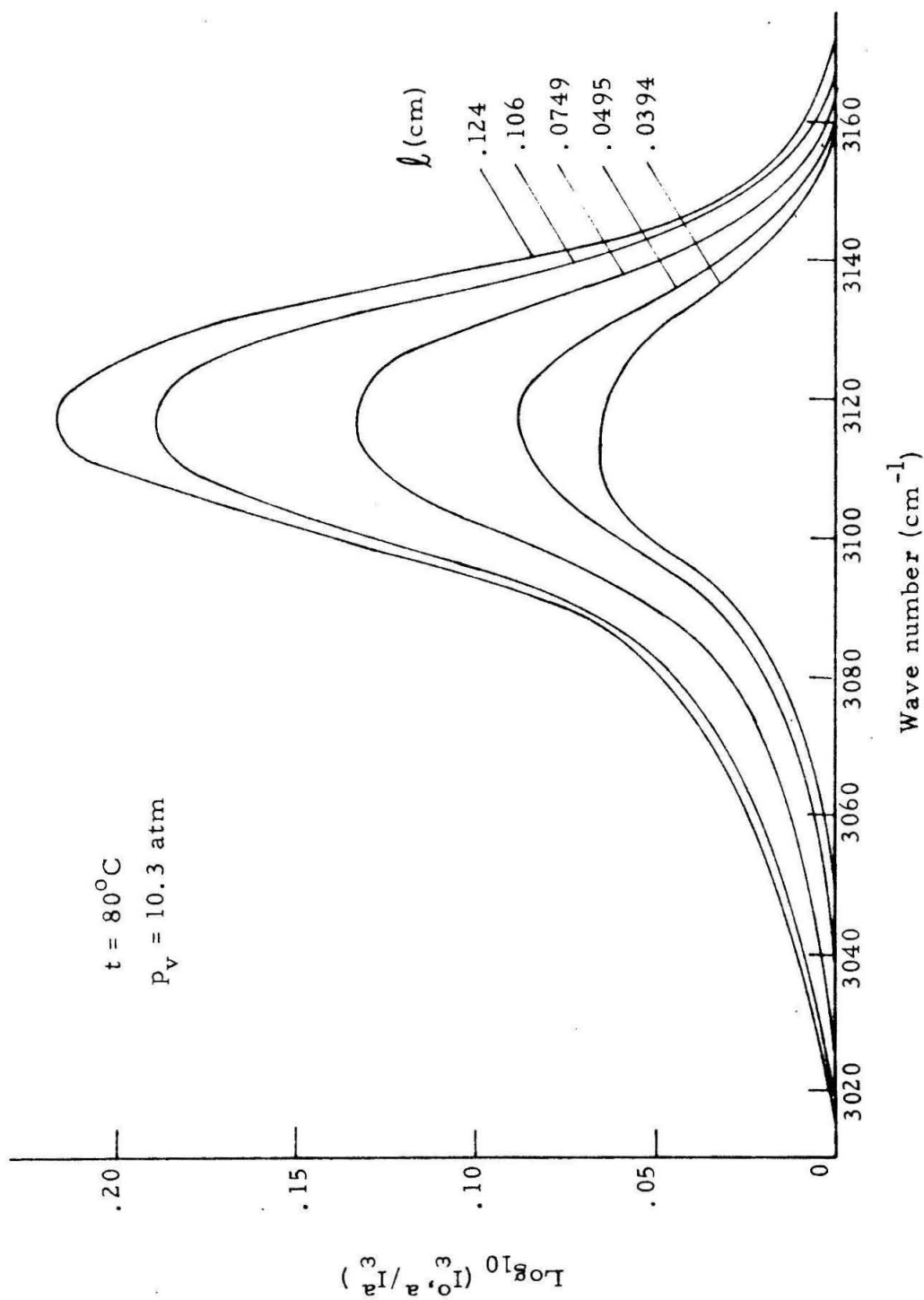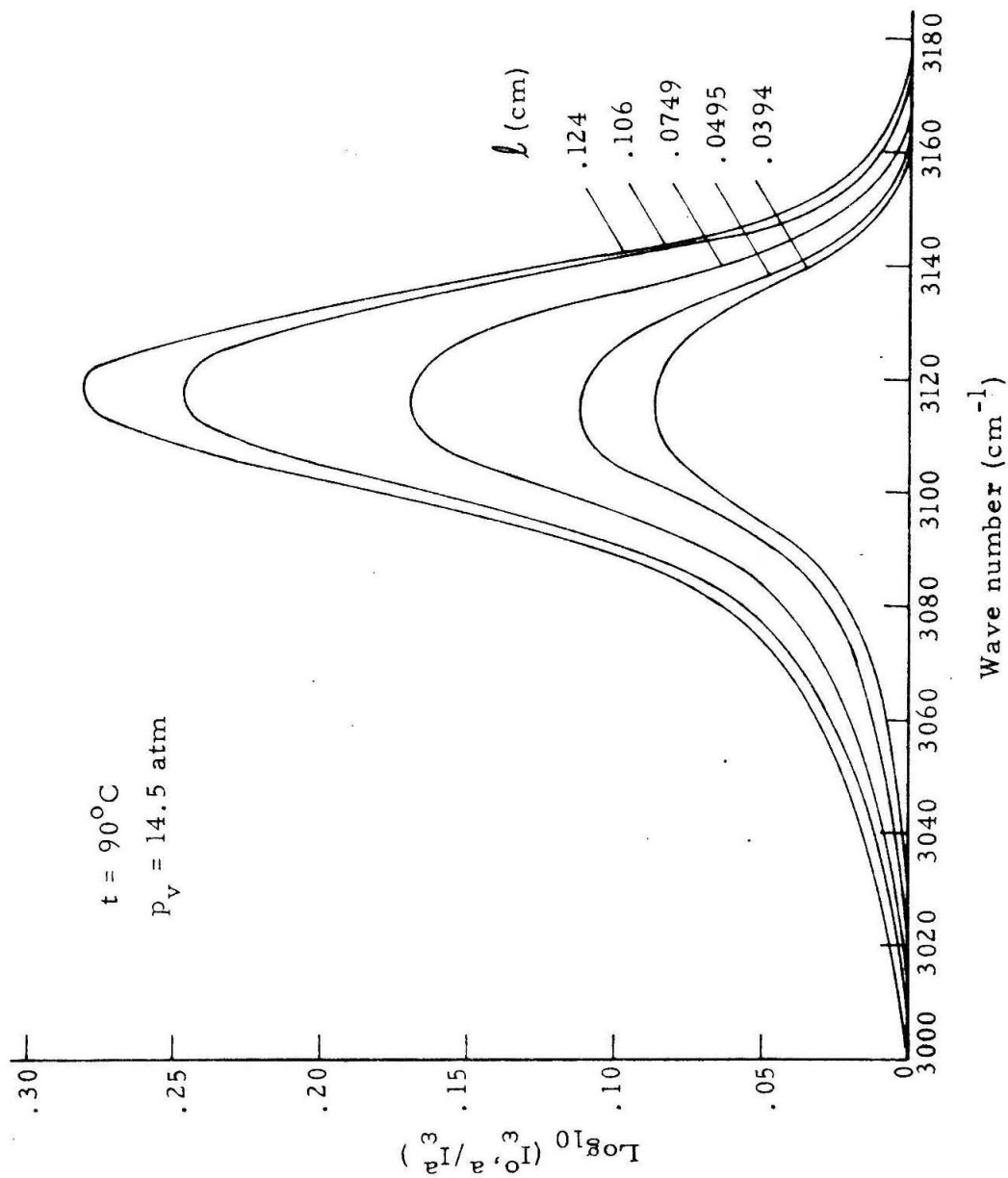
Fig. 34. Logarithm of the reciprocal of apparent spectral transmission for the 2618 cm^{-1} band of gaseous N_2O_4 at various optical depths.
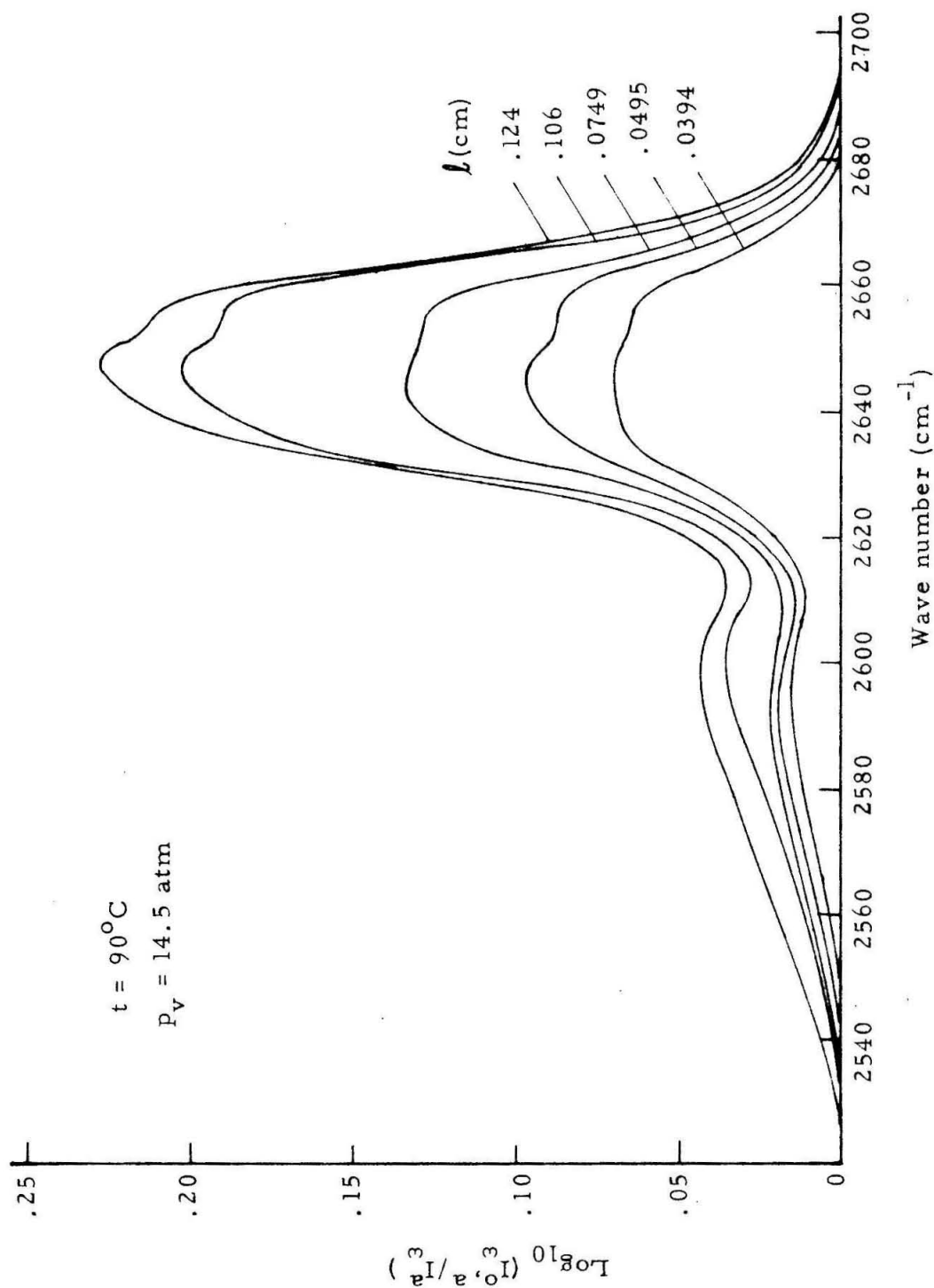
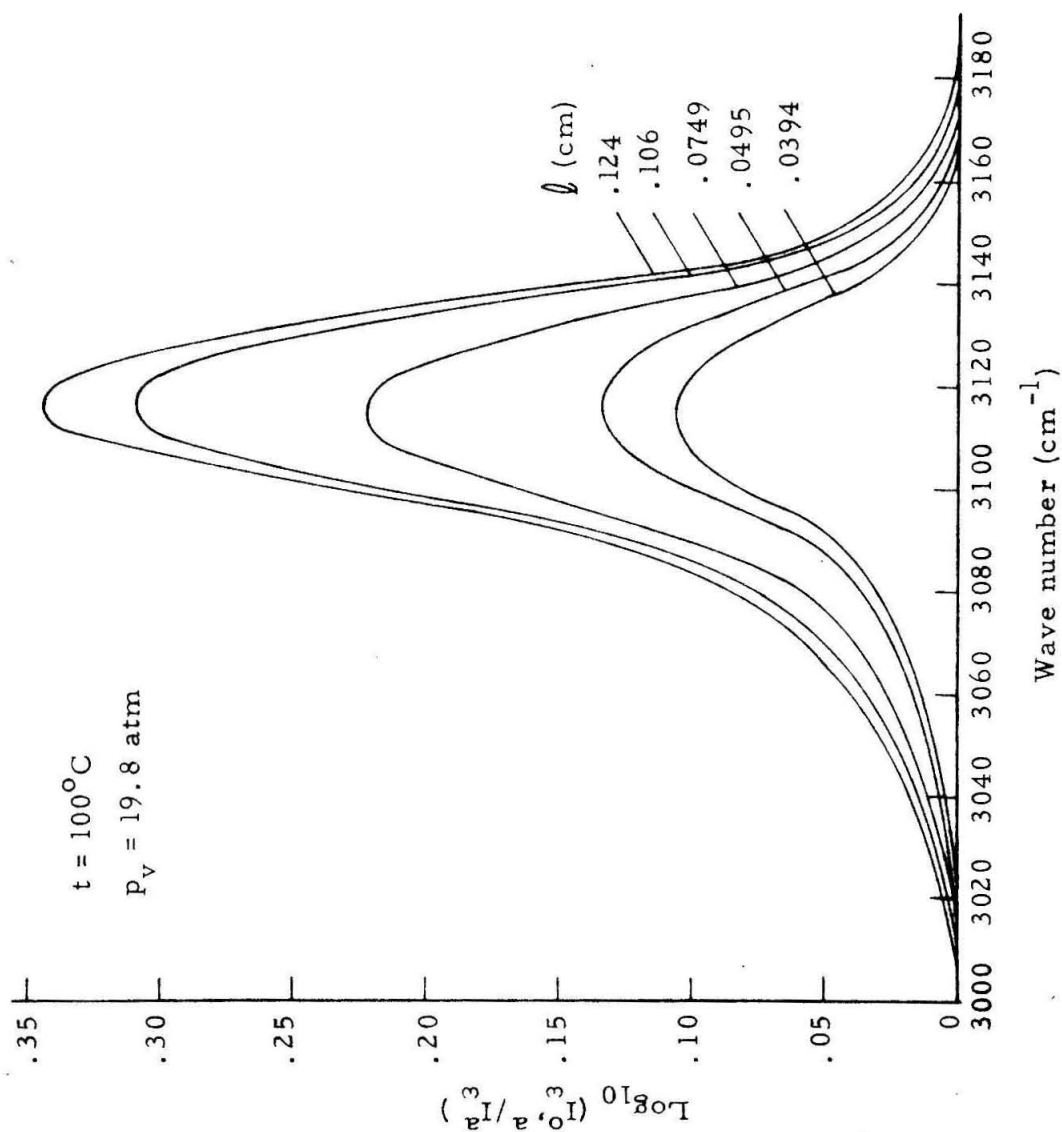Fig. 35. Logarithm of the reciprocal of apparent spectral transmission for the 2618 cm^{-1} band of gaseous N_2O_4 at various optical depths.
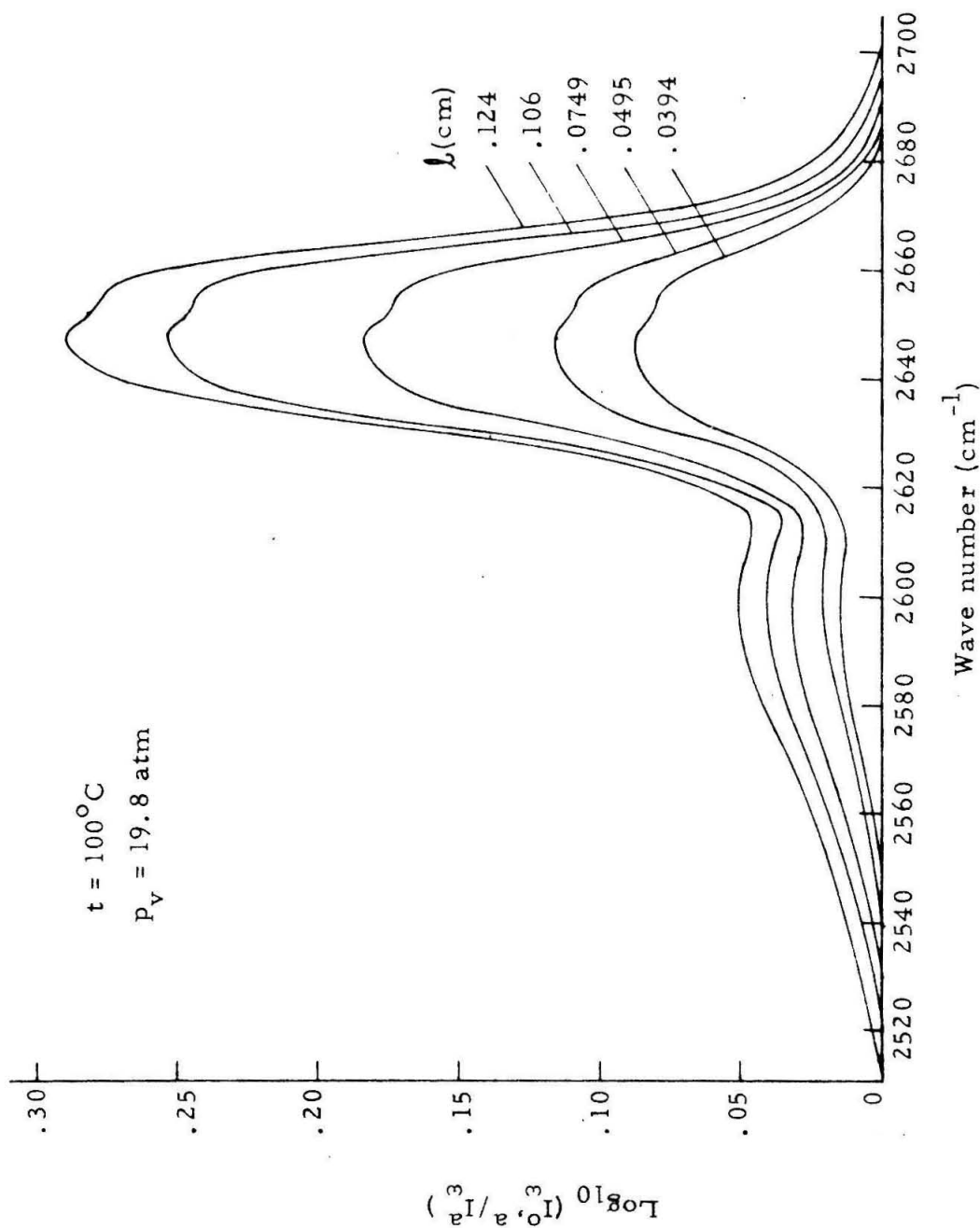
Fig. 36. Logarithm of the reciprocal of apparent spectral transmission for the 2618 cm^{-1} band of gaseous N_2O_4 at various optical depths.
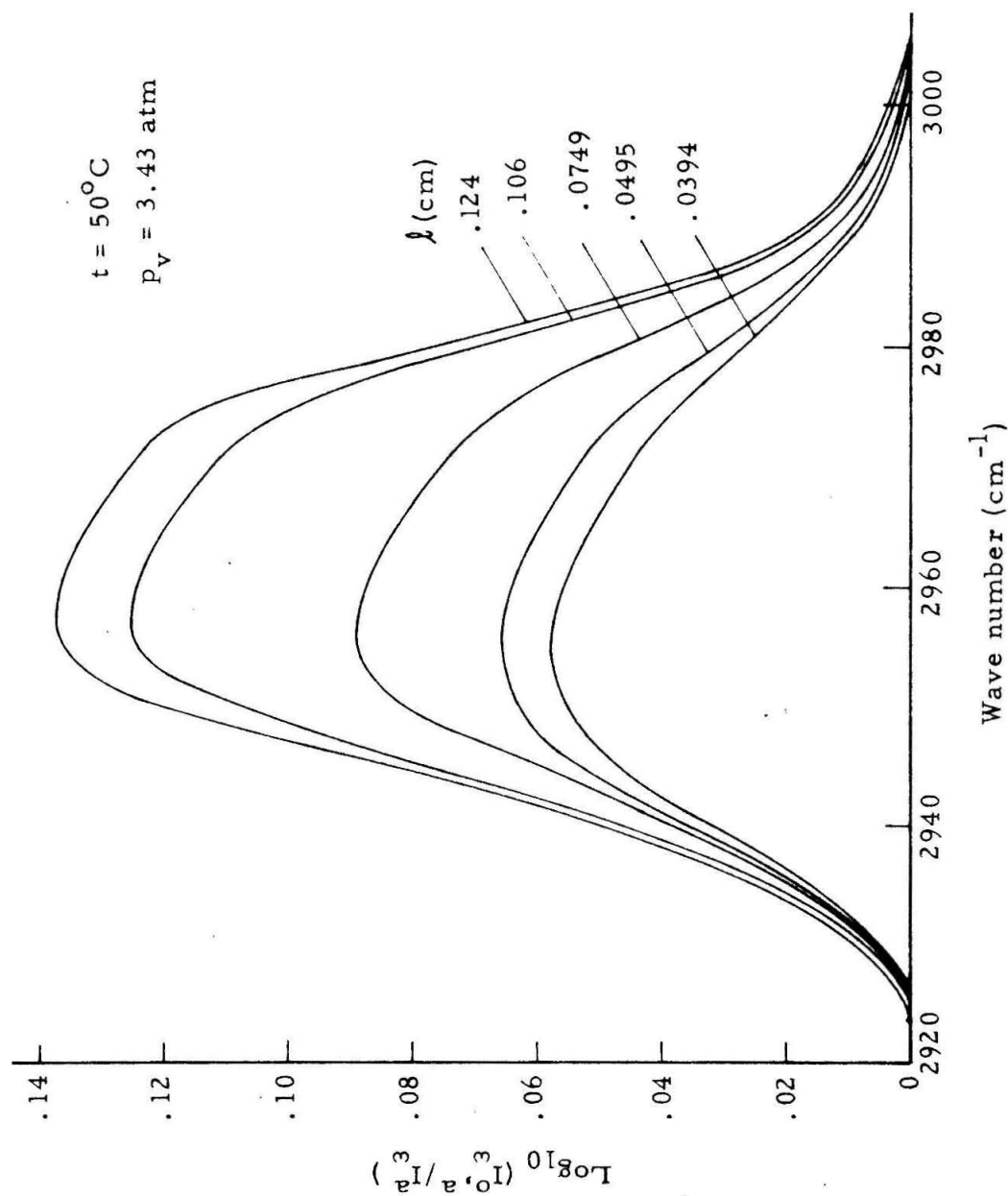
Fig. 37. Logarithm of the reciprocal of apparent spectral transmission for the 2962 cm^{-1} band of gaseous N_2O_4 at various optical depths.
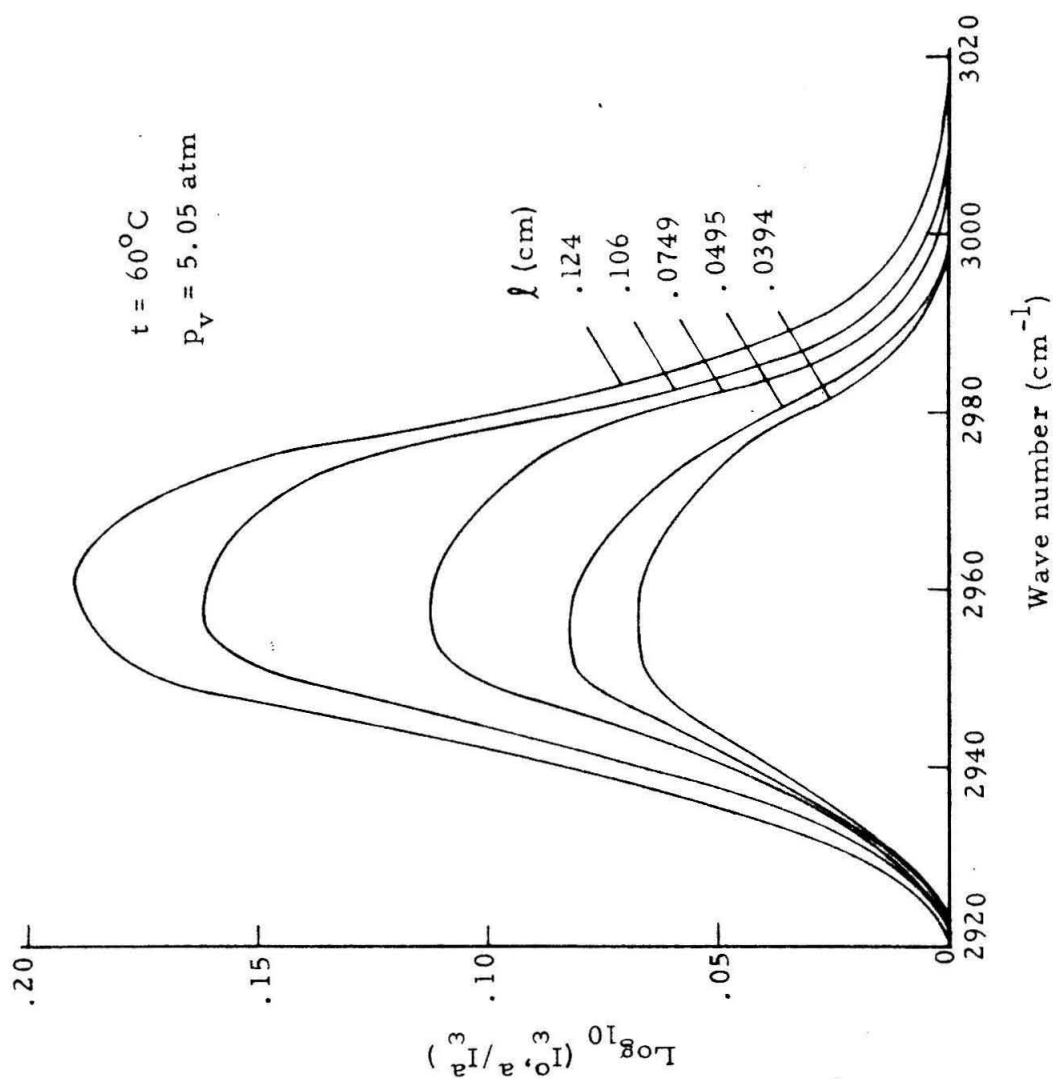
Fig. 38. Logarithm of the reciprocal of apparent spectral transmission for the 2962 cm^{-1} band of gaseous N_2O_4 at various optical depths.
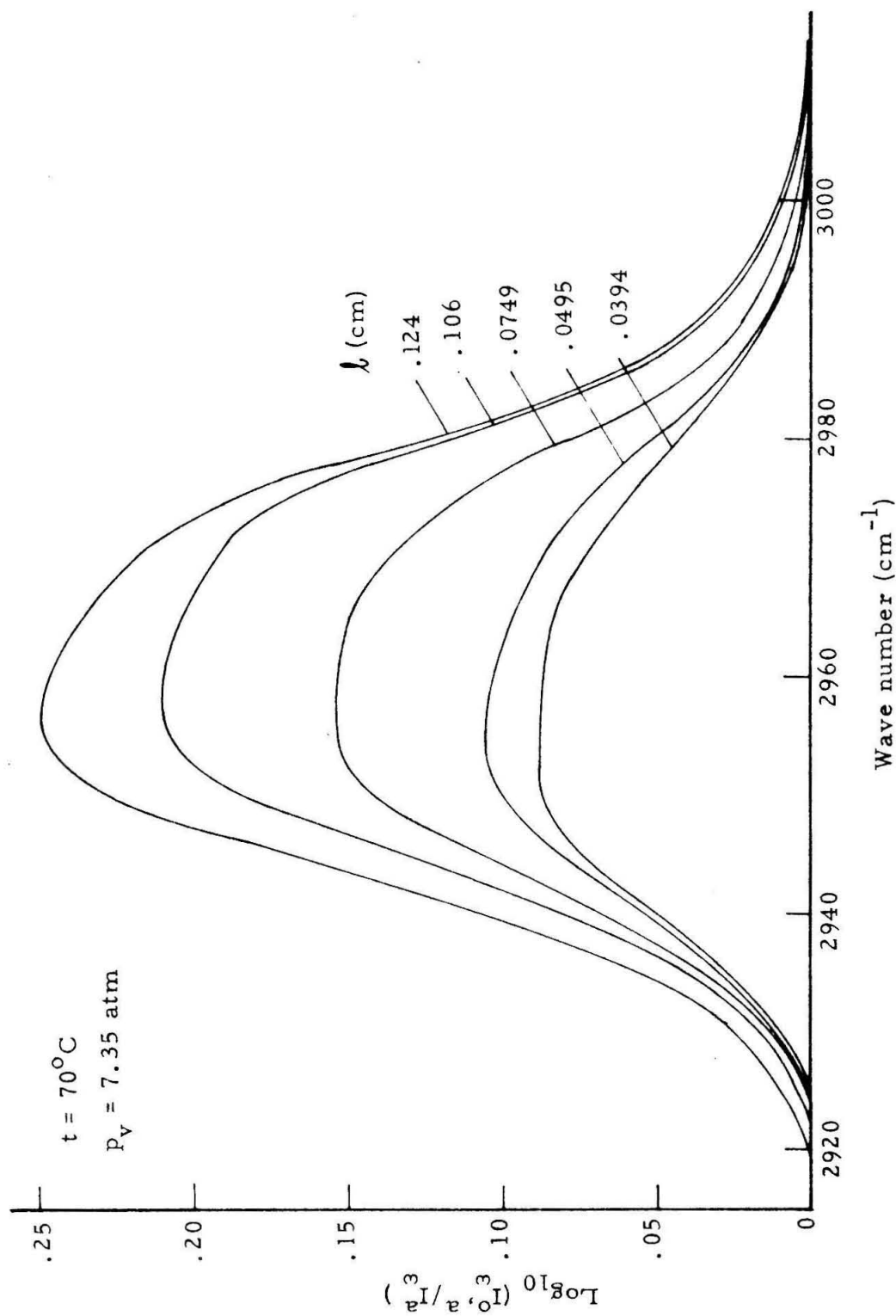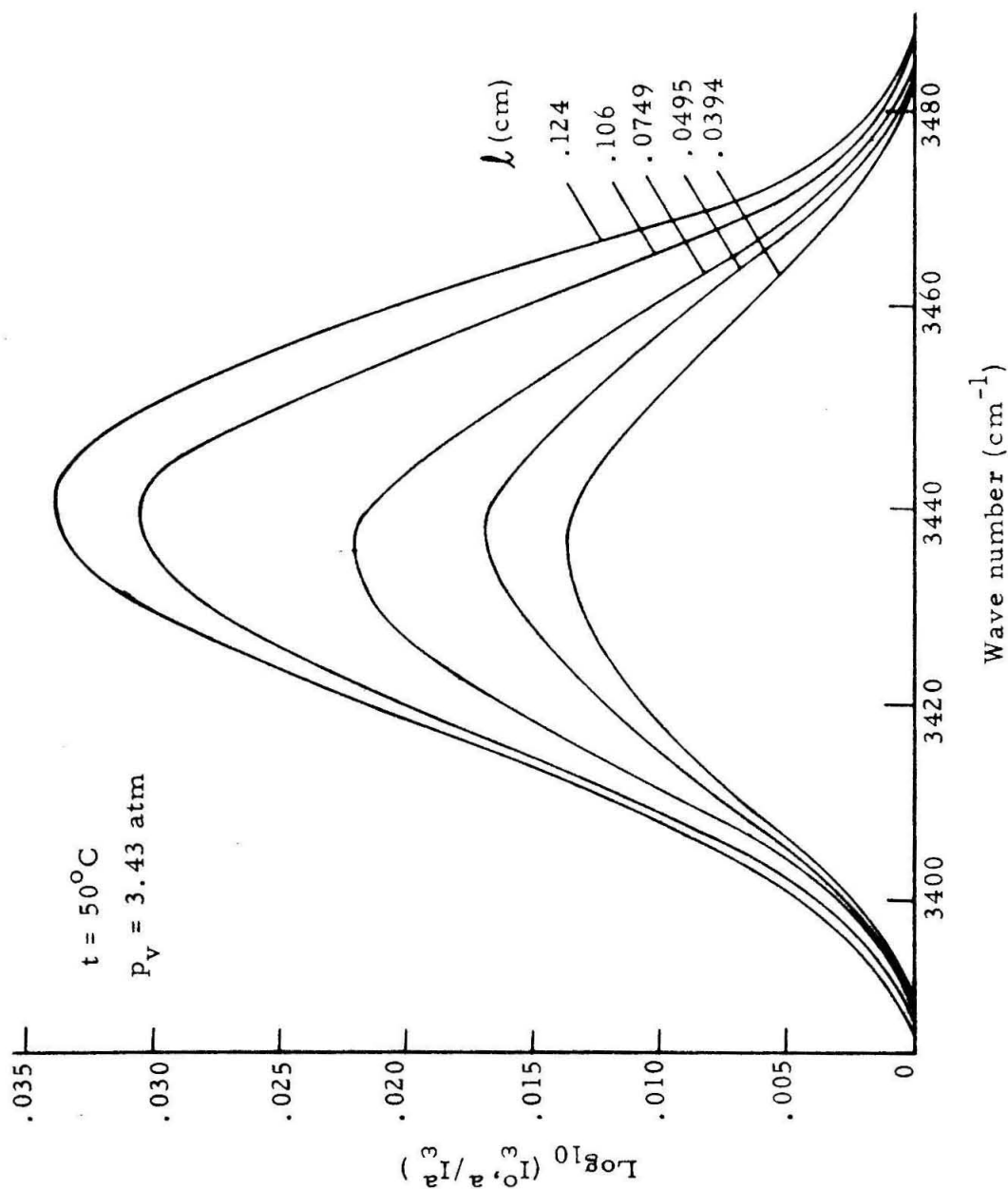
Fig. 39. Logarithm of the reciprocal of apparent spectral transmission for the 2962 cm^{-1} band of gaseous N_2O_4 at various optical depths.
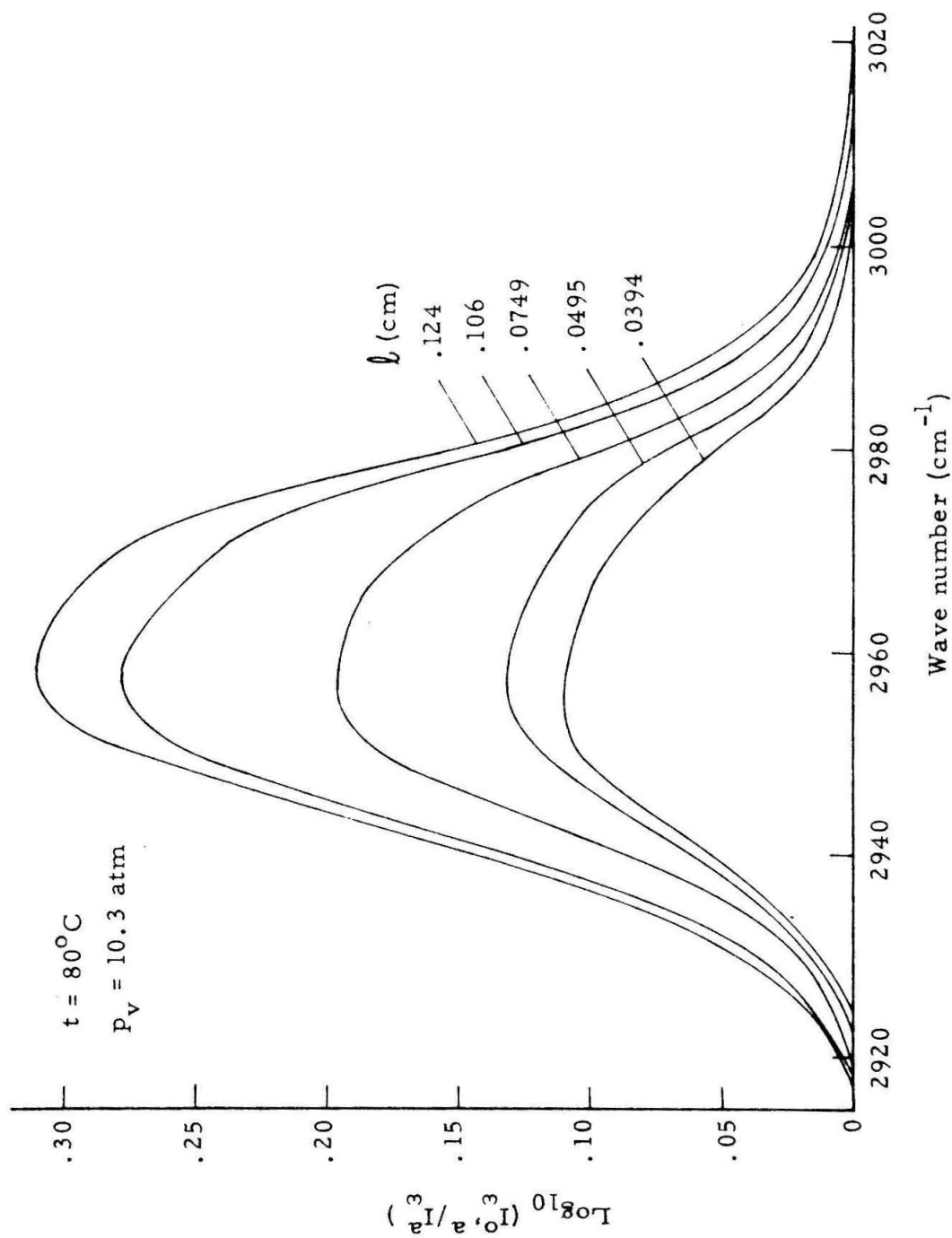
Fig. 40. Logarithm of the reciprocal of apparent spectral transmission for the 2962 cm^{-1} band of gaseous N_2O_4 at various optical depths.
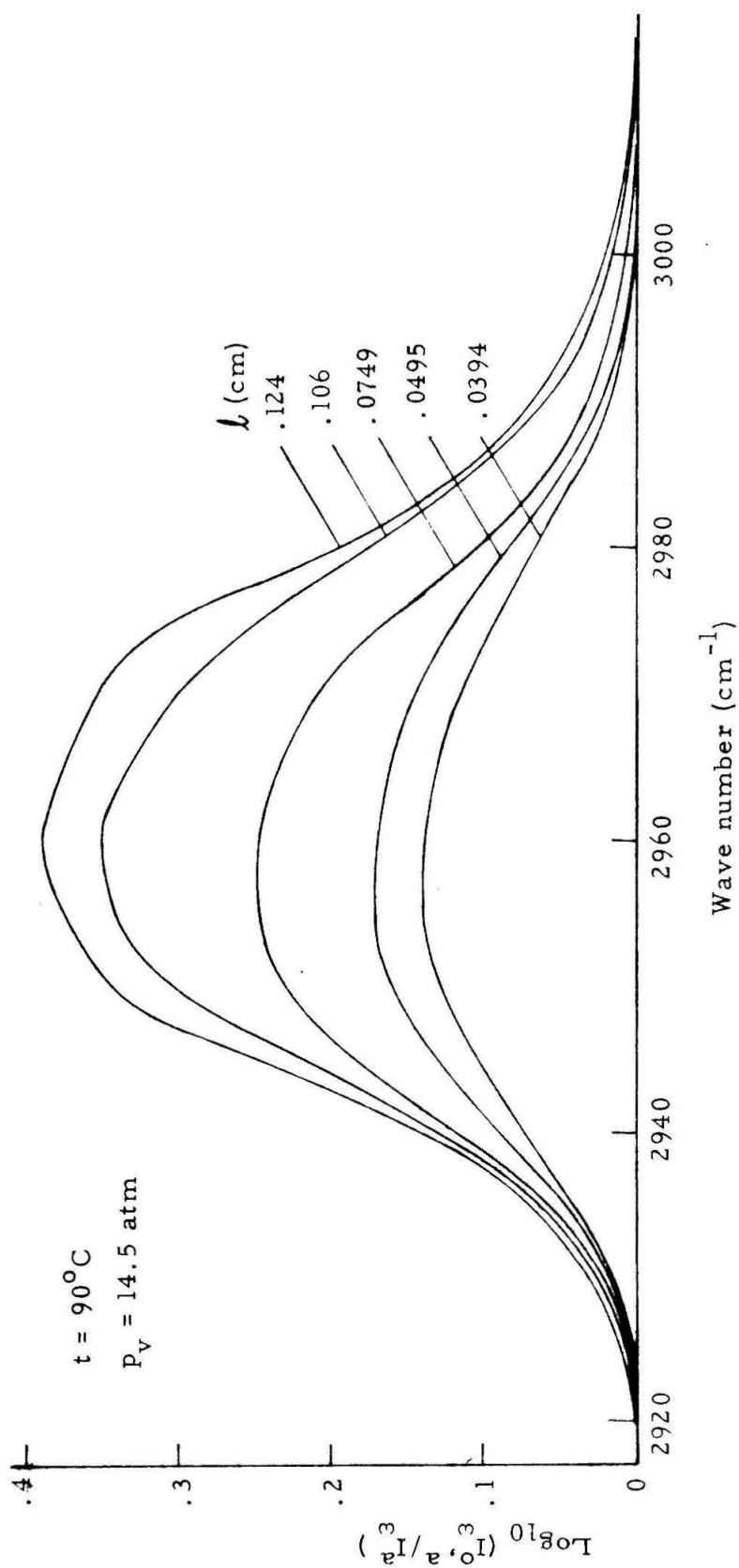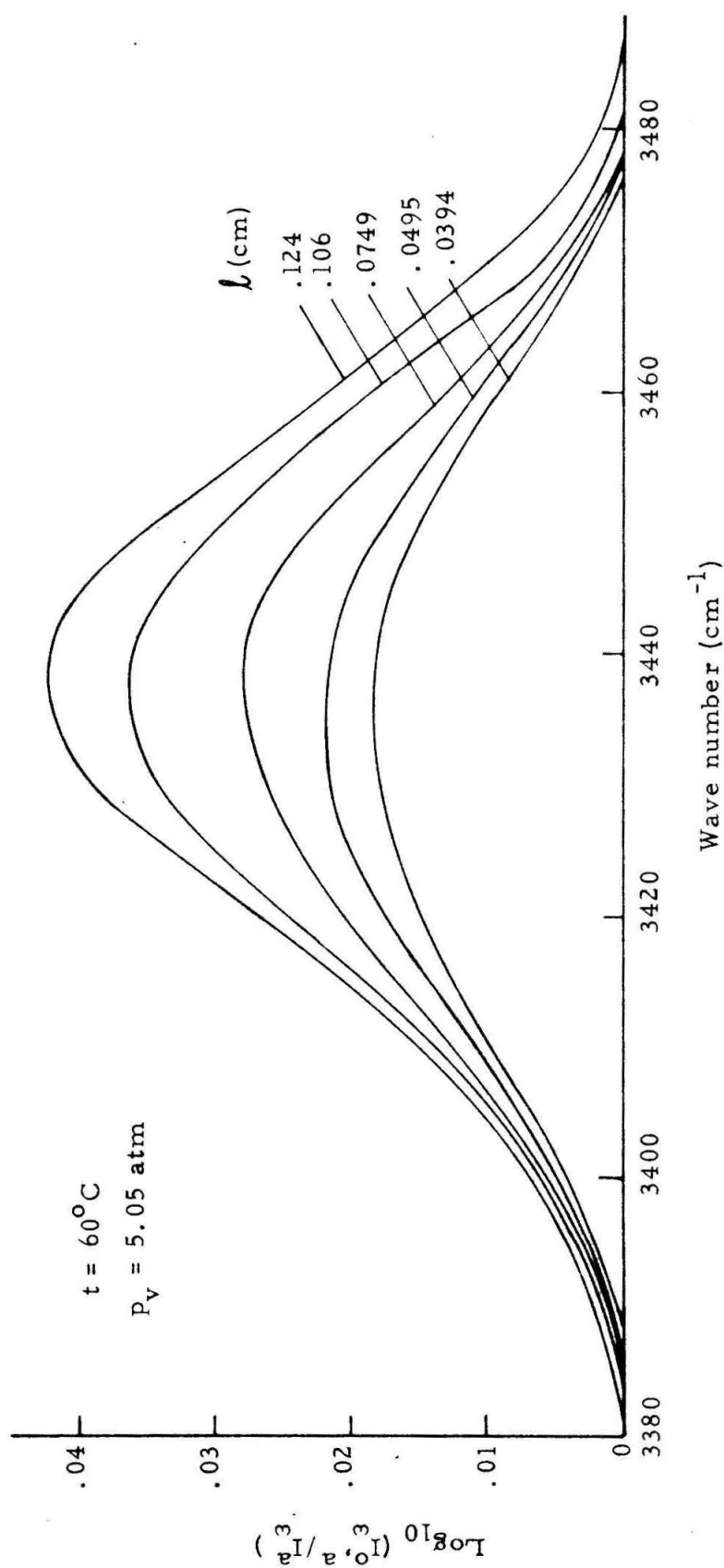
Fig. 41. Logarithm of the reciprocal of apparent spectral transmission for the 2962 cm^{-1} band of gaseous N_2O_4 at various optical depths.
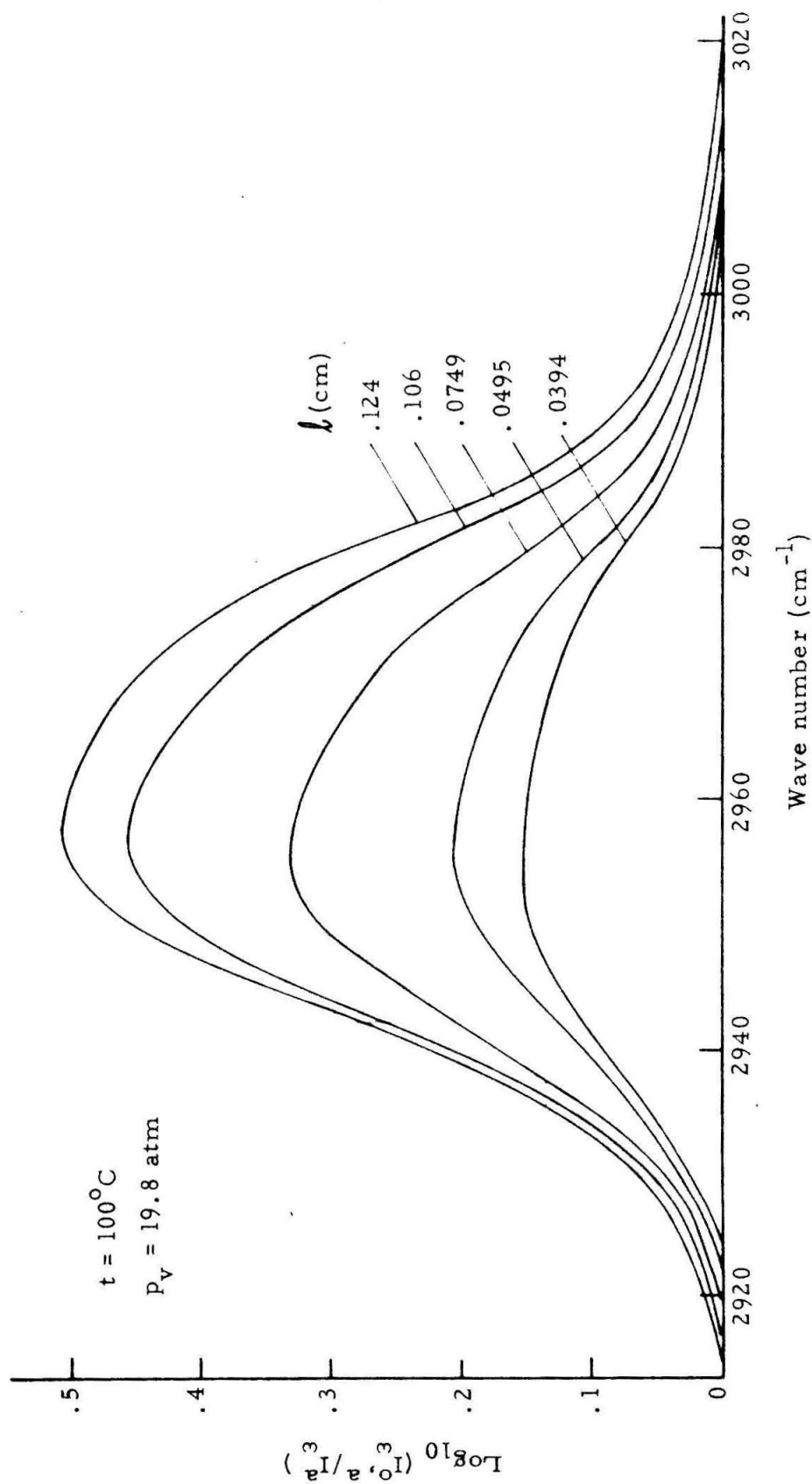
Fig. 42. Logarithm of the reciprocal of apparent spectral transmission for the 2962 cm^{-1} band of gaseous N_2O_4 at various optical depths.
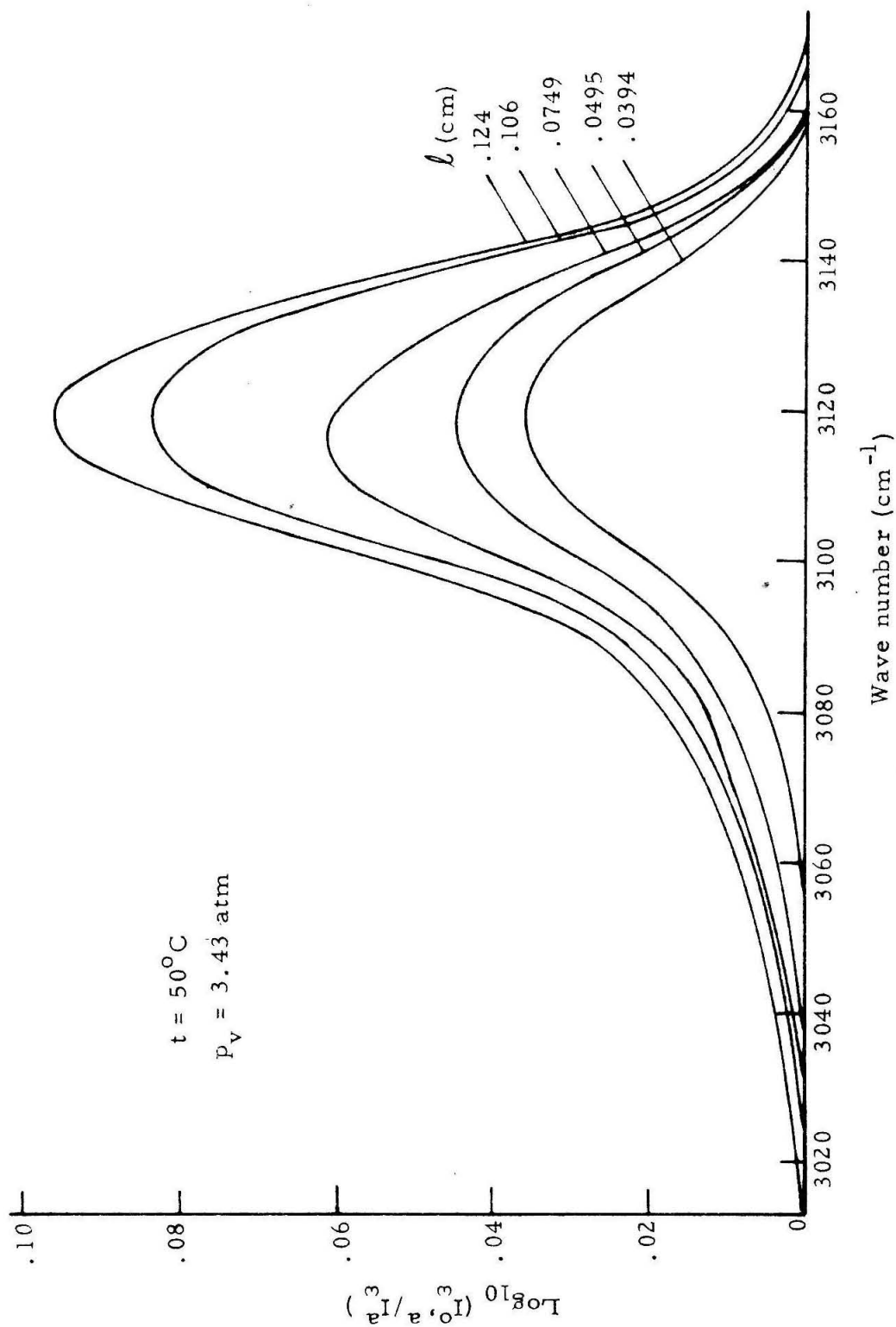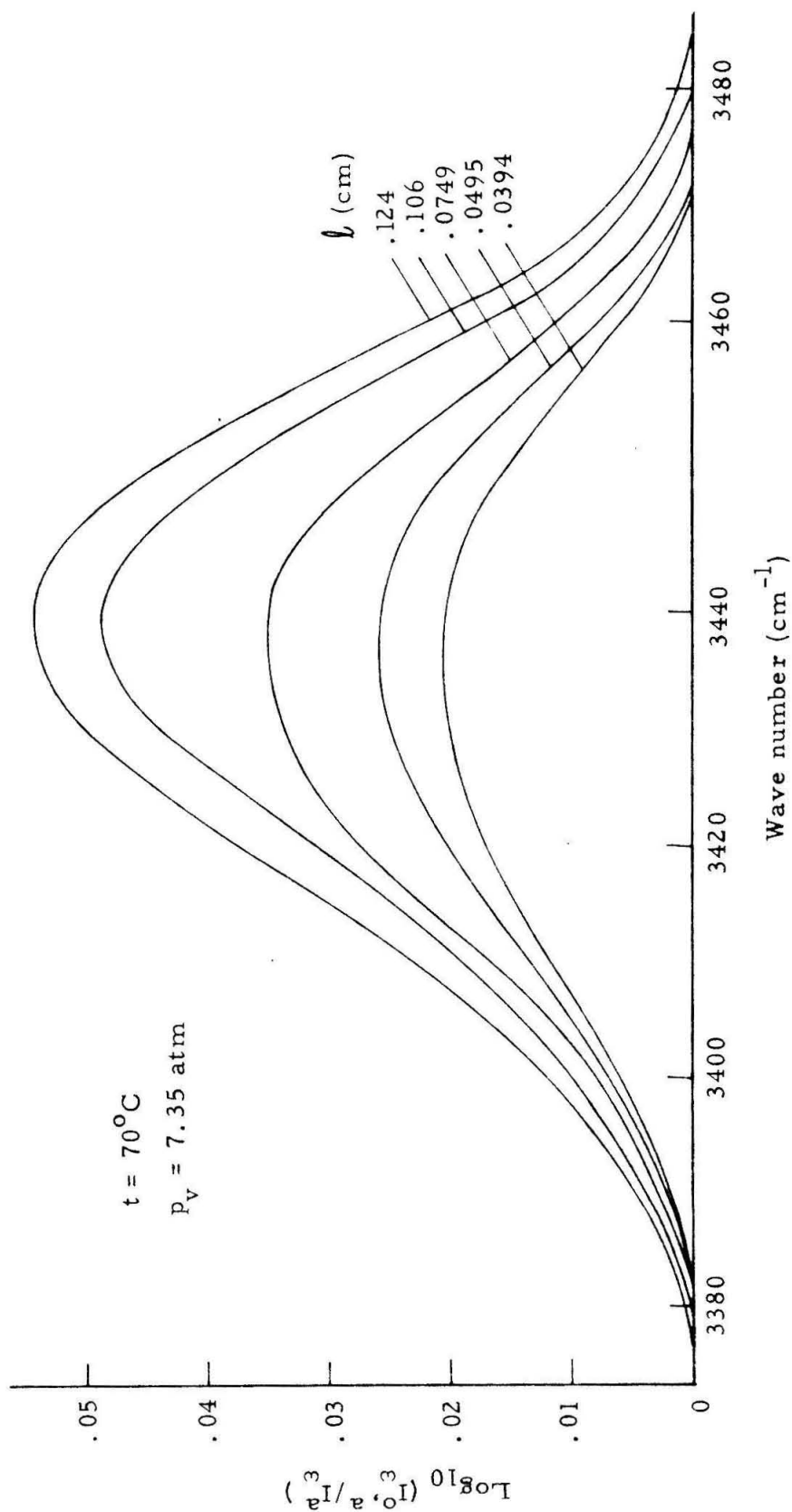
Fig. 43. Logarithm of the reciprocal of apparent spectral transmission for the 3120 cm^{-1} band of gaseous N_2O_4 at various optical depths.
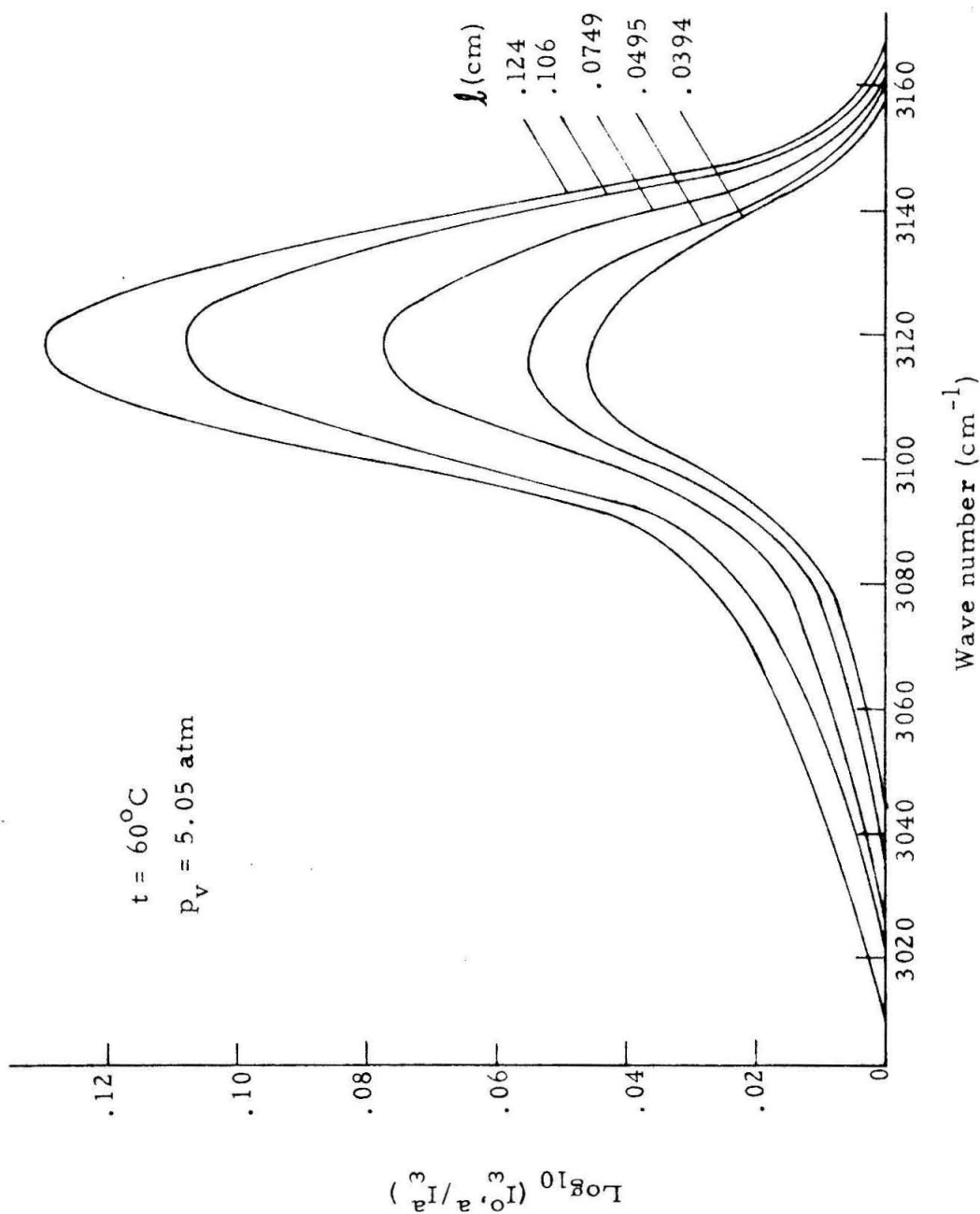
Fig. 44. Logarithm of the reciprocal of apparent spectral transmission for the 3120 cm^{-1} band of gaseous N_2O_4 at various optical depths.
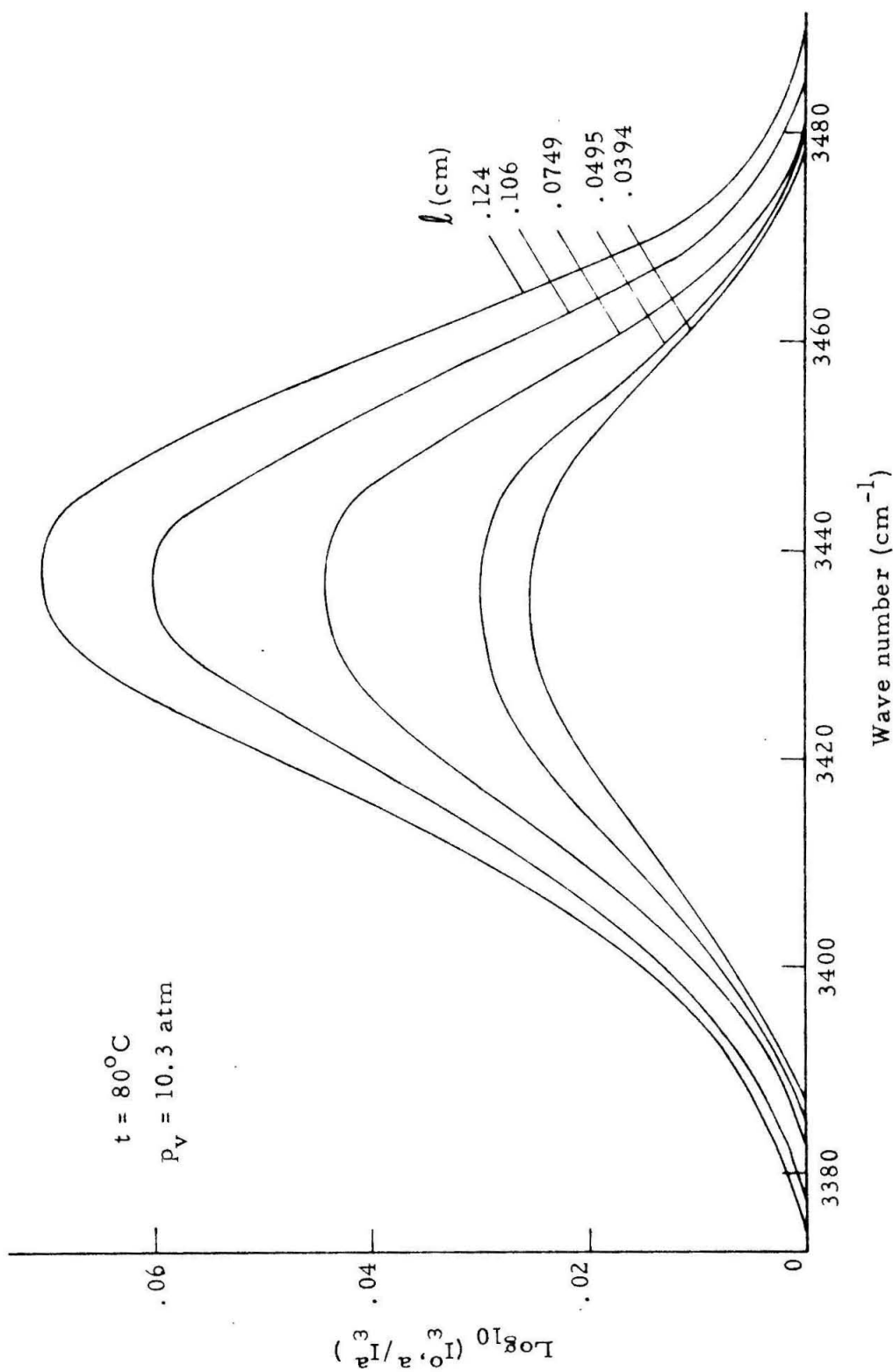
Fig. 45. Logarithm of the reciprocal of apparent spectral transmission for the 3120 cm^{-1} band of gaseous N_2O_4 at various optioal depths.

Fig. 46. Logarithm of the reciprocal of apparent spectral transmission for the 3120 cm^{-1} band of gaseous N_2O_4 at various optical depths.
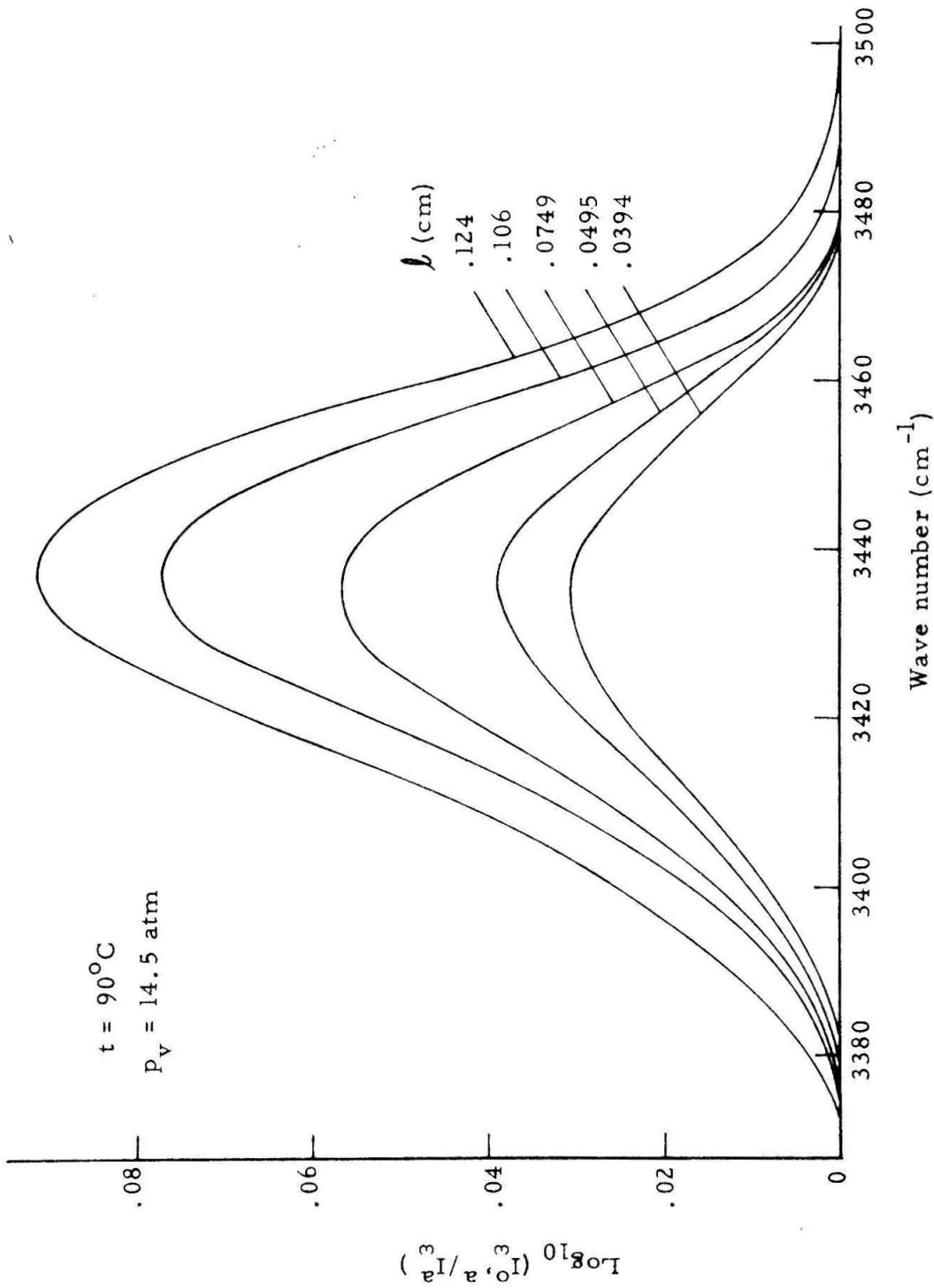
Fig. 47. Logarithm of the reciprocal of apparent spectral transmission for the 3120 cm^{-1} band of gaseous N_2O_4 at various optical depths.
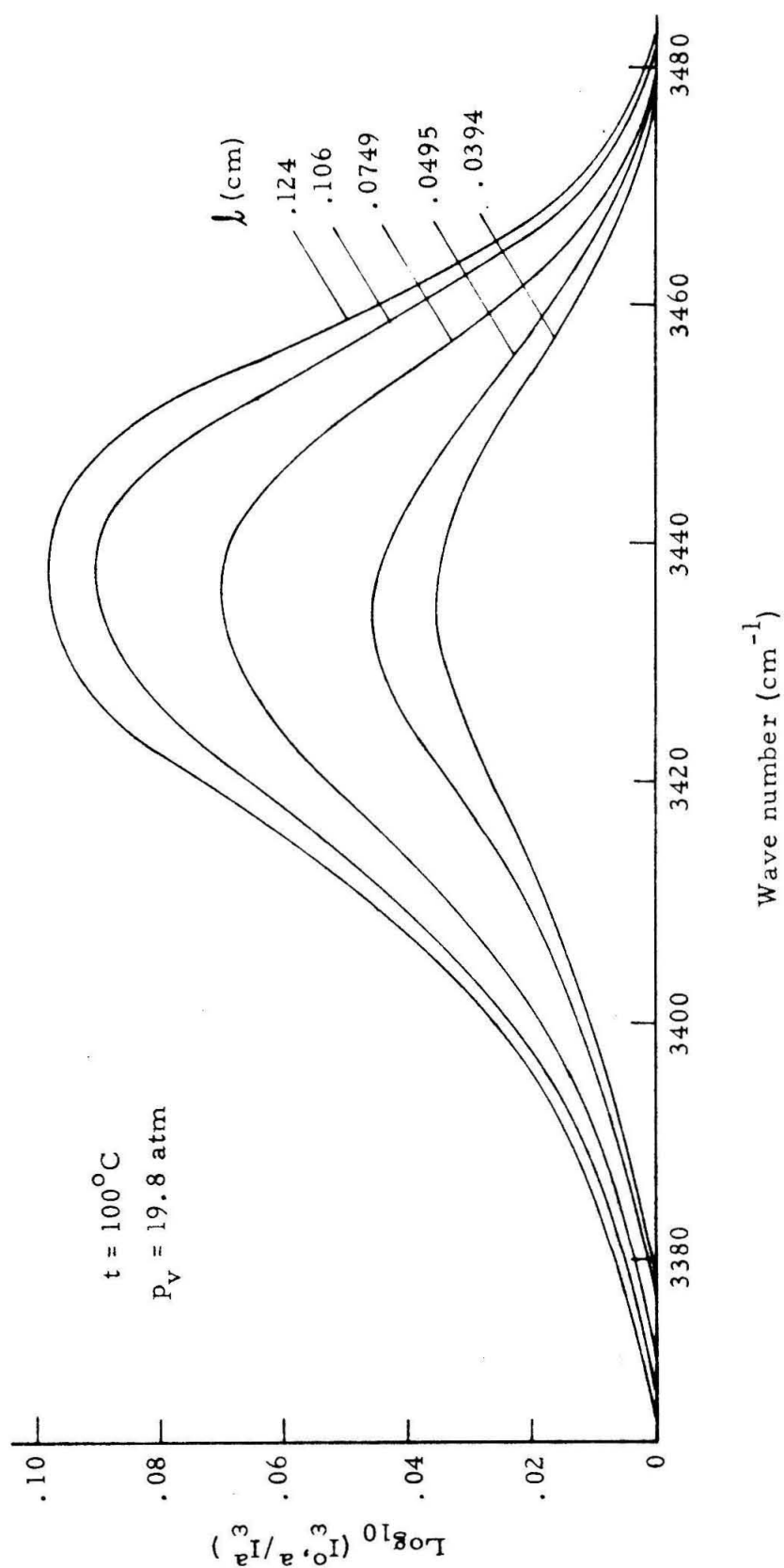
-66-

Fig. 48. Logarithm of the reciprocal of apparent spectral transmission for the 3120 cm^{-1} band of gaseous N_2O_4 at various optical depths.

Fig. 49. Logarithm of the reciprocal of apparent spectral transmission for the 3442 cm^{-1} band of gaseous N_2O_4 at various optical depths.

Fig. 50. Logarithm of the reciprocal of apparent spectral transmission for the 3442 cm^{-1} band of gaseous N_2O_4 at various optical depths.

Fig. 51. Logarithm of the reciprocal of apparent spectral transmission for the 3442 cm^{-1} band of gaseous N_2O_4 at various optical depths.

Fig. 52. Logarithm of the reciprocal of apparent spectral transmission for the 3442 cm^{-1} band of gaseous N_2O_4 at various optical depths.

Fig. 53. Logarithm of the reciprocal of apparent spectral transmission for the 3442 cm^{-1} band of gaseous N_2O_4 at various optical depths.

Fig. 54. Logarithm of the reciprocal of apparent spectral transmission for the 3442 cm^{-1} band of gaseous N_2O_4 at various optical depths.

APPENDIX II

Plots of Linear Absorption Coefficient as a Function of
Wave Number for Liquid N_2O_4 Combination Bands in the
Temperature Range 25 to $100^{\circ}C$.
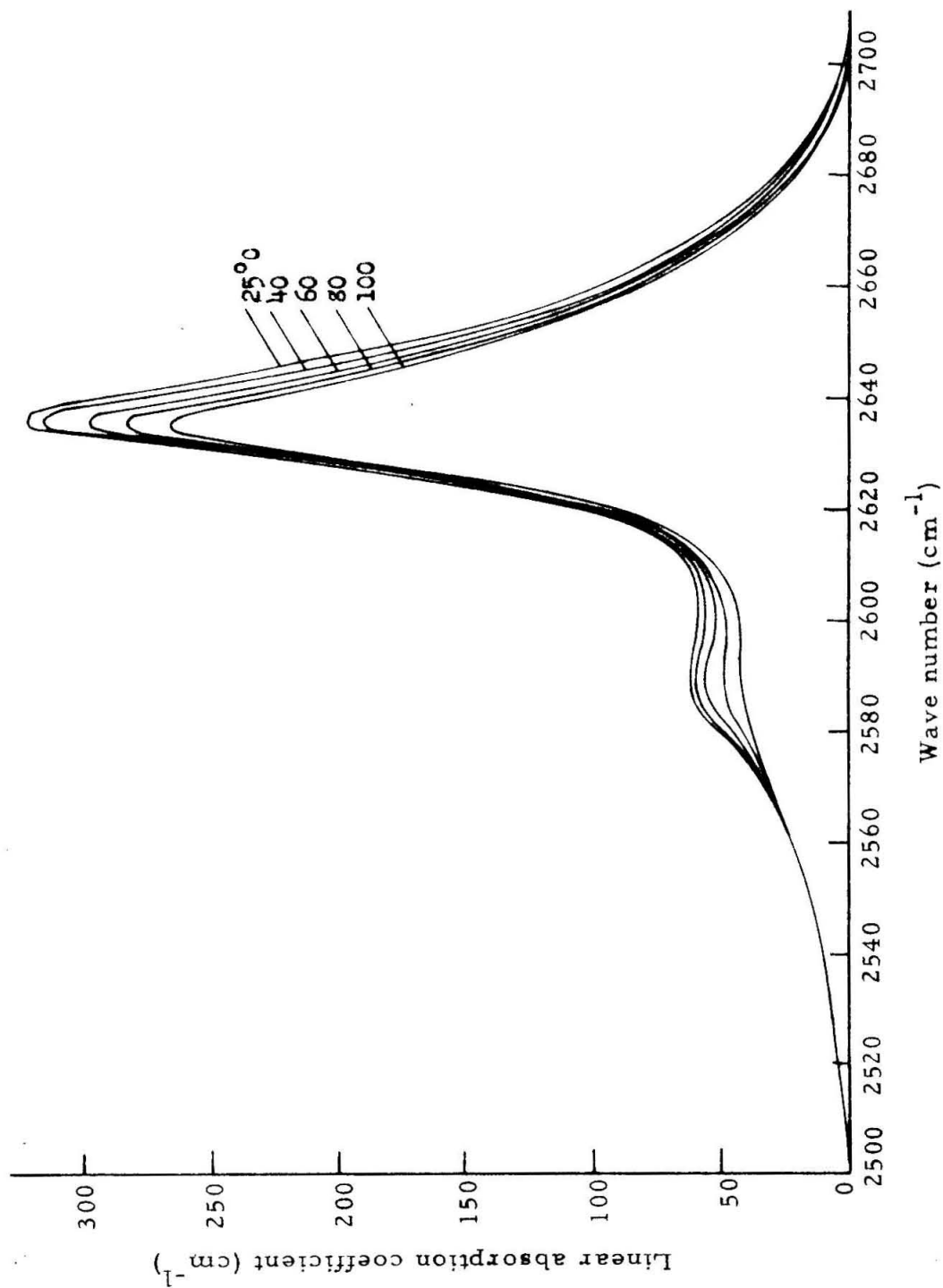
Fig. 55. Spectral absorption coefficient for the 2605 cm^{-1} band of liquid N_2O_4 at various temperatures.
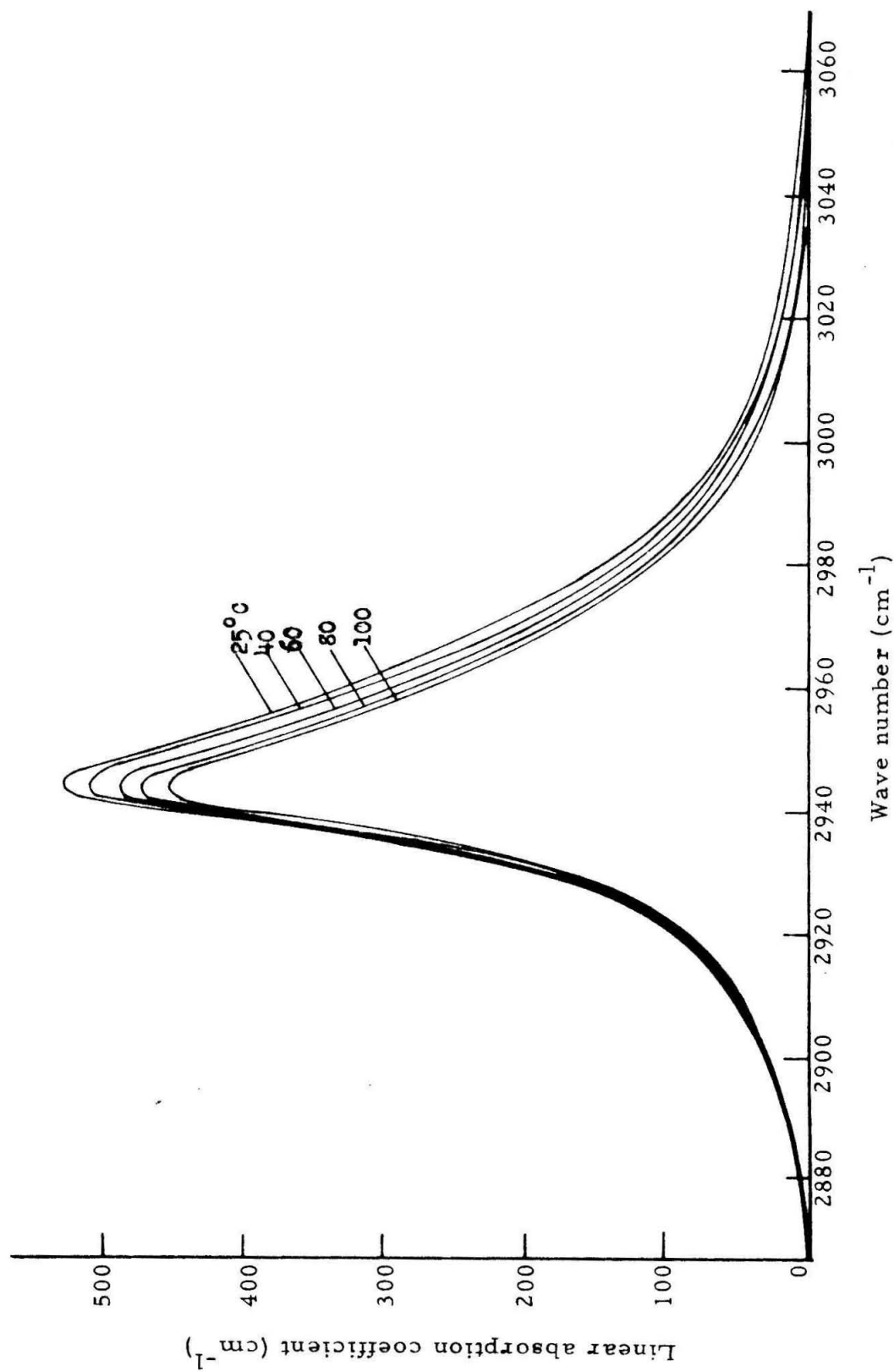
Fig. 56. Spectral absorption coefficient for the 2945 cm^{-1} band of liquid N_2O_4 at various temperatures.
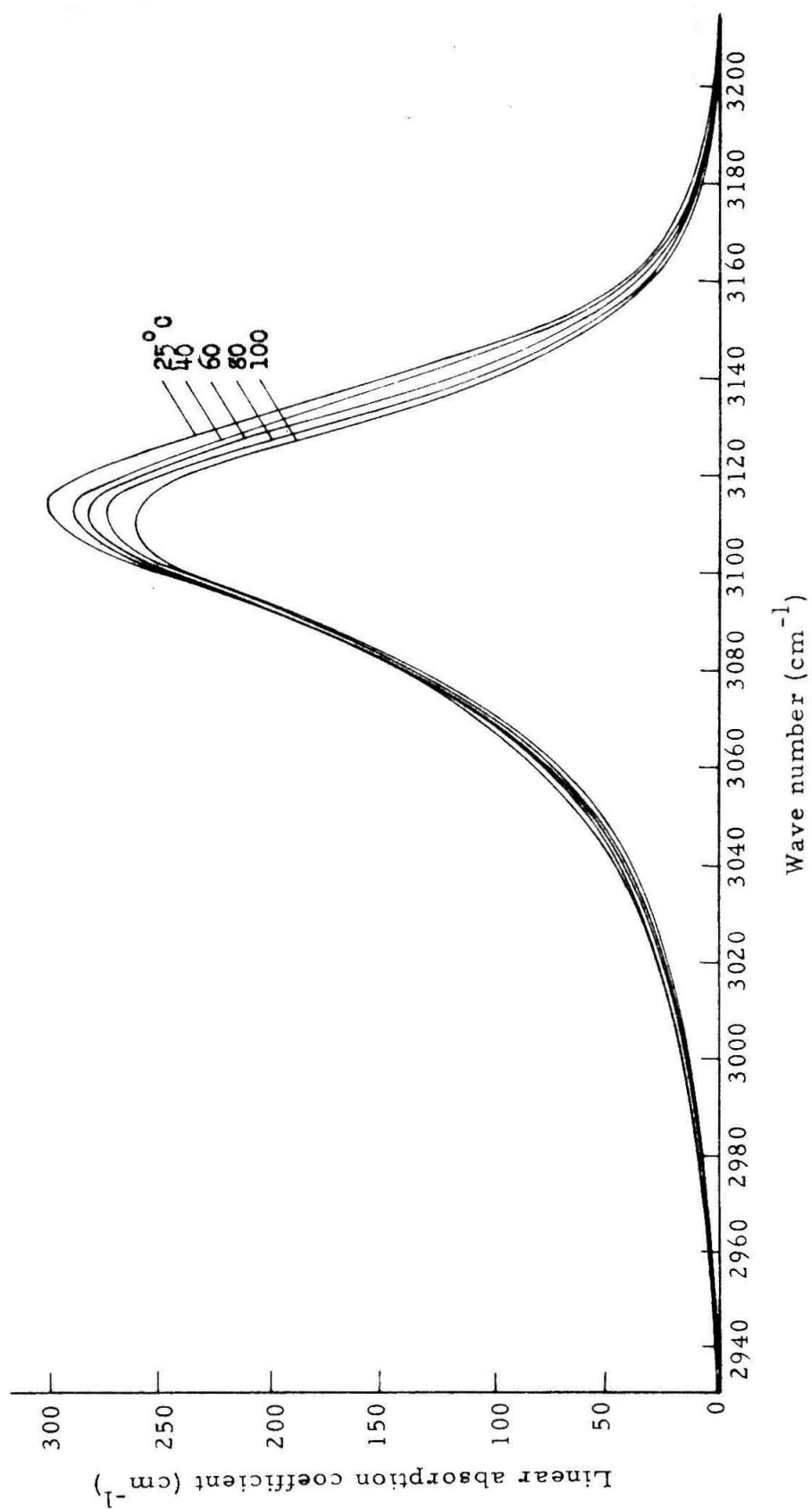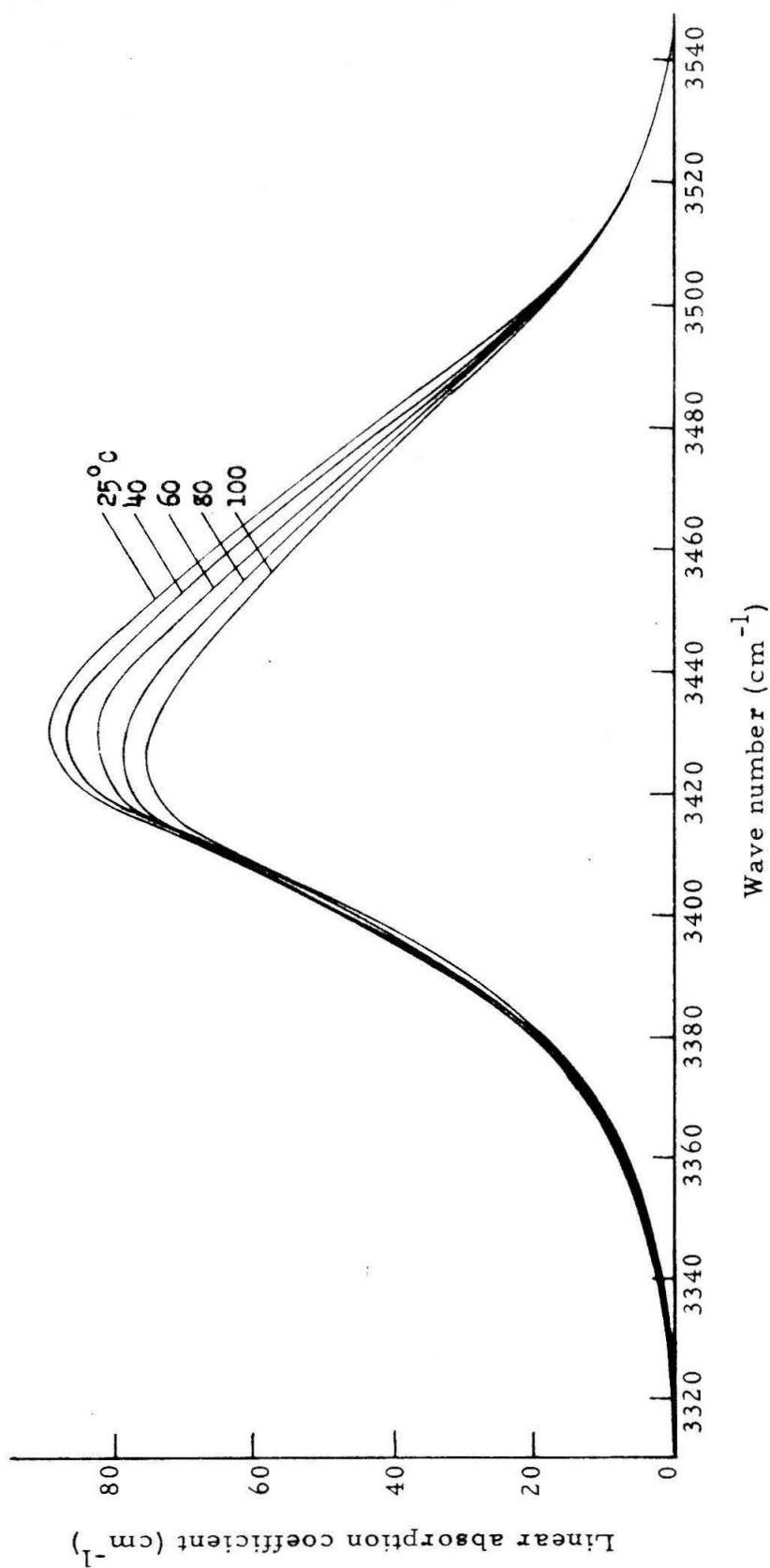
Fig. 57. Spectral absorption coefficient for the 3114 cm^{-1} band of liquid N_2O_4 at various temperatures.

Fig. 58. Spectral absorption coefficient for the 3429 cm^{-1} band of liquid N_2O_4 at various temperatures.

APPENDIX III

Plots of $\text{Log}_{10}(I^{o,a}_{\omega}/I^a_{\omega})$ as a Function of Wave Number
for Gaseous NO_2 and N_2O_4 Fundamental Bands at 25^oC.
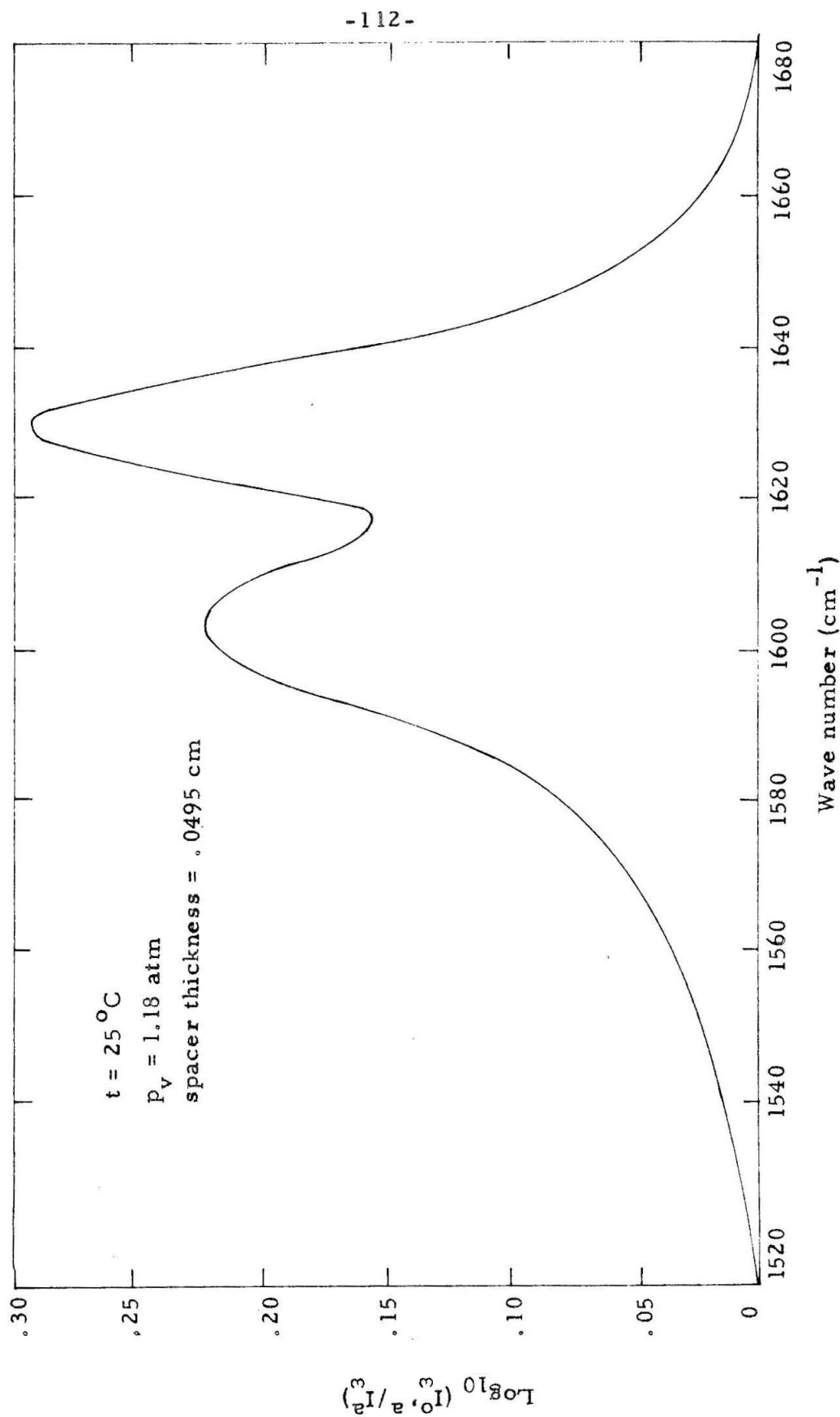
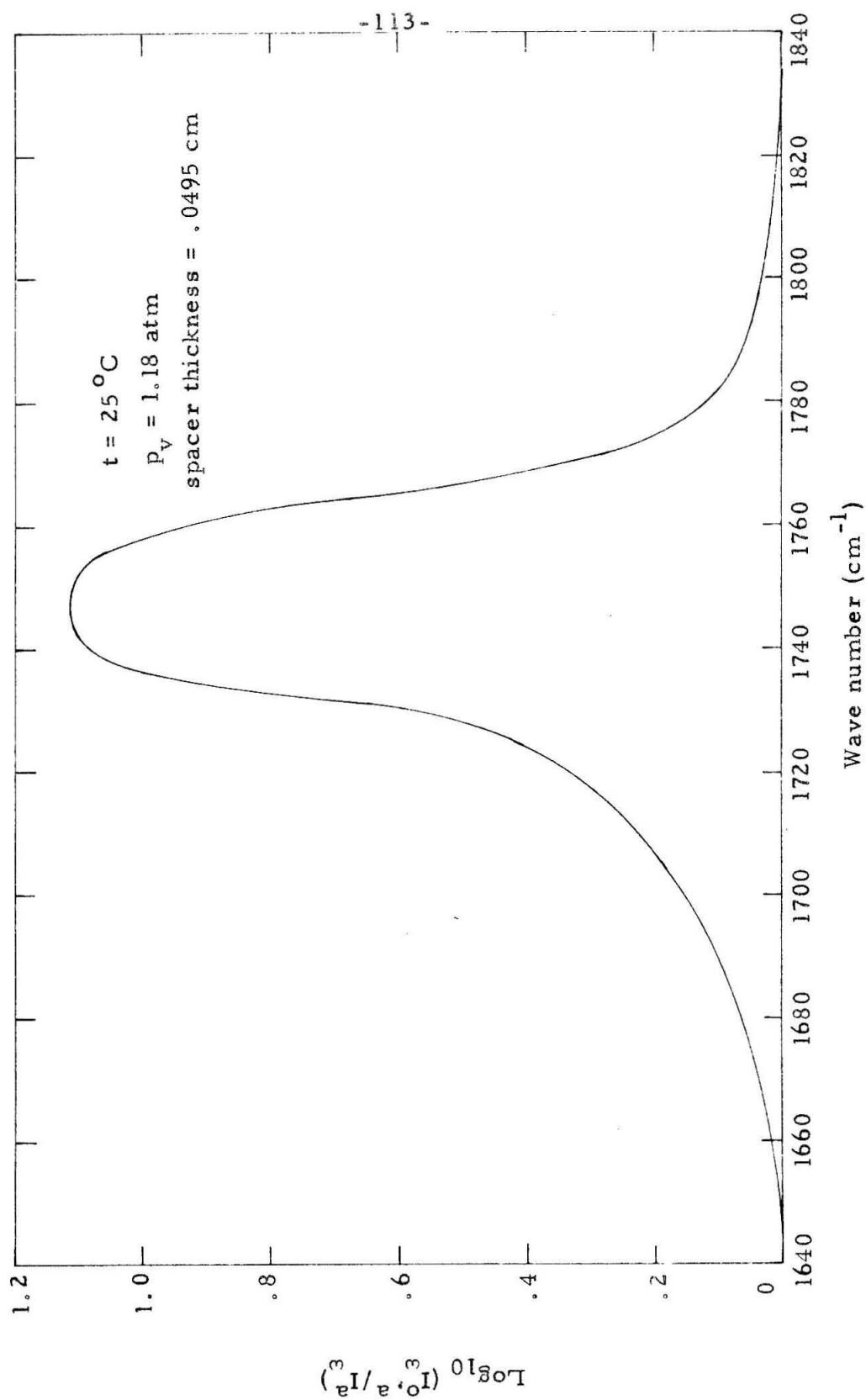Fig. 59. Logarithm of the reciprocal of apparent spectral transmission for the 1618 cm^{-1} fundamental of NO_2.

Fig. 60. Logarithm of the reciprocal of apparent spectral transmission for the 1748 cm^{-1} fundamental of gaseous N_2O_4.

t = 25 $^{\circ}$C

p_v = 1.18 atm

spacer thickness = .0495 cm
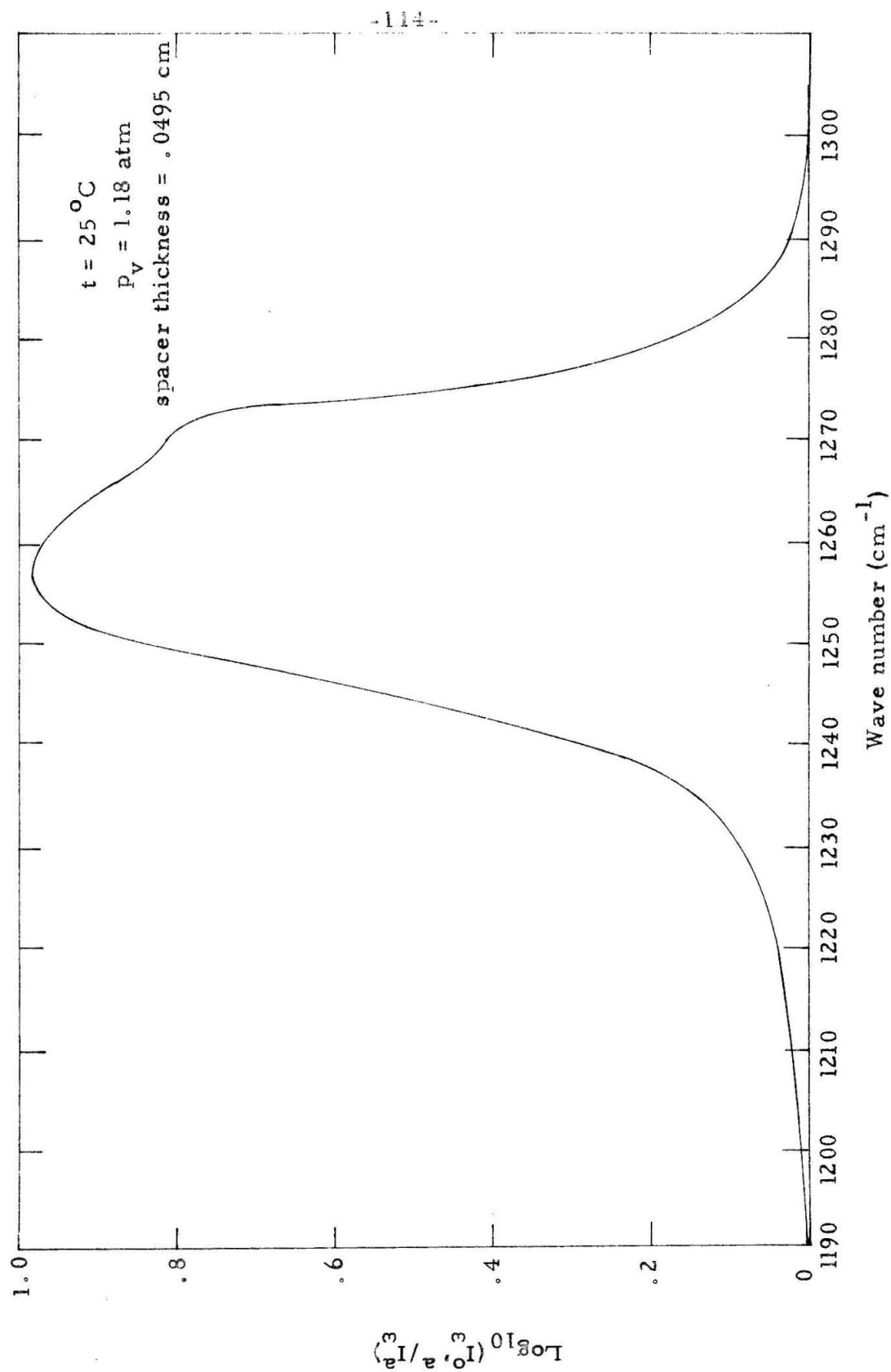
Wave number (cm^{-1})

Log_{10} ($I^{o,a}_{\omega}/I^a_{\omega}$)

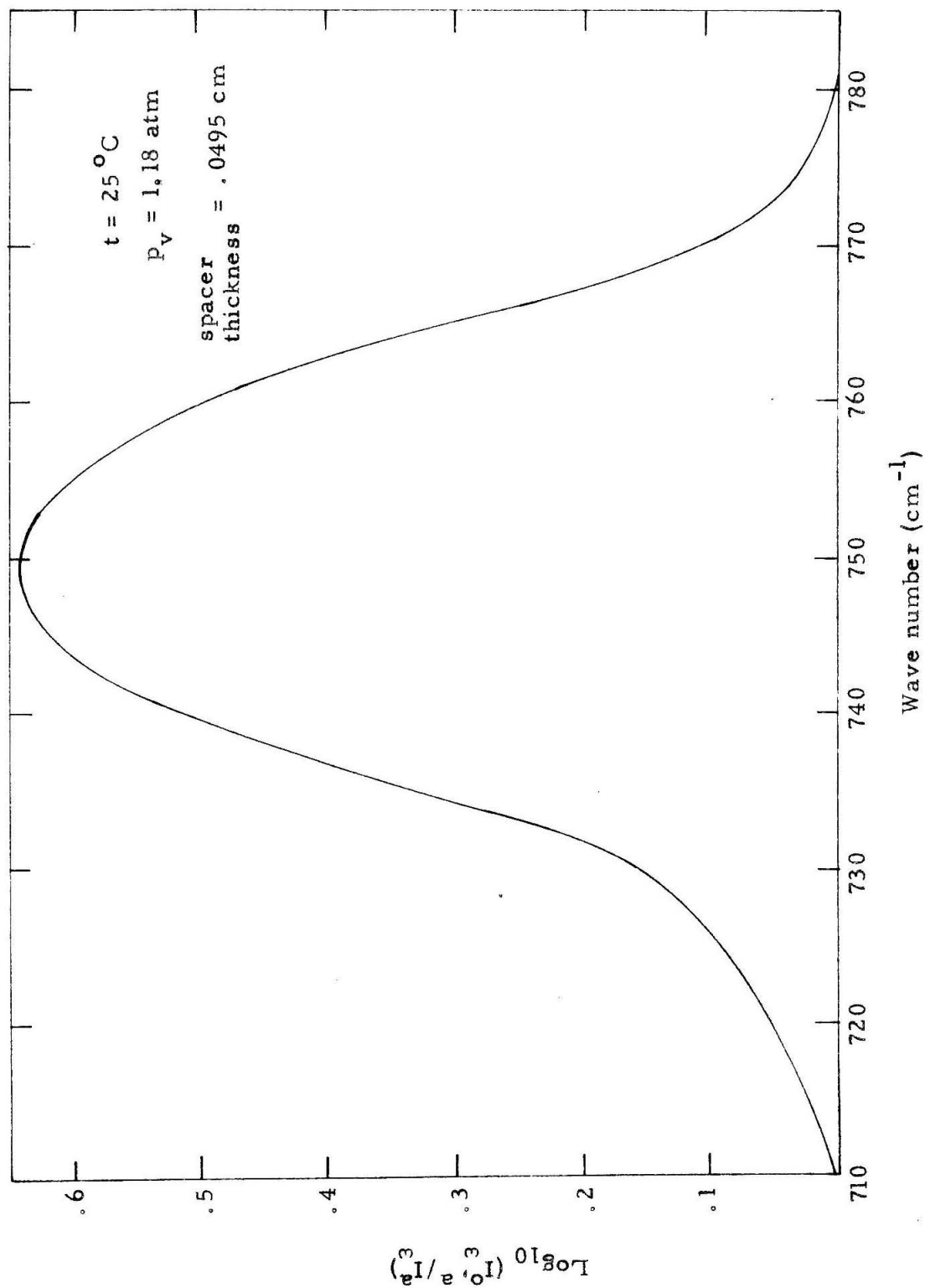Fig. 61. Logarithm of the reciprocal of apparent spectral transmission for the 1260 cm^{-1} fundamental of gaseous N_2O_4.

Fig. 62. Logarithm of the reciprocal of apparent spectral transmission for the 750 cm^{-1} fundamental of gaseous N_2O_4.